Lattice studies of quark spectra and supersymmetric quantum mechanics

Dissertation

zur Erlangung des Doktorgrades
der Naturwissenschaften (Dr. rer. nat.)
der Fakultät für Physik
der Universität Regensburg

vorgelegt von

Sebastian Schierenberg

aus Burghausen

Juni 2012

Promotionsgesuch eingereicht am: 24.06.2012

Die Arbeit wurde angeleitet von: Dr. F. Bruckmann

Prüfungsausschuss:	Vorsitzender:	Prof. Dr. K. Rincke
	1. Gutachter:	Prof. Dr. T. Wettig
	2. Gutachter:	Prof. Dr. A. Schäfer
	weiterer Prüfer:	Prof. Dr. M. Grifoni

Contents

1. Introduction

The standard model (SM) of particle physics is one of the most well-tested theories in physics. It explains high-energy experiments like those performed at the Large Hadron Collider (LHC) in a framework that unifies all relevant particle interactions occurring in these experiments. Only recently, there has been first experimental evidence for the Higgs boson [1, 2], which has been predicted back in 1964 [3]. It is connected to the Higgs mechanism of the SM, which provides an elegant explanation for the masses of weak gauge bosons via spontaneous symmetry breaking. The part of the SM that describes the strong force between the quarks is the theory of quantum chromodynamics (QCD). Due to asymptotic freedom [4], QCD is accessible by perturbative methods in the high energy regime. On the other hand, perturbation theory cannot be used to study non-analytical properties of QCD like the phase diagram. The latter is relevant for the description of heavy-ion collisions and the understanding of the early universe. A non-perturbative approach to the theory is thus necessary to gain insight into these subjects.

Despite its success, the SM has some flaws, e.g. the so-called hierarchy problem that parameters of a fundamental high-energy theory must be unnaturally fine-tuned in order to produce the known low-energy physics [6]. Furthermore, the cold dark matter which explains many astronomical observations (see Ref. [7] for a review) is not contained in the standard model. A possible way to overcome the mentioned issues is supersymmetry (SUSY), which is an extension of the usual space-time symmetries that relates fermions with bosons. However, no evidence has yet been found for a supersymmetric extension of the standard model. Thus, if SUSY exists in reality, it must be broken on the energy scales of the experiments done so far, either spontaneously or explicitly. As in the case of QCD, this calls for non-perturbative methods to study supersymmetric theories.

A promising candidate for such an approach is a numerical treatment of the theories, since the development of supercomputers has made great progress in the last decades. At present, the fastest supercomputer in the world is the IBM Sequoia, with a performance of $16.3 \cdot 10^{15}$ floating-point operations per second (FLOPS) based on the LINPACK benchmark [8]. For comparison, the fastest computer in November 1999 was the ASCI Red with about $2.4 \cdot 10^{12}$ FLOPS [9]. The calculations performed on these computers

have a wide range of applications from weather forecasts to the simulation of molecular dynamics.

Large amounts of computer time are also required for the numerical investigation of quantum field theories like QCD, which is done with great success by a branch called lattice QCD. Here, lattice refers to the discretization of space-time, which is necessary in order to make the theory feasible for the numerical calculations. Lattice QCD provides a non-perturbative way to gain theoretical insight e.g. into the structure of hadrons [10] and the QCD phase diagram [11]. The latter amounts to the study of QCD at non-zero temperature and/or density, which is the first main part of this work. However, the mentioned discretization of space-time causes some fundamental changes compared to the continuum theory. For example, gauge symmetry on the lattice requires the use of link variables which are elements of the gauge group instead of the continuum fields that are elements of the gauge algebra. Furthermore, exact chiral symmetry can only be obtained on the lattice by the cost of non-local actions or fermionic doublers [12]. However, a remnant of the continuum chiral symmetry is comprised by the so-called overlap operator [13–15], which is considered the 'best' lattice operator concerning chiral symmetry.

Similar issues are encountered in the numerical treatment of supersymmetry, which has also been studied on the lattice, see Refs. [16, 17] for reviews. Similar to the chiral symmetry, exact SUSY on the lattice can only be achieved by either non-local or quadratic actions [18], the latter being trivial. However, as in the case of chiral symmetry mentioned above, a remnant of SUSY may be satisfied by a local action. Our findings related to the search for such an action are comprised in the second main part of this work, along with a different approach to construct a lattice action that aims at a compromise between locality and supersymmetry.

This thesis is organized in the following way. After giving a brief introduction to the necessary theoretical basics in Sec. 2, the results are divided in two major parts. Firstly, we analyze quark spectra in two-color lattice QCD at non-zero temperature or non-zero density, with a focus on eigenvalue correlations, in Sec. 3. For the case of non-zero temperature considered in Sec. 3.1, we establish a connection between low eigenmodes of two different lattice Dirac operators and local Polyakov loops. Furthermore, we present a random matrix model that mimics many features of these operators. In Sec. 3.2, we consider the spacing distributions of the overlap Dirac operator for various values of the chemical potential, i.e., at non-zero density. We show that these are very well approximated by the spacing distributions we derive for small real random matrices

with a tunable degree of non-hermiticity. The latter also provide good approximations for the spacing distributions of corresponding large random matrices in the regime of weak non-hermiticity.

In Sec. 4, which contains the second part of the results, we consider various aspects of supersymmetry on the lattice. We begin with a status report on our search for a remnant of SUSY on the lattice with the blocking approach in Sec. 4.1. In Sec. 4.2, we construct lattice actions of supersymmetric quantum mechanics (SUSYQM), that are improved with respect to supersymmetry and ultra-local. We show numerically that the Ward identities, which can be used to quantify the breaking of SUSY, are indeed much smaller for the improved than for the naive discretizations. Finally, we summarize our findings and conclude in Sec. 5.

2. Theoretical basics

This Section provides the theoretical foundations on which the results of this thesis are based. It includes a short introduction into QCD in the continuum and on the lattice in Sec. 2.1, SUSY in Sec. 2.2, Monte Carlo (MC) integration in Sec. 2.3 and random matrix theory (RMT) in Sec. 2.4.

2.1. Quantum chromodynamics

For a detailed introduction to QCD and quantum field theories in general, we refer the reader to the book of Peskin and Schroeder [19]. The theory of quantum chromodynamics forms, together with the theory of the electro-weak interaction, the standard model of particle physics. It describes the interaction between the constituents of hadrons, the quarks, via non-abelian gauge fields called gluons. The action of QCD is given by

$$S_{\mathrm{QCD}} = \int d^4x \; \mathcal{L}_{\mathrm{QCD}} \,, \tag{2.1}$$

with the Lagrangian

$$\mathcal{L}_{\mathrm{QCD}} = \sum_f \left[\bar{\psi}_f \left(iD - m_f\right) \psi_f\right] - \frac{1}{4} F^a_{\mu\nu} F^{a\,\mu\nu} \,, \tag{2.2}$$

which is composed of fermion fields ψ_f and $\bar{\psi}_f (= \psi_f^\dagger \gamma_0)$ that represent the quarks with the flavor index f and mass m_f, the field strength tensor

$$F^a_{\mu\nu} = \partial_\mu A^a_\nu - \partial_\nu A^a_\mu + g f^{abc} A^b_\mu A^c_\nu \,, \tag{2.3}$$

and the Dirac operator

$$D = \gamma^\mu D_\mu = \gamma^\mu \left(\partial_\mu - igA_\mu\right) \text{ , with } \quad A_\mu = A^a_\mu t^a \,. \tag{2.4}$$

We denote the Dirac γ matrices by γ^μ, the gluon fields by A^a_μ, and the structure constants by f^{abc}. The Gell-Mann matrices denoted by t^a span the $\mathfrak{su}(3)$ algebra. $a, b, c = 1, \ldots, 8$ are color indices, whereas $\mu, \nu = 0, \ldots, 3$ are Lorentz indices and a sum over double indices is understood. The structure constants are related to the Gell-Mann matrices via

$$[t^a, t^b] = i\, f^{abc}\, t^c\,. \tag{2.5}$$

The fermion fields $\bar{\psi}_f$ and ψ_f are vectors in a 12-dimensional complex vector space which is a direct product of the 4-dimensional spinor space and the 3-dimensional color space. The γ-matrices act in the spinor space, while all matrices related to the $SU(3)$ group or the $\mathfrak{su}(3)$ algebra act in color space.

In accordance with the theory of special relativity, the action of QCD is symmetric with respect to Poincaré transformations. Additionally, it is invariant under local gauge transformations, which are defined by

$$\bar{\psi}_f(x) \to \bar{\psi}_f(x) V^\dagger(x)\,, \tag{2.6}$$

$$\psi_f(x) \to V(x)\psi_f(x)\,, \tag{2.7}$$

$$A_\mu(x) \to V(x) A_\mu(x) V^\dagger(x) + V(x)\frac{i}{g}\left[\partial_\mu V^\dagger(x)\right]\,, \tag{2.8}$$

with an arbitrary differentiable field of $SU(3)$ matrices $V(x)$. The covariant derivative D_μ then transforms like

$$\begin{aligned} D_\mu &\to \partial_\mu - igV(x)A_\mu(x)V^\dagger(x) + V(x)\left[\partial_\mu V^\dagger(x)\right] \\ &= V(x)\partial_\mu V^\dagger(x) - igV(x)A_\mu(x)V^\dagger(x) = V(x)D_\mu V^\dagger(x)\,, \end{aligned} \tag{2.9}$$

so $\bar{\psi}_f(iD)\psi_f$ and $\bar{\psi}_f\psi_f$ are invariants under gauge transformations. The field strength tensor can be expressed in terms of the covariant derivative as

$$F^a_{\mu\nu}\, t^a = \frac{i}{g}[D_\mu, D_\nu]\,. \tag{2.10}$$

Making use of the property $\mathrm{tr}(t^a t^b) = \delta_{ab}$ of the Gell-Mann matrices, the last term in Eq. (2.2) can be thus written as $\frac{1}{4g^2}\,\mathrm{tr}\left([D_\mu, D_\nu]\,[D^\mu, D^\nu]\right)$, which is clearly also invariant under gauge transformations.

For a quark flavor with zero mass, the action of QCD is also invariant under a chiral

transformation of the resp. fermion fields, given by

$$\bar{\psi} \to \bar{\psi} e^{i\epsilon\gamma_5} \text{ , and } \quad \psi \to e^{i\epsilon\gamma_5}\psi \,, \tag{2.11}$$

because the massless Dirac operator fulfills

$$\{D, \gamma_5\} = 0 \,. \tag{2.12}$$

However, this chiral symmetry may be spontaneously broken, as considered below.

2.1.1. QCD at non-zero temperature and density

The study of quantum chromodynamics at non-zero temperature and density is crucial for the understanding of the physics of the hot early universe and systems with a high baryon density like neutron stars. A recent review about the phase diagram of QCD in given in Ref. [5]. The grand canonical partition function of QCD in a heat bath of temperature T, spatial volume V and chemical potentials μ_f for the different quark flavors is given by

$$\begin{aligned} Z(T, V, \mu_f) &= \text{tr}\left[e^{-\frac{1}{T}(H - \sum_f \mu_f Q_f)}\right] \\ &= \int DAD\bar{\psi}D\psi \, \exp\left[-\int_0^{1/T} dt \int_V d^3x \left(\mathcal{L}_{\text{QCD}} + \sum_f \bar{\psi}_f \mu_f \gamma_4 \psi_f\right)\right] . \end{aligned} \tag{2.13}$$

Here, H is the QCD Hamiltonian, $Q_f = \bar{\psi}_f \gamma_4 \psi_f$ are the quark number operators for the different flavors and $\mathcal{L}_{\text{QCD}}$ is the imaginary-time version of the QCD Lagrangian defined in Eq. (2.2). Due to the imaginary time, space-time is Euclidean. Thus, the indices μ, ν run from 1 to 4, the metric is $g_{\mu\nu} = \delta_{\mu\nu}$ and the γ matrices fulfill $\{\gamma_\mu, \gamma_\nu\} = \delta_{\mu\nu}$. The non-zero temperature is simply introduced by a compactification of the time dimension, while the density is controlled by the quark chemical potentials. To ensure proper Bose/Fermi statistics, the boundary conditions in time direction have to be periodic for bosons and anti-periodic for fermions.

The (traced) Polyakov loop is the trace of a closed Wilson loop around the temporal direction, defined by

$$L(\vec{x}) = \frac{1}{3}\text{tr}\left\{\mathcal{P}\exp\left[ig\int_0^{1/T} dt A_4(\vec{x}, t)\right]\right\} , \tag{2.14}$$

where $\mathcal{P}$ is the path-ordering operator. We consider the pure gauge theory in the following. In this case, the action of QCD is invariant under gauge transformations that are periodic up to a center element of the gauge group, denoted by z, in the temporal direction. However, the Polyakov loop becomes $L(\vec{x}) \to zL(\vec{x})$ under such a transformation. Therefore, the expectation value[1] $\langle L \rangle$ of the Polyakov loop is zero, if center symmetry is not spontaneously broken, which is the case for $T = 0$. It is furthermore related to the quark free energy F_Q via $\langle L \rangle = e^{-(F_Q - F_0)/T}$, which means that $F_Q = \infty$ for $\langle L \rangle = 0$, and the theory is confining. For $T \to \infty$, the center symmetry is spontaneously broken, the expectation value of L becomes non-zero and the quark free energy becomes finite. Thus, there is a confinement-deconfinement transition in the zero-flavor approximation of QCD as the temperature is increased.

Another phase transition of QCD is related to chiral symmetry. As mentioned above, the massless Dirac operator is chiral, which means that the chiral condensate $\langle \bar{\psi}_f \psi_f \rangle$ should be zero for $m_f = 0$. However, this is not the case for $T = 0$, because chiral symmetry is spontaneously broken in this regime. Above a certain critical temperature denoted by T_c, the symmetry is restored, and the chiral condensate becomes zero. This means that there is again a non-analytical phase transition, which is denoted as chiral phase transition.

For dynamical QCD at physical quark masses, these are no exact phase transitions but rather crossovers, however the Polyakov loop and the chiral condensate still serve as approximate order parameters. In this case, recent lattice simulations have shown that the critical temperature for the chiral phase crossover is about $T_c \approx 154$ MeV [20].

An approximate restoration of chiral symmetry is also expected for sufficiently large values of the chemical potential at zero temperature and physical quark masses. Furthermore, for asymptotically large values of the potential, a superconducting phase is assumed from to the analysis of QCD with weak-coupling methods.

2.1.2. QCD on the lattice

We briefly summarize the very basics of lattice QCD in this Section, for a detailed introduction the reader is referred to Ref. [21]. The fundamental difference between continuum and lattice QCD is the discretization of space-time. In actual computer simulations, the lattice extent in all directions has also to be restricted leading to finite size effects, but this is not our main concern here. Furthermore, a Wick rotation the imaginary time is performed in order to make the path integrals introduced below in

[1] This means that the path integral over the gauge fields is taken.

Sec. 2.1.2.3 feasible by numerical methods. This means that the Metric becomes $g_{\mu\nu} = \delta_{\mu\nu}$ and the theory lives in Euclidean space.

2.1.2.1. The gauge action

We firstly consider the pure gauge theory in a discretized Euclidean four-dimensional space-time with lattice spacing a and arbitrary extent. In order to maintain local gauge symmetry in this setting, the continuum gauge fields, which are elements of the $\mathfrak{su}(3)$ algebra, have to be replaced by elements of the $SU(3)$ group. These $SU(3)$ elements are called gauge links and connect neighboring lattice sites. We denote the link at the lattice site x by $U_\mu(x)$, where $\mu = 1, \ldots, 4$ is the direction of the link, i.e., it connects the site x and the site $x + \hat{\mu}$, with the vector $\hat{\mu}$ of length a pointing along one of the four coordinate axis. Backward-pointing links are defined by $U_{-\mu}(x) = U_\mu^\dagger(x - \hat{\mu})$.

The gauge links transform under local gauge transformations as

$$U_\mu(x) \to g(x)\, U_\mu(x)\, g^\dagger(x + \hat{\mu})\,, \tag{2.15}$$

where the $g(x) \in SU(3)$ define the transformation. It can be easily shown that every product of links along a closed loop is a gauge-invariant quantity. The product around the smallest possible non-trivial closed loop is the so-called plaquette, which is given by

$$U_{\mu\nu}(x) = U_\mu(x)\, U_\nu(x + \hat{\mu})\, U_{-\mu}(x + \hat{\mu} + \hat{\nu})\, U_{-\nu}(x + \hat{\nu})\,. \tag{2.16}$$

The first gauge symmetric action for QCD on the lattice has been introduced by Wilson [22], and reads

$$S_G[U] = \frac{\beta}{3} \sum_x \sum_{\mu<\nu} \mathfrak{Re}\,\mathrm{tr}\,(\mathbb{1} - U_{\mu\nu}(x))\,, \tag{2.17}$$

where $\beta = 6/g^2$ is the so-called inverse coupling. One can show that in the continuum limit $a \to 0$, the term in the trace becomes proportional to the continuum Lagrange density of the pure gauge theory. Thus, the Wilson action approaches the gauge part of the continuum action of QCD, given in Eq. (2.1), in this limit up to a factor of -1 (due to the Euclidean metric as opposed to the Minkowski metric) and a rescaling of the gauge fields.

2.1.2.2. Fermions on the lattice

Unlike the gauge links, the fermionic fields $\bar{\psi}$ and ψ (we consider only one flavor here for convenience) are placed at the lattice points. Under the gauge transformation, they transform as

$$\bar{\psi}(x) \to \bar{\psi}(x)g^\dagger(x) \text{ , and } \quad \psi(x) \to g(x)\psi(x)\,. \tag{2.18}$$

Therefore, all terms of the form $\bar{\psi}(x)C(U)\psi(y)$, where $C(U)$ is a path-ordered product of gauge links along some curve from x to y, are gauge invariant.

Hence, a gauge invariant discretization of the fermionic action is given by

$$S_F[\bar{\psi},\psi,U] = a^4 \sum_{x,x'} \bar{\psi}(x) D_{xx'}\, \psi(x')\,, \tag{2.19}$$

with the naive choice for the lattice Dirac operator

$$D_{xx'} = \left[\sum_\mu \gamma_\mu \frac{U_\mu(x)\,\delta_{x+\hat{\mu},x'} - U_\mu^\dagger(x')\,\delta_{x-\hat{\mu},x'}}{2a}\right] + m\mathbb{1}\,\delta_{xx'}\,, \tag{2.20}$$

where γ_μ are Euclidean γ matrices. However, this operator suffers from the serious so-called doubling problem, which can be easily understood by considering the free[2] massless lattice Dirac operator (2.20) in momentum space, which reads

$$D(p) = \frac{i}{a}\ \sum_\mu \gamma_\mu \sin(ap_\mu)\,. \tag{2.21}$$

This operator has a total of 16 zero modes, since the sine function is zero for $p_\mu = 0$ or $p_\mu = \pi/a$, but only the zero mode at $p = (0,0,0,0)$ is also present in the continuum theory. Since each of the zero modes corresponds to a pole of the quark propagator, there exist 15 unphysical poles. A possible way to get rid of those is to use a different (massless) Dirac operator

$$D^W(p) = \frac{i}{a}\ \sum_\mu \gamma_\mu \sin(ap_\mu) + \frac{\mathbb{1}}{a}\ \sum_\mu [1-\cos(ap_\mu)]\,, \tag{2.22}$$

where the second summand is an additional term called Wilson mass. The only zero mode of this operator is the one that is also present in the continuum, while all others

[2] This means that the gauge links are set to $\mathbb{1}$.

are lifted to a non-zero value. In real space and with non-trivial gauge links, the Wilson mass term reads

$$-\frac{a}{2}\sum_{\mu}\frac{U_\mu(x)\,\delta_{x+\hat{\mu},x'}-\mathbb{1}_3\,2\delta_{xx'}+U_\mu^\dagger(x')\,\delta_{x-\hat{\mu},x'}}{a^2}\,, \tag{2.23}$$

which is the discretization of a Laplacian times $a/2$, so it vanishes in the continuum limit $a \to 0$. In principle, the Wilson mass can be conveniently rescaled by any non-zero real number without spoiling its properties.

A problem of the Wilson mass is that it breaks chiral symmetry explicitly, so the Dirac operator D^W is not chirally symmetric for massless quarks. Another approach which partially removes the doublers, but keeps a remnant of chiral symmetry, is the staggered operator [23]. It is obtained from the naive discretization (2.20) by an unitary transformation of the fermion fields via

$$\bar{\psi}(x) \to \bar{\psi}(x)\gamma_4^{x_4}\gamma_3^{x_3}\gamma_2^{x_2}\gamma_1^{x_1}\ \text{, and} \qquad \psi(x) \to \gamma_1^{x_1}\gamma_2^{x_2}\gamma_3^{x_3}\gamma_4^{x_4}\psi(x)\,. \tag{2.24}$$

In this basis, the operator becomes block-diagonal, with four blocks that are exactly identical and read

$$D^S_{xx'} = \frac{1}{2a}\sum_{\mu=1}^{4}\eta_\mu(x)\left[\delta_{x+\hat{\mu},x'}U_\mu(x)-\delta_{x-\hat{\mu},x'}U_\mu^\dagger(x')\right]\,, \tag{2.25}$$

where $\eta_\mu(x) = (-1)^{\sum_{\nu<\mu} x_\nu}$. The staggered operator is defined as one of those blocks. Thus, the number of doublers is reduced to 4, and one can show that these can be considered as 4 so-called tastes of fermions which however interact non-trivially [24].

A third possibility to discretize the Dirac operator is the overlap operator [13–15], which is defined by

$$D^{\text{ov}} = \frac{1}{a}\left(1+\gamma_5\,\text{sign}(\gamma_5 D^W)\right)\,, \tag{2.26}$$

with the Wilson Dirac operator D^W as given in Eq. (2.22). The matrix sign function is defined by diagonalizing the argument, taking the sign of the eigenvalues, and transforming back into the initial basis. This procedure is well-defined since $\gamma_5 D^W$ is Hermitian (for vanishing chemical potential).

The overlap operator has no undesired doublers and is not exactly chiral in the

conventional sense, but it fulfills the Ginsparg-Wilson relation [25],

$$\{D^{\text{ov}}, \gamma_5\} = aD^{\text{ov}}\gamma_5 D^{\text{ov}}\,. \tag{2.27}$$

This relation can be seen as the lattice version of chiral symmetry, which tends towards the continuum relation, $\{D, \gamma_5\} = 0$, for $a \to 0$. It is considered the lattice operator with the mildest breaking of chiral symmetry, which also has no doublers. The zero modes of the overlap operator are sensitive to the topological charge of the gauge background, similar to the continuum Dirac operator [26]. However, the overlap is also the most costly discretization in terms of computer time, because it is not ultra-local like the operators discussed before.

2.1.2.3. The path integral on the lattice

The fundamental task of lattice QCD is the approximate calculation of expectation values, i.e., path integrals over certain operators. For an operator $O[\bar{\psi}, \psi, U]$, and with one quark flavor, such an integral reads

$$\langle O[\bar{\psi}, \psi, U]\rangle = \frac{1}{\mathcal{N}} \int D\psi D\bar{\psi} DU\, O[\bar{\psi}, \psi, U]\, e^{-S_F[\bar{\psi},\psi,U]-S_G[U]}\,, \tag{2.28}$$

with the partition function

$$\mathcal{N} = \int D\psi D\bar{\psi} DU\, e^{-S_F[\bar{\psi},\psi,U]-S_G[U]}\,, \tag{2.29}$$

and the bosonic and fermionic actions S_G and S_F (with a convenient choice of the Dirac operator D) that are given in Eqs. (2.17) and (2.19), respectively. The factor i is missing in the exponent in comparison to continuum path integrals because of the Wick rotation to imaginary time mentioned above. The Grassmann valued fermionic fields can be integrated out analytically, resulting in a determinant

$$\langle O[\bar{\psi}, \psi, U]\rangle = \frac{1}{\mathcal{N}} \int DU\, \tilde{O}[U]\, \det[D]\, e^{-S_G[U]}\,, \tag{2.30}$$

where the operator $\tilde{O}$ emerges from the initial operator O in a well-defined way. For a finite-sized lattice, the integral over the gauge fields can now be calculated numerically by the use of importance sampling techniques, which are introduced in Sec. 2.3 below.

If the determinant of the Dirac operator is neglected in the probability used for the importance sampling, this is called the quenched approximation. On the other hand,

if the determinant is real and positive as in the case of the staggered Dirac operator defined in Eq. (2.25), one can rewrite Eq. (2.30) as

$$\langle O[\bar{\psi}, \psi, U] \rangle = \frac{1}{\mathcal{N}} \int DU \, \tilde{O}[U] \, e^{-S_G[U] + \log \det[D]} \,, \tag{2.31}$$

and use an effective action of $S[U] = S_G[U] - \log \det[D]$ for the importance sampling. In this case, the integration is called 'dynamical'. If the Dirac operator is γ_5-Hermitian, i.e.,

$$D^\dagger = \gamma_5 D \gamma_5 \,, \tag{2.32}$$

as is the case for all the discretizations considered above, one can show that the determinant is real, but not necessarily positive. However, by introducing a second quark flavor with the same mass like the first, one obtains a factor of $\det[D]^2$ in the expectation value of O, which is real and positive.

2.1.2.4. Non-zero temperature and chemical potential

In lattice QCD, a non-zero temperature T is introduced by a compactification of the time dimension as in the continuum. For a lattice with n_t sites in time direction, we obtain a temperature of $T = 1/(an_t)$, which is inversely proportional to the length of the time dimension. For actual simulations on the computer, all dimensions have to compactified anyway to have a finite number of lattice points. For simulations at a temperature close to zero, one thus uses lattices with a large extent in the temporal direction, while high temperature studies require a short time dimension.

To introduce a non-vanishing quark density in lattice QCD, a quark chemical potential is required. A way to insert the chemical potential μ is to multiply all hopping terms in the Dirac operator pointing in the forward temporal direction by $e^{a\mu}$ and the ones pointing backwards by $e^{-a\mu}$. This is explained in detail in Ref. [21].

A non-zero chemical potential causes the so-called sign problem, because it breaks the γ_5-hermiticity of the Dirac operator, so the determinant of the latter may become complex. This is a serious problem for dynamical Monte Carlo simulations, since a complex determinant cannot be interpreted as a probability in the importance sampling any more. We comment on this in more detail in Sec. 3.2.

2.2. Supersymmetry

Symmetries play an important role in classical as well as in quantum physics. In the classical case, the Noether theorem [27] states that every invariance of the action of a given system under a certain symmetry results in a conserved quantity. Such conserved quantities restrict the dynamics of the system, which often strongly simplifies the solution of equations of motion. In quantum physics, symmetries lead to 'good' quantum numbers, which means that eigenstates of the Hamiltonian can be chosen to be also eigenstates of the generators of the resp. symmetry. Mostly, this results in degenerate energy levels of the system.

The latter holds also for supersymmetry, which extends the well-known space-time and gauge symmetries by connecting fermions and bosons, see Ref. [28] for an introduction. According to the Coleman-Mandula-Theorem [29], there is no symmetry which mixes space-time and internal symmetries in a non-trivial way and whose action can be represented by a Lie group (or an infinite parameter group). For SUSY, the last point does not apply, which is why it avoids this no-go theorem [30]. The action of SUSY transformations is rather represented by a Lie supergroup, which is generated by a Lie superalgebra. Such an algebra (also referred to as $\mathbb{Z}_2$-graded algebra) is composed of a Lie algebra $\mathbb{L}_0$, a vector space $\mathbb{L}_1$ and a product $\circ$, such that for all $x_l \in \mathbb{L}_l$ holds

$$\text{Grading and Completeness:} \qquad x_i \circ x_j \in \mathbb{L}_{(i+j) \bmod 2} \tag{2.33}$$

$$\text{Supersymmetry:} \qquad x_i \circ x_j = -(-1)^{i \cdot j}\, x_j \circ x_i \tag{2.34}$$

$$\text{Jacobi-identity:} \qquad x_k \circ (x_i \circ x_j)(-1)^{k \cdot j} + x_i \circ (x_j \circ x_k)(-1)^{i \cdot k} + x_j \circ (x_k \circ x_i)(-1)^{j \cdot i} = 0\,. \tag{2.35}$$

The product $\circ$ can thus be antisymmetric or symmetric, depending on the factors. For physical applications, the algebra $\mathbb{L}_0$ usually is the Poincaré algebra while $\mathbb{L}_1$ contains the supersymmetry generators. These are the very basics of supersymmetry in a nutshell.

Supersymmetry solves some problems of quantum field theories in an elegant way. For example, supersymmetric theories are easier to renormalize due to the cancellation of bosonic and fermionic loop integrals. Furthermore, the ground state of a supersymmetric theory has a finite energy, if SUSY is not spontaneously broken. A recent review about the research on SUSY is given in Ref. [31].

2.2.1. Supersymmetric quantum mechanics

Supersymmetric quantum mechanics is a simple toy model which can be viewed as a one-dimensional quantum field theory with two bosonic, real valued fields $\tilde{\chi}$, $\tilde{F}$ and two fermionic, Grassmann valued fields $\tilde{\psi}$, $\tilde{\bar{\psi}}$. These depend on one real time coordinate denoted by t and are combined into a multiplet

$$\tilde{\Phi}^b(t) = [\tilde{\chi}(t), \tilde{F}(t), \tilde{\psi}(t), \tilde{\bar{\psi}}(t)]^b \,, \text{ with } \quad b = 1, \ldots, 4 \,, \tag{2.36}$$

to compactify the notation. In one dimension, the Poincaré group contains only translations, which are generated by the derivative with respect to t denoted by ∂_t. There are also two linearly independent generators of SUSY transformations

$$\tilde{M} = \begin{pmatrix} 0 & 0 & 0 & 1 \\ 0 & 0 & 0 & -\partial_t \\ -\partial_t & -1 & 0 & 0 \\ 0 & 0 & 0 & 0 \end{pmatrix} , \quad \tilde{\bar{M}} = \begin{pmatrix} 0 & 0 & -1 & 0 \\ 0 & 0 & -\partial_t & 0 \\ 0 & 0 & 0 & 0 \\ \partial_t & -1 & 0 & 0 \end{pmatrix} , \tag{2.37}$$

which are written in matrix representation as acting on the vector $\tilde{\Phi}$. It is easy to check that these operators form a graded algebra with $\partial_t \in \mathbb{L}_0$ and $\tilde{M}, \tilde{\bar{M}} \in \mathbb{L}_1$, where the product $\circ$ is defined as either the commutator $[\cdot, \cdot]$ or the anti-commutator $\{\cdot, \cdot\}$. Then the following relations hold

$$[\partial_t, \partial_t] = \{\tilde{M}, \tilde{M}\} = \{\tilde{\bar{M}}, \tilde{\bar{M}}\} = [\partial_t, \tilde{M}] = [\partial_t, \tilde{\bar{M}}] = 0 \,, \quad \{\tilde{M}, \tilde{\bar{M}}\} = 2\partial_t \,, \tag{2.38}$$

so Eqs. (2.33)-(2.35) are fulfilled (the Jacobi identity is easily checked).

The Euclidean action of SUSYQM is given by

$$\tilde{S}[\tilde{\Phi}] = \int \mathrm{d}t \left[\frac{1}{2}(\partial_t \tilde{\chi})^2 + \tilde{\bar{\psi}} \partial_t \tilde{\psi} - \frac{1}{2}\tilde{F}^2 + \tilde{\bar{\psi}} \frac{\partial W}{\partial \tilde{\chi}} \tilde{\psi} - \tilde{F} W(\tilde{\chi}) \right] , \tag{2.39}$$

with an arbitrary so-called superpotential $W(\tilde{\chi})$. $\tilde{S}$ is invariant under infinitesimal supersymmetry transformations

$$\tilde{\Phi} \to \tilde{\Phi} + \delta\tilde{\Phi} \,, \text{ with } \quad \delta\tilde{\Phi} = (\epsilon \tilde{M} + \bar{\epsilon} \tilde{\bar{M}}) \tilde{\Phi} \,. \tag{2.40}$$

Here, ϵ and $\bar{\epsilon}$ are independent Grassmann valued parameters. The respective variations

of the component fields are

$$\begin{aligned} \delta\tilde{\chi} &= -\bar{\epsilon}\tilde{\psi} + \epsilon\tilde{\bar{\psi}}\,, \qquad \delta\tilde{F} = -\bar{\epsilon}\partial_t\tilde{\psi} - \epsilon\partial_t\tilde{\bar{\psi}}\,, \\ \delta\tilde{\psi} &= -\epsilon\partial_t\tilde{\chi} - \epsilon\tilde{F}\,, \quad \delta\tilde{\bar{\psi}} = \bar{\epsilon}\partial_t\tilde{\chi} - \bar{\epsilon}\tilde{F}\,. \end{aligned} \tag{2.41}$$

The field F is a non-dynamical field which occurs only up to quadratic order in the action and can therefore be integrated out analytically. This amounts to replacing F by $-W(\chi)$ and results in the 'on-shell' action

$$\tilde{S}^{\text{on}} = \int \mathrm{d}t \left[\frac{1}{2}(\partial_t\tilde{\chi})^2 + \tilde{\bar{\psi}}\partial_t\tilde{\psi} + \tilde{\bar{\psi}}\frac{\partial W}{\partial\tilde{\chi}}\tilde{\psi} + \frac{1}{2}W^2(\tilde{\chi})\right]. \tag{2.42}$$

After eliminating F, the SUSY transformations of the component fields are given by

$$\delta\tilde{\chi} = -\bar{\epsilon}\tilde{\psi} + \epsilon\tilde{\bar{\psi}}\,, \quad \delta\tilde{\psi} = -\epsilon\partial_t\tilde{\chi} + \epsilon W(\tilde{\chi})\,, \quad \delta\tilde{\bar{\psi}} = \bar{\epsilon}\partial_t\tilde{\chi} + \bar{\epsilon}W(\tilde{\chi})\,, \tag{2.43}$$

which can now be non-linear, depending on $W(\tilde{\chi})$.

Some properties of SUSYQM are easily obtained by considering the Hamiltonian of the theory, which is given by

$$H = -\frac{1}{2}\frac{d^2}{d\tilde{\chi}^2} + \frac{1}{2}W^2(\tilde{\chi}) + \frac{\partial W}{\partial\chi}[f^-, f^+]\,, \tag{2.44}$$

with fermionic ladder operators fulfilling $\{f^-, f^+\} = 1$ and $(f^-)^2 = (f^+)^2 = 0$. The Hamiltonian commutes with the supercharges

$$Q^{\pm} = \frac{1}{\sqrt{2}}\left[W(\tilde{\chi}) \mp \frac{d}{d\tilde{\chi}}\right] f^{\pm}\,, \tag{2.45}$$

and can be written as $H = (Q^+ + Q^-)^2$, i.e., the square of a Hermitian operator (since $[Q^{\pm}]^\dagger = Q^{\mp}$). It therefore has non-negative eigenvalues, and one can show that these are doubly degenerate. The only exception is a possible ground state with zero energy, which is unique. If such a state exists, the supersymmetry is unbroken, otherwise it is spontaneously broken.

2.3. Monte Carlo integration

One of the main numerical tasks occurring in lattice field theory is the calculation of very high dimensional integrals. Typically, expressions like

$$\big\langle O(A_1,\ldots,A_D)\big\rangle = \frac{1}{\mathcal{N}}\int\prod_{i=1}^{D} dA_i\, O(A_1,\ldots,A_D)\, e^{-S(A_1,\ldots,A_D)}\,, \tag{2.46}$$

have to be computed, see e.g. Eqs. (2.30) and (2.31), with a number of D integration variables and

$$\mathcal{N} = \int\prod_{i=1}^{D} dA_i\, e^{-S(A_1,\ldots,A_D)}\,. \tag{2.47}$$

Here, O and S are arbitrary functions, with the restriction that S is real and bounded from below as it corresponds to the action of the physical system under consideration. If the number of integration variables D is very large, these integrals only become feasible by the use of statistical methods. We describe the basic idea of Monte Carlo integration with importance sampling and Hybrid Monte Carlo integration as a more sophisticated method in the following.

2.3.1. Monte Carlo with importance sampling

The method of Monte Carlo integration with importance sampling is based on a random sampling of the domain of the respective integral. It is well suited for the expression given in Eq. (2.46) because the term $e^{-S(A_1,\ldots,A_D)}$ has a probabilistic interpretation. With the factor $1/\mathcal{N}$, we can define a probability

$$P(A_1,\ldots,A_D) = \frac{1}{\mathcal{N}}\, e^{-S(A_1,\ldots,A_D)}\,, \tag{2.48}$$

which is properly normalized, i.e.,

$$\int\prod_{i=1}^{D} dA_i\, P(A_1,\ldots,A_D) = 1\,. \tag{2.49}$$

We now rewrite Eq. 2.46 as

$$\langle O(A_1, \ldots, A_D) \rangle = \int \prod_{i=1}^{D} dA_i \, O(A_1, \ldots, A_D) \, P(A_1, \ldots, A_D) \,, \tag{2.50}$$

where the right hand side is the expectation value of the function O with respect to the random variables $A_1, \ldots, A_D$, which are distributed according to the probability density P. A statistical estimate of the integral can then be obtained by creating a large number of realizations of the random numbers and computing the average of O for these realizations. However, if the probability density P is very complicated, which will be the case in our applications, a straightforward draw of the random variables is unlikely to be possible. Instead, advanced methods like Markov chains have to be used, which are explained now.

Definition: A time-homogeneous Markov chain is a sequence of random numbers X_t with the integer t that all share the same sample space $\mathfrak{X}$. These have the property that for all $x, x' \in \mathfrak{X}$, the probability $P_T(X_t = x \wedge X_{t+1} = x')$ depends only on x and x'.

We also call x and x' possible states of the chain and P_T the transition probability between them. In other words, the probability to go from one state to another does neither depend on any of the previously drawn random numbers nor on the position (or time) t in the sequence. The transition probability is then the defining property for a specific Markov chain, alongside with the sample space of the random variables. For simplicity, we only consider a finite set $\mathfrak{X}$ in the following, the elements of which we label by the integers i and j. The transition probabilities from state x_i to state x_j can thus be organized in a matrix defined by

$$T_{ij} = P_T(X_t = x_i \wedge X_{t+1} = x_j) \,, \tag{2.51}$$

which satisfies $\sum_j T_{ij} = 1$ due to normalization of the probabilities. We now define the probability that the system is in the state i by π_i. Then the evolution of this probability function after a time step is simply given by

$$\pi_j(t+1) = \sum_i \pi_i(t) T_{ij} \,. \tag{2.52}$$

In the following, we consider only Markov chains that are irreducible and all of whose states are positive recurrent. Irreducible means that there is a non-zero probability to

reach every state from every other state in a finite number of steps. A positive recurrent state is defined by the property of having a finite expected return time, i.e., the average time it takes for the chain to hit the same state again is finite. If these requirements are met, the Markov chain has a unique stable (or equilibrium) distribution of the states, which satisfies

$$\pi_j^{\mathrm{eq}} = \sum_i \pi_i^{\mathrm{eq}} T_{ij} \,, \tag{2.53}$$

i.e., it is a (left) eigenvector of the matrix T. We furthermore assume now that all states of the chain are aperiodic[3], i.e., returns to each state do not have to occur in a certain period of time. The Markov chain will then converge to the equilibrium distribution for $t \to \infty$, independent of the starting distribution. Furthermore, if a distribution π fulfills the so-called detailed balance equation

$$\pi_j T_{ji} = \pi_i T_{ij} \,, \tag{2.54}$$

for all values of i and j, it also fulfills Eq. (2.53) and is therefore equal to the equilibrium distribution π^{eq}. This can easily be seen by taking the sum over i in Eq. (2.54).

A possible way to create an ensemble of random variables with an arbitrary distribution π is thus the construction of an algorithm that simulates a Markov chain with transition probabilities T_{ij} satisfying Eq. (2.54). After a sufficient number of time steps, the algorithm will then produce random variables with the desired distribution. A simple example of such an algorithm similar to the Metropolis algorithm [32] is presented in the following.

The algorithm generates a series of realizations of the real random variables $A_1, \ldots, A_D$ with the distribution P defined in Eq. (2.48). In principle, the configuration space of the random variables is now of infinite size, unlike in our considerations above. However, in real simulations it is still finite because of the limited memory of the computer, so the statements we have made are still valid. The update procedure is defined as follows. We denote the current state of the Markov chain by a with the corresponding realizations of the random variables $a_1, \ldots, a_D$. To obtain the next state a', independent Gaussian random numbers g_k $(k = 1, \ldots, D)$ with mean zero and variance v (which has to be chosen according to the specific distribution P) are added, i.e.,

$$a_k(t+1) = a_k(t) + g_k \,. \tag{2.55}$$

[3]If all states of a Markov chain are aperiodic and positive recurrent, the chain is also called ergodic.

The new realization is accepted with the probability

$$A[a \to a'] = \min\left\{1, \frac{P[a']}{P[a]}\right\}, \tag{2.56}$$

where we defined $P[a] = P(a_1, \ldots, a_D)$ to compactify the notation. If the realization is not accepted, the old one is kept meaning $a'_k = a_k$. The total probability for a transition from the realization a to a' is therefore

$$P_T[a \to a'] \sim A[a \to a'] \prod_{k=1}^{D} e^{-\frac{1}{2}\left(\frac{a'_k - a_k}{v}\right)^2}. \tag{2.57}$$

It is easily verified that this transition probability and the distribution P fulfill the detailed balance equation

$$P[a]P_T[a \to a'] = P[a']P_T[a' \to a], \tag{2.58}$$

which in turn means that P is the equilibrium distribution of the Markov chain generated by the algorithm. After a sufficient number of steps, the realizations of random numbers are thus subject to the distribution P and the integral in Eq. (2.50) can be calculated numerically as described above.

2.3.2. Hybrid Monte Carlo

The method to create a new realization of random variables by adding Gaussian numbers as introduced in Sec. 2.3.1 has a lot of drawbacks. As the choice of the new realization is independent of the distribution P, a large variance v of the Gaussian numbers will result in a low acception rate. On the other hand, a small variance grants a larger acception rate but means that the configuration space of the random variables is covered very slowly.

The method of Hybrid Monte Carlo (HMC) [33] solves this problem by introducing a more sophisticated way to select a new realization of random variables. Here, a Hamiltonian dynamics with a virtual time is used to create new states, making use of the conservation of virtual energy. The update step works as follows. At first, a virtual momentum p_k is drawn from a Gaussian distribution with mean zero and variance one for each of the realizations a_k. Then the system propagates for a virtual time τ where

the motion is governed by the Hamiltonian

$$H[a,p] = \frac{1}{2}\sum_{k=1}^{D} p_k^2 + S[a]\,, \tag{2.59}$$

where S is the action from Eq. 2.46, i.e., $P \sim e^{-S}$. The equations of motion are thus

$$\frac{da_k}{d\tau} = \frac{\partial H}{\partial p_k} = p_k\,, \tag{2.60}$$

$$\frac{dp_k}{d\tau} = -\frac{\partial H}{\partial a_k} = -\frac{\partial S}{\partial a_k}\,. \tag{2.61}$$

After the time τ, the system is in a new state which we denote by a'_k and p'_k. Due to the conservation of virtual energy, the Hamiltonian does not change during the propagation, i.e.,

$$\frac{1}{2}\sum_{k=1}^{D} p_k^2 + S[a] = \frac{1}{2}\sum_{k=1}^{D} {p'_k}^2 + S[a']\,. \tag{2.62}$$

The probability for this transition to happen is given by the probability to draw the momenta p_k, which is[4]

$$P_H[a \to a'] \sim e^{-\frac{1}{2}\sum_{k=1}^{D} p_k^2}\,. \tag{2.63}$$

On the other hand, if the system is in state a', the starting momenta $-p'_k$ lead to a transition to state a after the virtual time τ due to the time-reversal properties of the Hamilton formalism. The probability for this to happen is

$$P_H[a' \to a] \sim e^{-\frac{1}{2}\sum_{k=1}^{D} {p'_k}^2} = e^{-\frac{1}{2}\sum_{k=1}^{D} p_k^2 - S(a) + S(a')}\,, \tag{2.64}$$

where we have made use of Eq. 2.62. This transition probability fulfills the detailed balance equation with $P[a]$.

In most practical applications however, the Hamiltonian motion defined in Eqs. (2.60) and (2.61) cannot be solved analytically. Rather, an algorithm like leapfrog integration [33] has to be applied to obtain a numerical solution for the Hamilton equations. In this case, the virtual motion is still reversible, but the energy is not conserved exactly any more. To take this into account, we accept the realization generated by the Hamiltonian

[4] There may be multiple possible draws of momenta that propagate to a' through different paths in phase space. In this case, one just has to take sum over those paths in the following considerations.

motion with the probability

$$A[a \to a'] = \min\left\{1, e^{H[a,p]-H[a',p']}\right\}, \tag{2.65}$$

so the total transition probability from state a to a' is

$$P_T[a' \to a] = P_H[a' \to a]A[a \to a'], \tag{2.66}$$

which again satisfies detailed balance with $P[a]$. The advantage of the HMC algorithm compared to the Metropolis algorithm discussed above is that it is possible to achieve very high acceptance rates while the configuration space is covered with large steps. This can be done by putting much numerical effort into the Hamiltonian motion in order to minimize the violation of virtual energy. Then, the acceptance probability in Eq. (2.65) is close to 1.

2.4. Random matrix theory

2.4.1. Generalities

Random matrix theory is a mathematical tool that is very successfully used to describe certain statistical properties of various complex systems. A good introduction to RMT is given in the book of Mehta [34], broad overviews can furthermore be found in Refs. [35, 36]. The success of RMT is based on its universality, i.e., many different physical or mathematical models can be described by a few ensembles from RMT. There are three classical Gaussian ensembles which are most commonly used, the Gaussian Orthogonal Ensemble (GOE) consisting of real symmetric matrices, the Gaussian Unitary Ensemble (GUE) consisting of complex Hermitian matrices and the Gaussian Symplectic Ensemble (GSE) consisting of real quaternionic Hermitian matrices. The applicability of those to a given sufficiently complex system described by a Hermitian matrix H is classified by the anti-unitary symmetries of the system. Such a symmetry implies that H commutes with an anti-unitary operator V, which can be written as

$$V = O\,K, \tag{2.67}$$

where O is a unitary operator and K is the complex conjugation operator. We consider only anti-unitary operators which obey $V^2 = \pm 1$, i.e., $OO^* = \pm 1$. In the first case $V^2 =$

1, one can construct a basis[5] in which H is real which makes the GOE its counterpart from random matrix theory. If there is no anti-unitary symmetry, H is complex and described by the GUE, whereas for $V^2 = -1$, H can be made quaternionic real in a suitable basis and is thus described by the GSE. In the latter case, all eigenvalues are doubly degenerate and the dimension of the matrix has to be even. The Gaussian ensembles share the same probability density of the matrix elements, which reads up to normalization for the $N \times N$ ($2N \times 2N$ for GSE) random matrix H

$$P(H) = e^{-\frac{1}{2}\mathrm{tr}HH^\dagger}\,. \tag{2.68}$$

Actually, the original definition of the Gaussian ensembles in [34] is slightly more general, but all interesting quantities that involve eigenvalue correlations are maintained by our definition. With this choice, all the matrix elements of H are, up to constraints resulting from hermiticity, independently Gaussian distributed and the probability measure

$$d\mu(H) = P(H)dH \tag{2.69}$$

is invariant under orthogonal (GOE), unitary (GUE) or symplectic (GSE) transformations of H. The joint probability density function (jpdf) of the eigenvalues $\theta_1, \ldots, \theta_N$ is obtained by integrating out the degrees of freedom associated with the eigenbasis of the random matrix, resulting up to normalization in

$$P(\theta_1, \ldots, \theta_N) = |\Delta(\theta_1, \ldots, \theta_N)|^\beta\, e^{-\frac{1}{2}\sum_{i=1}^N \theta_i^2}\,, \tag{2.70}$$

with the Dyson index $\beta = 1$ (GOE), $\beta = 2$ (GUE), $\beta = 4$ (GSE) and the Vandermonde determinant

$$\Delta(\theta_1, \ldots, \theta_N) = \prod_{i<j=1}^{N} (\theta_i - \theta_j)\,. \tag{2.71}$$

The Vandermonde determinant is responsible for the repulsion of eigenvalues, because is suppresses the probability to find eigenvalues which are very close to each other. From the jpdf of the eigenvalues, all correlations between eigenvalues can be derived [34].

[5] Note that this basis depends only on O, but not on H. The same is true for the basis in which the GSE becomes quaternionic real.

2.4.2. Non-Hermitian Gaussian ensembles

Other Gaussian ensembles can be obtained by dropping the constraint of hermiticity and thus allowing for complex eigenvalues. These ensembles have first been introduced by Ginibre [37], and can be classified by their anti-unitary symmetries like the Hermitian ones, again resulting in real, complex or quaternionic real matrices. The probability density of the matrix elements is again given by Eq. 2.68, but now all the elements are independent. However, the jpdf of the eigenvalues differs strongly for these ensembles. For arbitrary complex $N \times N$ matrices ($\beta = 2$), it reads up to normalization [37]

$$P(z_1, \ldots, z_N) = |\Delta(z_1, \ldots, z_N)|^2 \, e^{-\frac{1}{2}\sum_{l=1}^{N} |z_l|^2} \,, \tag{2.72}$$

where $z_1, \ldots, z_N$ are the complex eigenvalues of the random matrix. For real quaternionic $2N \times 2N$ matrices ($\beta = 4$), the jpdf of the eigenvalues is up to normalization [37]

$$P(z_1, \ldots, z_N) = \prod_{k=1}^{N} |z_k - z_k^*|^2 \prod_{i<j=1}^{N} \left(|z_i - z_j|^2 |z_i - z_j^*|^2\right) e^{-\frac{1}{2}\sum_{i=1}^{N} |z_i|^2} \,, \tag{2.73}$$

where the eigenvalues come in complex conjugate pairs. For real matrices, the eigenvalues are either real or come in complex conjugate pairs. In this case, the jpdf of the eigenvalues is more involved and has to be classified with respect to the number of complex eigenvalue pairs denoted by ν. It reads up to normalization [38]

$$\begin{aligned} P(\theta_1, \ldots, \theta_{N-2\nu}, z_1, \ldots, z_\nu) = {} & |\Delta(\theta_1, \ldots, \theta_{N-2\nu}, z_1, z_1^*, \ldots, z_\nu, z_\nu^*)| \\ & \times \prod_{k=1}^{\nu} \operatorname{erfc}(\sqrt{2}\,\mathfrak{Im} z_k) e^{-\frac{1}{2}\sum_{i=1}^{N-2\nu} \theta_i^2} e^{-\frac{1}{2}\sum_{i=1}^{\nu} \left[(\mathfrak{Re} z_i)^2 - (\mathfrak{Im} z_i)^2\right]} \,, \end{aligned} \tag{2.74}$$

with the real eigenvalues $\theta_1, \ldots, \theta_{N-2\nu}$ and complex eigenvalues $z_1^{(*)}, \ldots, z_\nu^{(*)}$.

2.4.3. Unfolding

The correlations in the eigenvalue spectrum of a large variety of chaotic systems can be described by random matrix theory. These correlations are consequently called universal quantities, as they are the same in many different systems. In contrast, the eigenvalue density is not such a universal quantity. Therefore, a method called 'unfolding' [39] has to be applied to disentangle spectral correlations from the average density and thus local from global eigenvalue fluctuations. There are a lot of ways to do this, and one of the simplest is to sort all eigenvalues and replace them by their index in the sorted list [40].

However, this works only if a large number of matrices with independent spectra from the same ensemble is available. Otherwise, one can obtain a smoothed spectral density by application of an appropriate filter and use this density to normalize the local scale of eigenvalue distances. A method to unfold general complex spectra, i.e. spectra with two degrees of freedom, is introduced in Ref. [41].

2.4.4. The next-neighbor spacing distribution

The next-neighbor spacing distribution is a universal quantity which is well suited to describe the short range correlations of a spectrum and is easily accessible numerically. It is defined as the probability distribution of finding two neighboring eigenvalues at a certain distance.[6] The unfolded spacing distributions of the three Gaussian ensembles in the limit of infinite matrix size are very well approximated by the spacing distributions of 2×2 matrices (4×4 for the GSE) of the respective ensemble. This fact has first been pointed out by Wigner [42] for the GOE and is therefore called 'Wigner's surmise'. The spacing distributions of the 2×2 (4×4) matrices read

$$P_\beta(s) = c_\beta s^\beta e^{-d_\beta s^2} \,, \tag{2.75}$$

where β is the Dyson index of the respective ensemble. The constants

$$c_\beta = 2\,\frac{\Gamma^{1+\beta}(1+\frac{\beta}{2})}{\Gamma^{2+\beta}(\frac{1+\beta}{2})} \text{ , and} \qquad d_\beta = \frac{\Gamma^2(1+\frac{\beta}{2})}{\Gamma^2(\frac{1+\beta}{2})} \,, \tag{2.76}$$

with the gamma function Γ ensure the proper normalization, i.e.,

$$\int_0^\infty ds\, P_\beta(s) = \int_0^\infty ds\, s P_\beta(s) = 1 \,. \tag{2.77}$$

This normalization of spacing distributions is a usual convention which we will use throughout this work.

While the Gaussian ensembles from RMT describe the spectral correlations of sufficiently chaotic systems, integrable systems typically have uncorrelated eigenvalues. The unfolded spacing distribution of the latter is a Poissonian distribution given by

$$P_0(s) = e^{-s} \,, \tag{2.78}$$

which is why random matrix ensembles with uncorrelated eigenvalues are usually denoted

[6] Note that for general complex spectra, the notion of next neighbor is not uniquely defined.

as 'Poissonian' ensembles.

2.4.5. Chiral random matrix theory

Many spectral properties of the lattice QCD Dirac operator are described by a branch of random matrix theory called chiral RMT with great success, as reviewed in Ref. [43]. A specific example of such a property is the distribution of the lowest eigenvalue of the Dirac operator, which has been found to coincide with chiral RMT in lattice simulations [40, 44]. For a certain finite-volume regime called the ε-regime, one can even establish an analytical relation between the QCD Dirac spectrum below a certain energy and chiral RMT [45]. Here, the spontaneous breaking of chiral symmetry, which gives rise to a chiral condensate, plays a crucial role.

3. Analysis of quark spectra on the lattice with two-color QCD

Many important properties of QCD are encoded in the spectrum of the Dirac operator. For example, the Banks-Casher relation [46] relates the eigenvalue density of the Dirac operator at zero to the chiral condensate, which in turn is an order parameter for the chiral phase transition. Furthermore, exact zero modes of the Dirac operator are sensitive to the topological charge of the underlying gauge fields. A powerful tool to describe spectral properties of generic complex systems is random matrix theory. As stated in Sec. 2.4.5, the appropriate random matrix counterparts of the QCD Dirac operator are the ensembles from chiral RMT. However, at larger energies the correlations of Dirac eigenvalues can be described by the standard Gaussian RMT ensembles [47, 48], and chiral symmetry is no longer important. In fact, the unfolded eigenvalue correlations in the bulk of the spectrum of chiral RMT can be shown to coincide with the correlations of the respective Gaussian ensembles [49–51].

The conventional Gaussian and chiral ensembles from RMT describe chaotic systems with a certain anti-unitary symmetry. In actual physical systems however, one may often find only approximate symmetries or compositions of parts with different symmetries. A simple ansatz to mimic such systems by RMT is to take the sum of two different ensembles, i.e., to consider a random matrix

$$H = H_1 + \lambda H_2 \,, \tag{3.1}$$

where H_1 and H_2 are taken from different ensembles of RMT and λ denotes the strength of the coupling between the two. For the Gaussian ensembles, most of the transitions of this form have already been considered in [34]. While the jpdf of the eigenvalues and even the correlation functions of these composite ensembles are in many cases feasible analytically, this does not hold for the spacing distribution. However, the latter is often very well approximated by the spacing distribution of small (2×2 or 4×4) composite random matrices of the form given in Eq. (3.1), which can be calculated analytically.

This 'generalized Wigner surmise' has firstly been found in Ref. [52]. In Ref. [53], the surmise has been shown for all possible transitions between the three Gaussian and the Poissonian ensemble, when the mixed system is the mentioned form. The latter reference in essentially a compact version of the diploma thesis of the author.

In the following, we consider the spectral properties of the lattice QCD Dirac operator with $SU(2)$ gauge links at either non-zero temperature (in Sec. 3.1) or chemical potential (in Sec. 3.2). In both cases, pure RMT may not be applicable and a composite ansatz becomes necessary. At high temperature, integrable and chaotic behavior has been found in different spectral regions of the Dirac operator, as detailed below. A chemical potential μ, on the other hand, breaks the hermiticity of the Dirac operator, which leads to a gradual change of its spectral properties as μ is increased. We also consider the case of an imaginary chemical potential, where the anti-unitary symmetry of the Dirac operator is broken.

3.1. Quark spectra at high temperature

The contents of this Section have been published in Ref. [54].

Lattice simulations of QCD have shown that the smallest eigenvalues of the Dirac operator near or above the critical temperature of the chiral phase transition are not described by chiral RMT very well [55, 56]. Instead, a tendency towards Poissonian behavior of these small eigenvalues has been found close to the critical temperature [57]. Recent studies have clearly revealed a transition from Poisson to RMT-like spectral statistics in the low end of the Dirac spectrum well above the critical temperature. This has been found for both the overlap [58] and the staggered discretization [59] in quenched two-color QCD. It has furthermore been observed there that the corresponding eigenmodes are very localized in the Poissonian regime and delocalize as the RMT regime is entered. Here, the physical size of the localized uncorrelated low lying modes is independent of the resolution and the physical volume of the lattice. However, the number of those low modes is proportional to the volume. This strongly suggests that these phenomena are no lattice artifacts but rather physical. Findings of the same effects in dynamical three-color lattice simulations [60], i.e., a much more realistic setting, back this assumption.

The mentioned localization of low eigenmodes is similar to Anderson localization in disordered media [61], which is linked to a strongly fluctuating underlying potential. We show that in two-color lattice QCD at high temperature, the local traced Polyakov loop plays the role of this potential. We firstly observe a correlation between low lying eigenmodes of the staggered and the overlap Dirac operator on the same gauge configurations. This hints at a connection of the modes to the gauge background. Note that similarities between the small eigenvalues of these two operators have previously been found in the Schwinger model [62] and also in QCD [63]. Returning to the low modes, we find that indeed those of both operators are correlated to structures in the gauge fields, namely Polyakov loops. More precisely, these modes are attracted by local Polyakov loops that are smaller than the average loop. Similar localization effects have already been observed in [64] for the gauge-covariant Laplace operator, which has been a main inspiration for our studies. We are unable to connect the localized modes to fundamental topological objects like magnetic monopoles, but composite objects like molecules of dyons could be an explanation [54]. While our findings rely on quenched lattice simulations with $SU(2)$ gauge links, we strongly believe that the observed phenomena persist in more realistic gauge theories.

The average traced Polyakov loop is an order parameter for the phase transition

between the confined and the deconfined sector of QCD, which approaches 1 as the temperature increases[1]. On the other hand, the local Polyakov loop is a strongly fluctuating quantity that may also take values close to -1. Such small loops can locally compensate for the anti-periodic boundary condition of the fermions in the temporal direction. This leads to a small local Matsubara frequency and thus favors small Dirac eigenvalues. These considerations are backed by the existence of a non-zero chiral condensate in configurations where the average Polyakov loop is close to center elements that are not the identity [65–72]. This means that the eigenvalue density at zero is non-zero and very small eigenvalues are present, which is also necessary for the breaking of center symmetry [73].

The Polyakov loops obtained from our high temperature lattice simulations are hardly correlated and thus a possible cause of the Poissonian tail of the Dirac spectrum. Indeed, in a certain basis the staggered Dirac operator takes a similar form like a Hamiltonian in condensed matter physics, i.e. three dimensional next-neighbor hopping terms plus an on-site potential. The latter is essentially a function of the local traced Polyakov loops, which on the lattice are defined by

$$L(\vec{x}) = \frac{1}{2}\,\mathrm{tr}\prod_{x_4=1}^{n_t} U_4(x_4,\vec{x})\,, \tag{3.2}$$

where n_t denotes the number of lattice points in the time direction. We construct a chiral random matrix model of the same form like the staggered operator in the mentioned basis, yet with uncorrelated matrix entries. We show numerically, that this model reproduces a spectral gap at zero, a Poisson-RMT transition and localized low modes. We consider these very important features of the Dirac operator at high temperature.

The outline of this Section is as follows. We describe the spectra and low eigenmodes of both staggered and overlap Dirac operator at high temperature and compare them in Sec. 3.1.1. In Sec. 3.1.2, we establish a connection between the lowest eigenmodes of the Dirac operators and local Polyakov loops and interpret this finding in Sec. 3.1.3. We introduce a random matrix model for the staggered Dirac operator and explore its properties in Sec. 3.1.4.

[1] In quenched lattice simulations, the sector of negative average loop has to be discarded by hand, because it is not suppressed by the fermion determinant as in the dynamical case.

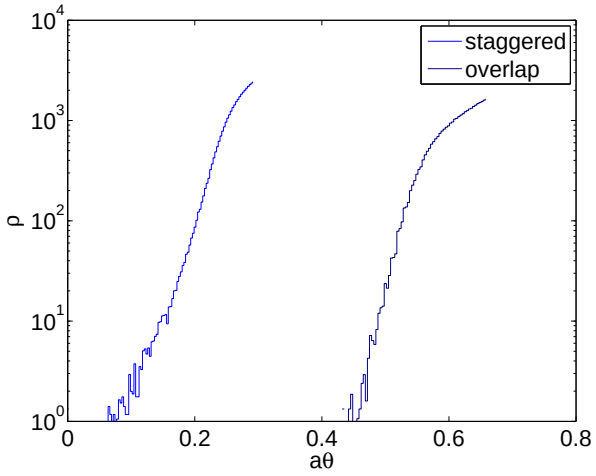

Figure 3.1.: The spectral density along the imaginary axis for the staggered (at smaller θ) and the overlap Dirac operator from the lowest 256 eigenvalues.

3.1.1. Comparison between the staggered and overlap operator

We explore quenched $SU(2)$ lattice configurations that have been generated by T. G. Kovács with the Wilson gauge action on a $24^3 \cdot 4$ lattice ($n_t = 4$) of spacing a with $\beta = 2.6$. This corresponds to a temperature of $T = 2.6\,T_c$, i.e., well above the critical temperature of the chiral phase transition T_c. Furthermore, the average traced Polyakov loop is $\langle L \rangle = 0.37$, so the system is in the deconfined phase.

We consider the staggered and the overlap (with parameter $s = 0.4$ cf. [58]) Dirac operator at zero quark mass. For both operators, the 256 lowest eigenvalues with positive imaginary parts[2] have been measured on a number of 1136 configurations for the overlap and 3149 for the staggered. For a set of 1102 configurations, also the 12 resp. lowest eigenmodes (normalized to 1) of both staggered and overlap operator have been computed. All of these numerical calculations have also been done by T. G. Kovács.

The eigenvalue densities of both operators as a function of the imaginary part of the eigenvalues in lattice units, denoted by $a\theta$, are plotted in Fig. 3.1. For the overlap operator, the eigenvalues were projected onto the imaginary axis by setting their real part to zero, before the density has been calculated. We observe a gap around $a\theta = 0$, with the eigenvalue density starting to rise from zero considerably at $a\theta \approx 0.15$ (staggered) and $a\theta \approx 0.5$ (overlap). The overlap operator also possesses exact zero modes, which have been used in order to determine the topological charge of the configurations.

To show the transition from Poissonian to RMT behavior in the Dirac spectra, we

[2]The non-zero eigenvalues come in pairs of opposite imaginary part due to chiral symmetry, but we restrict ourselves to the half with positive imaginary part.

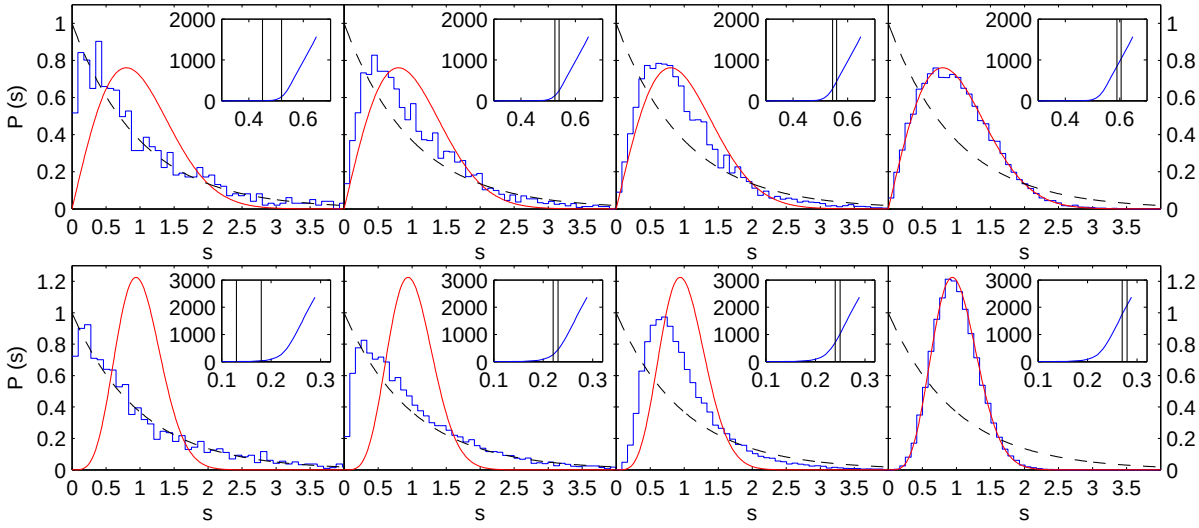

Figure 3.2.: The histograms show the spacing distributions of the overlap (top) and staggered (bottom) spectrum in spectral windows indicated by the insets showing the spectral density (cf. Fig. 3.1). The pure RMT predictions (solid) and the Poissonian distribution (dashed) are plotted for comparison.

have measured the unfolded[3] spacing distribution $P(s)$, which is very sensitive to the eigenvalue correlations, in different windows in the spectra. For $SU(2)$ gauge links, the appropriate RMT ensembles are the GOE for the overlap operator (see Sec. 3.2.5.1.2 below, where this is discussed for arbitrary chemical potential) and the GSE for the staggered operator (see e.g. Refs. [74, 75]). These ensembles differ strongly in the repulsion strength of nearby eigenvalues, which results in a linear (GOE) and quartic (GSE) behavior of their spacing distribution $P(s)$ near $s = 0$. The approximations we use for these spacing distributions are the surmises explicitly given in Eq. (2.75). For uncorrelated eigenvalues, which do not repel each other, a Poissonian spacing distribution is expected, i.e., $P(s) = e^{-s}$.

It is shown in Fig. 3.2, that the spacing distribution of both the overlap and the staggered operator is almost Poissonian at the low end of the spectrum. The distribution undergoes a transition to RMT behavior as the spectral window is shifted towards the bulk. Note that for the staggered operator, this is a mere reproduction of the findings in Ref. [59].

In the following, we are mainly interested in the low end of the spectrum. Before considering the eigenmodes, we remark that for every exact overlap zero eigenvalue we find an exceptionally small staggered eigenvalue. In the topological sector $|Q| = 0$, the average smallest staggered eigenvalue is 0.175, while for $|Q| = 1$ it is 0.109. This can

[3]We unfolded by means of a sorted list, as described in Ref. [40]

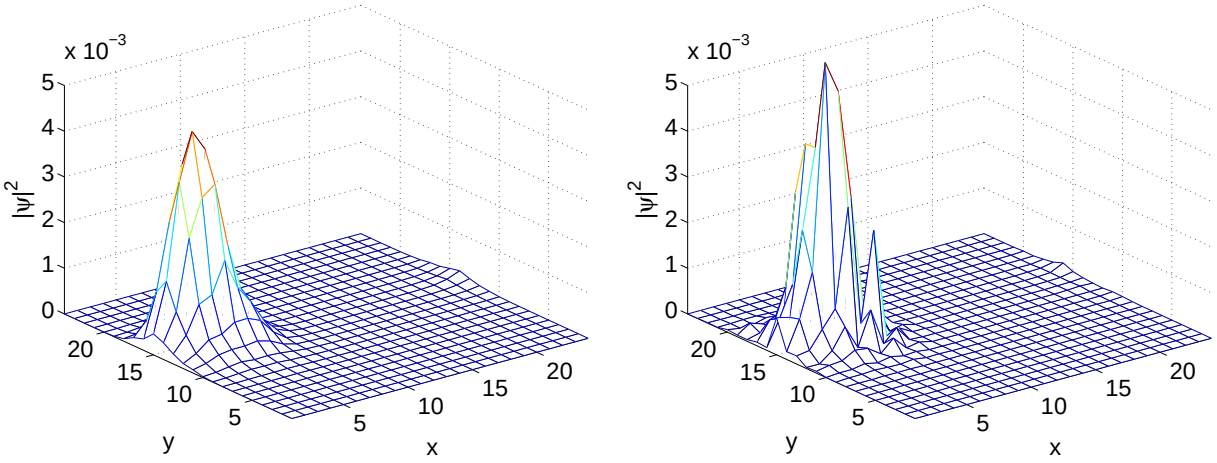

Figure 3.3.: The profile, as defined in Eq. (3.3), of the lowest overlap mode (left) and matched (see text) staggered mode (right) in a certain x-y-plane for a gauge configuration with $|Q| = 0$. The remaining spatial and the time coordinate are fixed to values in which the overlap mode takes on its maximum.

also be read off from Fig. 3.6 (right).

We want to check whether there is a correlation between the low modes of the staggered operator and those of the overlap operator on the same resp. gauge configurations. To this end, we compare the profiles of these low modes to find out if they are placed at the same locations. We define the profile of an eigenmode ψ by

$$|\psi(x)|^2 = \sum_b |\psi_b(x)|^2 \,, \tag{3.3}$$

where the index b denotes gauge – and in the case of overlap also spinor – degrees of freedom.

A first example of similar staggered and overlap low modes is visualized by the two-dimensional profiles in Fig. 3.3. For an actual quantification of the correlation and localization of two modes, we introduce the following 'interlocalization'

$$I = n \sum_x \left|\psi^{\mathrm{ov}}_{(m)}(x)\right|^2 \left|\psi^{\mathrm{st}}_{(l)}(x)\right|^2 \,, \tag{3.4}$$

where n is the total number of lattice sites, and $|\psi^{\mathrm{ov,st}}_{(m)}(x)|^2$ is the profile of the mth overlap/staggered eigenmode[4].

This positive quantity is large when both modes are similar *and* localized and becomes their inverse participation ratio (IPR) when the modes coincide exactly. The IPR is a

[4]This means that the mode belongs to the mth-smallest eigenvalue of the resp. operator.

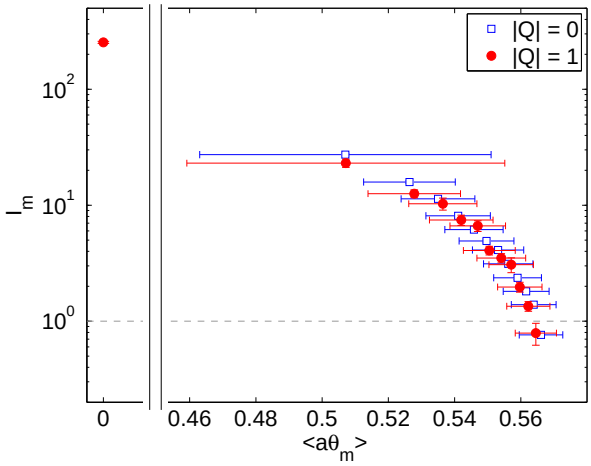

Figure 3.4.: The interlocalization I_m defined in Eq. (3.4), for matched modes (see text) as a function of the averaged overlap eigenvalue (in lattice units) $\langle a\theta_m \rangle$. The horizontal error bars show the standard deviation of the eigenvalues, obtained by the ensemble average, instead of the errors. The maximal possible value for I on our lattice is $24^3 \cdot 4 \approx 5.5 \cdot 10^4$, while delocalized modes yield $I \approx 1$, indicated by the dashed gray line.

prominent measure for localization, defined by

$$R = n \sum_x |\psi(x)|^4 \,, \tag{3.5}$$

for the eigenmode ψ. It takes a maximum value of n for a mode that is localized on a single lattice point and a minimum value of 1 for a mode that is constant in the whole volume. A reference value for the interlocalization of uncorrelated modes is set by two normalized modes with independent random Gaussian amplitudes (of mean zero) at each site, which is at the order of $I \approx 1$.

We match overlap and staggered modes using the interlocalization in the following way. We take the lowest overlap mode and pair it with the staggered mode which has the largest value of I with it. Then we do the same with the second lowest overlap mode, but consider only staggered modes that have not been paired yet. This procedure is continued until all available overlap modes have been assigned to a staggered mode. In this way, we obtain an interlocalization for each overlap mode $\psi^{\mathrm{ov}}_{(m)}$ (with the resp. paired staggered mode), which we denote by I_m. We plot these interlocalizations averaged over the gauge configurations as a function of the average overlap eigenvalue (in lattice units) $\langle a\theta_m \rangle$ of the corresponding mode in Fig. 3.4. We observe that the exact zero modes of the overlap operator are almost perfectly matched by a corresponding staggered mode.

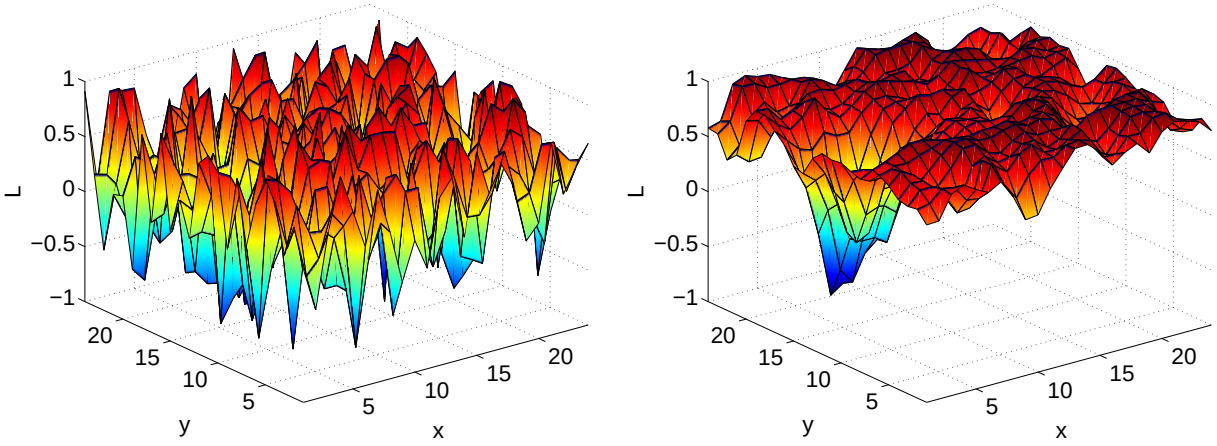

Figure 3.5.: Unsmeared (left) and smeared (right) traced Polyakov loops of the same configuration and in the same x-y-plane as in Fig. 3.3. While nothing seems particular in this plane for the unsmeared case, the smeared Polyakov loop takes its minimum of -0.70 (the average smeared Polyakov loop is 0.81 for this configuration) at the maximum of the fermion modes in Fig. 3.3.

Actually, the value of $I \approx 300$ is very close to the IPR of the these overlap zero modes[5], which indicates that these modes are close to identical. Also for the topological sector $|Q| = 0$, the lowest overlap modes have a quite large interlocalization with the respective staggered modes. Going up in the spectrum, the interlocalization quickly drops and after a few modes reaches the reference value of 1 discussed above.

3.1.2. Connection between eigenmodes and Polyakov loops

A natural explanation for the correlation between the low eigenmodes of the staggered and the overlap operator shown above is that both operators are sensitive to the gauge background in a similar way. In the following, we show that there is indeed a connection between the local Polyakov loops and the low eigenmodes of both operators.

As a first example for this phenomenon, we depict in Fig. 3.5 the traced Polyakov loops of the same configuration as used in Fig. 3.3, restricted to the same x-y-plane. As the Polyakov loop is dominated by ultraviolet fluctuations on the scale of the lattice spacing, it is impossible to observe any coarse structure by the naked eye. We therefore applied 6 steps of APE smearing [77] with $\epsilon = 0.2$ to the gauge configuration to smoothen the Polyakov loops. In this case, a valley of negative loops develops at the location where the lowest overlap mode has its maximum. We stress that this is the only occasion in which we consider a smeared quantity, in order to show an exemplary visualization of

[5]The corresponding staggered modes have a slightly larger IPR of about 400, which is presumably because the staggered operator is ultra-local in contrast to the overlap operator.

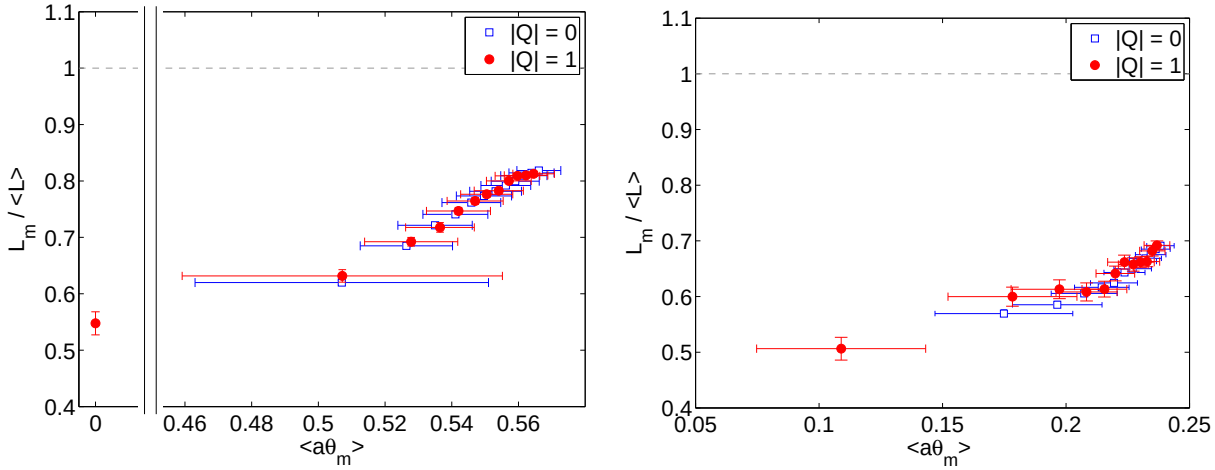

Figure 3.6.: The ratio of Polyakov loops weighted by low-lying modes L_m given in Eq. (3.6), to the average Polyakov loop of the resp. configuration for overlap (left) and staggered modes (right). These are plotted as a function of the resp. averaged eigenvalues (in lattice units) $\langle a\theta_m \rangle$, where the horizontal error bars show the standard deviation instead of the errors..

our findings. We consider unsmeared gauge configurations for the rest of this work.

To measure the correlation between Polyakov loops and low Dirac eigenmodes, we define the quantity

$$L_m = \sum_{\vec{x}} |\psi_{(m)}(\vec{x})|^2 L(\vec{x}) \,, \tag{3.6}$$

which is the local Polyakov loop weighted by the *spatial* profile of the Dirac mode $|\psi_{(m)}(\vec{x})|^2$. The spatial profile of a mode is defined like the profile introduced in Eq. (3.3), with an additional sum over the time variable. L_m is restricted to the range of the Polyakov loop, i.e. the interval $(-1, 1)$. A plane wave-like mode $\psi_{(m)}$ yields an L_m of the average Polyakov loop, while a localized mode mainly picks up the loop at the position of that mode.

We show the ratio of L_m to the average Polyakov loop of the resp. gauge configuration for the low-lying staggered and overlap modes in Fig. 3.6. These data have been obtained by taking the average over all the gauge configurations available. As can be seen, the Polyakov loop that is picked up by the low-lying Dirac modes is considerably smaller than the average loop. This tendency vanishes for the higher modes.

Another way to show the connection between low Dirac modes and local Polyakov loops is to consider the 'Polyakov loop distribution as seen by a mode'. To this end, we weight the probability density of the local Polyakov loops with the spatial profile of the

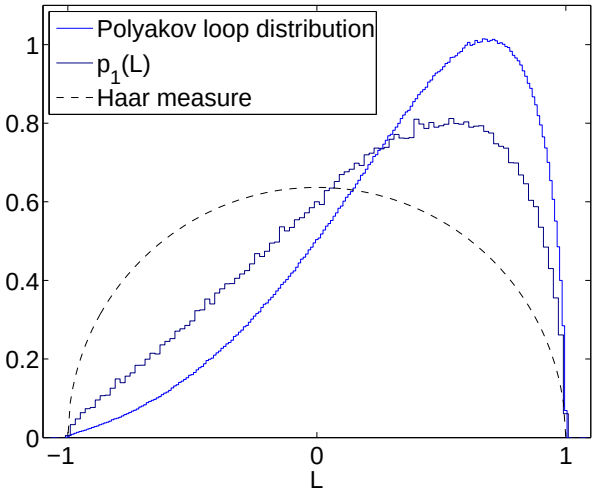

Figure 3.7.: The original Polyakov loop distribution (the curve with the larger maximum) compared to the 'Polyakov loop distribution as seen by the lowest overlap mode' $p_1(L)$, given in Eq. (3.7), in the topological sector with $|Q| = 0$. We also show the Haar measure, which is valid in the low temperature phase.

low Dirac eigenmodes by defining

$$p_m(L) = \sum_{\vec{x}} \delta\left[L - L(\vec{x})\right] |\, \psi_{(m)}(\vec{x})|^2 \,. \tag{3.7}$$

For constant modes, this reduces to the distribution of the local Polyakov loops. Taking the L-expectation value, we can obtain from $p_m(L)$ the quantity L_m, i.e.,

$$L_m = \int dL\, p_m(L)\, L \,. \tag{3.8}$$

This shows how the global quantity L_m is generated by a local deformation of the distribution of the Polyakov loops.

We show this probability distribution in Fig. 3.7 for the lowest mode of the overlap operator averaged aver all configurations in the $Q = 0$ sector. The distribution is clearly deformed towards $L = -1$, which confirms again that low Dirac eigenmodes see a smaller local Polyakov loop.

3.1.3. Interpretation

The effect of the Polyakov loops on the quark spectra can be easily understood in a gauge background with spatial links set to unity and time-like links U_4 that are constant in space and time. By a certain gauge transformation, all the time-like links except the

one on the last time-slice at each spatial site, can also be set to unity. Furthermore, the gauge transformation can be chosen such that all the links are diagonalized. The Polyakov loop is then the diagonal version of $(U_4)^{n_t}$ and reads

$$\exp\left[i\varphi\begin{pmatrix}1 & 0\\ 0 & -1\end{pmatrix}\right], \text{ with} \quad \varphi \in (0,\pi)\,, \tag{3.9}$$

where we introduced the phase of the Polyakov loop φ. The latter is related to the traced loop by $L = \cos\varphi$. For $\varphi = \pi$, the loop becomes $-\mathbb{1}$ and effectively cancels the anti-periodic boundary condition of the fermions. Therefore, the Polyakov loop can be seen as a modification of the boundary condition in the time direction.

A continuum Dirac operator with zero mass in an equivalent gauge background, i.e., spatial gauge fields set to zero and a Polyakov loop as above, possesses eigenmodes that are constant in space and plane waves in time. These are of the form

$$\psi(x) \sim e^{ipx_0T}\,, \text{ with} \quad p = \pi \pm \varphi + 2\pi z\,, \text{ and} \quad z \in \mathbb{Z}\,, \tag{3.10}$$

where T is the temperature and the different signs in the momentum quantum number p amount to the different color components. The eigenvalues corresponding to these modes are given by ipT. The lowest positive one is $i\theta_{\mathrm{M}}^{\mathrm{cont}}$, with

$$\theta_{\mathrm{M}}^{\mathrm{cont}} = (\pi - \varphi)T\,, \tag{3.11}$$

which we denote as effective Matsubara frequency. Returning to the lattice, where the number of time-slices is finite, these become

$$\theta_{\mathrm{M}} = \frac{1}{a}\sin\left(\frac{\pi-\varphi}{n_t}\right)\,. \tag{3.12}$$

For very high temperatures, the Polyakov loop approaches unity, so we have $L \to 1$ and $\varphi \to 0$, which yields $\theta_{\mathrm{M}} = \frac{1}{a}\sin(\pi/n_t)$. Inserting $L = 0.37$, which is the average traced loop on our the gauge configurations, we obtain a Matsubara frequency (in units of the inverse lattice spacing) of

$$a\theta_{\mathrm{M}} = \sin\left(\frac{\pi - \arccos 0.37}{4}\right) = 0.47\,. \tag{3.13}$$

This is in the same order of magnitude as the lower end of the bulk of the spectra we have measured and consistent with the findings in [78].

The main outcome of these considerations is that a Polyakov loop of $L \approx -1$ (i.e. $\phi \approx \pi$) yields a Matsubara frequency of $\theta_{\mathrm{M}} \approx 0$ and therefore a zero mode of the Dirac operator or at least a very small eigenvalue. Indeed, real gauge configurations comprise strongly fluctuating spatial and temporal links that spoil the analytical calculations above. However, the loops close to $L \approx -1$ still have the tendency to generate small Dirac eigenvalues, which could explain why they trap the corresponding modes.

3.1.4. Random matrix model for the staggered Dirac operator

There are many RMT models that can describe a transition between uncorrelated and correlated eigenvalues. One of the simplest ansätze is to take the sum of a diagonal matrix with independently distributed entries and add a matrix from one of the Gaussian ensembles times a coupling parameter. This is a specific case of the ansatz given in Eq. (3.1). As the coupling parameter is increased from zero, one then observes a transition from a Poissonian to an RMT-like spacing distribution. Furthermore, if the spectral density of the diagonal matrix is not constant, this transition proceeds faster in the parts of the spectrum where the density is larger. This has been worked out in [53], along with formulas that approximate the spacing distributions during the transitions very well. However, these distributions differ from the ones we encounter in the overlap and staggered spectrum, because the former typically show a maximum that strongly overshoots the Poisson curve. In case of the staggered operator, we assume that this is due to the sparseness of the operator, which connects only nearest neighbors in contrast to the full matrices of the Gaussian ensembles used in the additive ansatz. The overlap operator, on the other hand, is not a sparse matrix, but its matrix elements still decay with the lattice distance [79]. This distinguishes the overlap operator from the matrices of the Gaussian ensembles, too.

3.1.4.1. Motivation of the model

We construct a random matrix model that is better suited to describe the spectral properties of the staggered Dirac operator in the following. The model is based on sparse matrices and partially motivated by our findings about the Polyakov loop, which we will treat as a random potential. In Fig. 3.8, it is shown that the correlation of the local Polyakov loops drops very quickly with the lattice distance and that their unfolded spacing distribution (neglecting the spatial information) is very similar to a Poissonian distribution. Furthermore, the Polyakov loop distribution extends to negative values close to -1 (see Fig. 3.7) and thus small local effective Matsubara frequencies. Thus, it

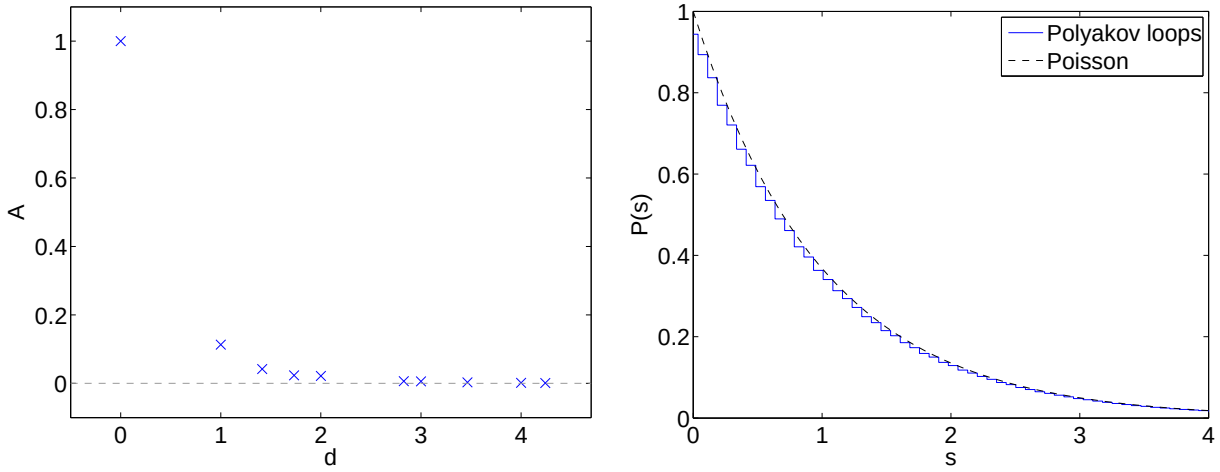

Figure 3.8.: Left: the auto-correlation of local Polyakov loops defined by $A = (\langle L(\vec{x})L(\vec{y})\rangle - \langle L(\vec{x})\rangle\langle L(\vec{y})\rangle) \,/\, (\langle L^2(\vec{x})\rangle - \langle L(\vec{x})\rangle^2)$ as a function of the distance in lattice units $d = |\vec{x} - \vec{y}|/a$. Right: the unfolded spacing distribution of the local Polyakov loop trace L compared to the Poisson distribution.

seems likely that the Polyakov loops are responsible for the Poissonian behavior in the low end of the Dirac spectrum. This becomes even more plausible by considering the staggered operator, which reads

$$D^S_{xx'} = \frac{1}{2a}\sum_{\mu=1}^{4}\eta_\mu(x)\left[\delta_{x+\hat{\mu},x'}U_\mu(x) - \delta_{x-\hat{\mu},x'}U^\dagger_\mu(x')\right] , \tag{3.14}$$

with $\eta_\mu(x) = (-1)^{\sum_{\nu<\mu} x_\nu}$ and $U_\mu(x) \in SU(2)$ in the case of two-color QCD. We can explicitly split this operator into temporal and spatial part,

$$D^S = D^{TE} + D^{SP}. \tag{3.15}$$

In this decomposition, D^{TE} contains the temporal and D^{SP} the spatial derivatives.

The temporal part is block diagonal, with one block for each spatial lattice site $\vec{x}$. These blocks can separately be diagonalized analytically, which yields two-fold degenerate eigenvalues $\pm i\gamma^{(k)}_{\vec{x}}$, with (for even n_t)

$$\gamma^{(k)}_{\vec{x}} = \frac{1}{a}\sin\left(\frac{\pi - \varphi_{\vec{x}} - 2\pi k}{n_t}\right) , \text{ where } \quad k = 0, \ldots, \frac{n_t}{2} - 1 . \tag{3.16}$$

Here, $\varphi_{\vec{x}}$ is the phase of the local Polyakov loop, i.e., $L(\vec{x}) = \cos\varphi_{\vec{x}}$. We consider only the four smallest of these eigenvalues with $k = 0$ in the following, and project to the eigenbasis that is spanned by their eigenmodes. At least four eigenvalues are needed

to maintain both the exact two-fold degeneracy[6] and the plus-minus degeneracy, which stems from chiral symmetry. In this way, the projected operator is in the same RMT universality class like the $SU(2)$ staggered operator and fulfills chiral symmetry.

In the restricted eigenbasis, the temporal operator can be cast in the form

$$D^{TE(k=0)}_{\vec{x}\vec{x}'} = i\,\delta_{\vec{x}\vec{x}'} \begin{pmatrix} -\gamma^{(0)}_{\vec{x}} & 0 & 0 & 0 \\ 0 & -\gamma^{(0)}_{\vec{x}} & 0 & 0 \\ 0 & 0 & \gamma^{(0)}_{\vec{x}} & 0 \\ 0 & 0 & 0 & \gamma^{(0)}_{\vec{x}} \end{pmatrix}, \tag{3.17}$$

where the entries are analytical functions of the local Polyakov loops. Therefore, the discussion above about the correlation of the local Polyakov loops applies also to the $\gamma^{(0)}_{\vec{x}}$. Indeed, the latter have the same unfolded spacing distribution like the Polyakov loops, which is Poissonian, as shown in Fig. 3.8 (right). Thus, the temporal part can be seen as a strongly fluctuating (chiral) on-site potential in three dimensions.

In the restricted basis, the spatial part has entries of the form

$$D^{SP(k=0)}_{\vec{x},\vec{x}+\hat{i}} = \begin{pmatrix} U_{\vec{x},\vec{x}+\hat{i}} & V_{\vec{x},\vec{x}+\hat{i}} \\ V_{\vec{x},\vec{x}+\hat{i}} & U_{\vec{x},\vec{x}+\hat{i}} \end{pmatrix}, \tag{3.18}$$

where the 2-by-2 matrices U and V represent real quaternions that are functions of the gauge links. $\hat{i}$ is a unit vector in one of the the spatial directions. Considering the spatial part of the staggered Dirac operator as a perturbation to the temporal part, these matrices can be given a concrete meaning: U connects eigenvalue pairs of equal sign, and therefore yields a GSE-like level repulsion between nearest neighbors. V on the other hand repels eigenvalues of different signs and so generates the gap around zero in the spectrum.

3.1.4.2. Construction and numerical test of the model

Based on the considerations above, we propose a random matrix model of the form

$$M = M^{TE} + M^{SP}, \tag{3.19}$$

[6] In RMT language, this is Kramers degeneracy of the GSE.

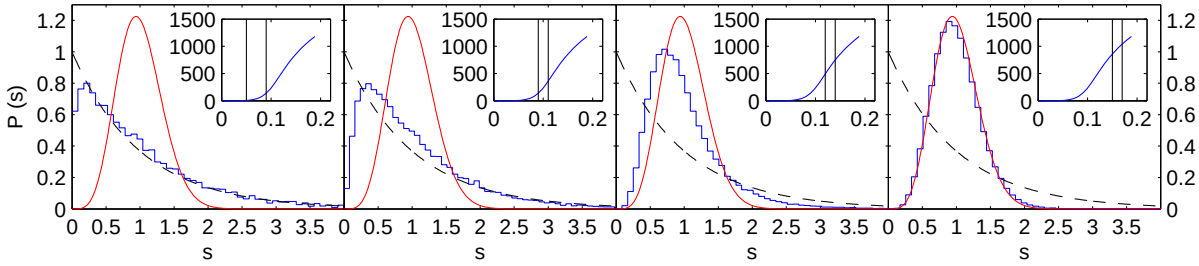

Figure 3.9.: Spacing distributions of the RMT spectrum plotted along with the GSE prediction (full curve) and the Poissonian distribution (dashed curve). The insets show the eigenvalue density as a function of the imaginary part of the eigenvalues and indicate the part of the spectrum that is measured, respectively. The data has been obtained by an ensemble average over 5 000 random matrices.

where M^{TE} has the same diagonal structure like $D^{TE(k=0)}$, i.e.,

$$M^{TE}_{\vec{x}\vec{x}'} = i\,\delta_{\vec{x}\vec{x}'} \begin{pmatrix} -\vartheta_{\vec{x}} & 0 & 0 & 0 \\ 0 & -\vartheta_{\vec{x}} & 0 & 0 \\ 0 & 0 & \vartheta_{\vec{x}} & 0 \\ 0 & 0 & 0 & \vartheta_{\vec{x}} \end{pmatrix}, \text{ with } \quad \vartheta_{\vec{x}} = T(\pi - \phi_{\vec{x}})\,. \tag{3.20}$$

The $\vartheta_{\vec{x}}$ are the local random equivalents of the effective Matsubara frequency in the continuum, see Eqs. (3.11) and (3.17). T is the temperature, which equals $1/n_t$, because we have set the lattice spacing to 1, which is just an irrelevant rescaling of the whole operator. The $\phi_{\vec{x}} \in (0, \pi)$ are random counterparts of the Polyakov loop phases. They are drawn independently from a distribution which has been obtained from lattice data by converting the histogram shown in Fig. 3.7 via $\phi_{\vec{x}} = \arccos L(\vec{x})$. This is an asymmetric distribution with a support in the interval $(0, \pi)$ and a maximum below $\pi/2$.

For the spatial part M_{SP} we still have to introduce a three-dimensional periodic lattice of some extent n_s in order to mimic the next-neighbor interaction of the staggered operator. To this end, we identify $\vec{x}$ with $\vec{x} + n_s\hat{i}$, with unit vectors $\hat{i}$ in each of the spatial directions. M^{SP}, like $D^{SP(k=0)}$, has non-vanishing entries only at positions that connect next neighbors. These entries have the form

$$M^{SP}_{\vec{x},\vec{x}+\hat{i}} = \begin{pmatrix} u_{\vec{x},\vec{x}+\hat{i}} & v_{\vec{x},\vec{x}+\hat{i}} \\ v_{\vec{x},\vec{x}+\hat{i}} & u_{\vec{x},\vec{x}+\hat{i}} \end{pmatrix}, \tag{3.21}$$

with the 2×2 random matrices u and v that are representations of real quaternions, like U and V in Eq. (3.18). The complex and real components of u and v are Gaussian distributed with mean zero and variances of σ_u^2 and σ_v^2, respectively, which are parameters

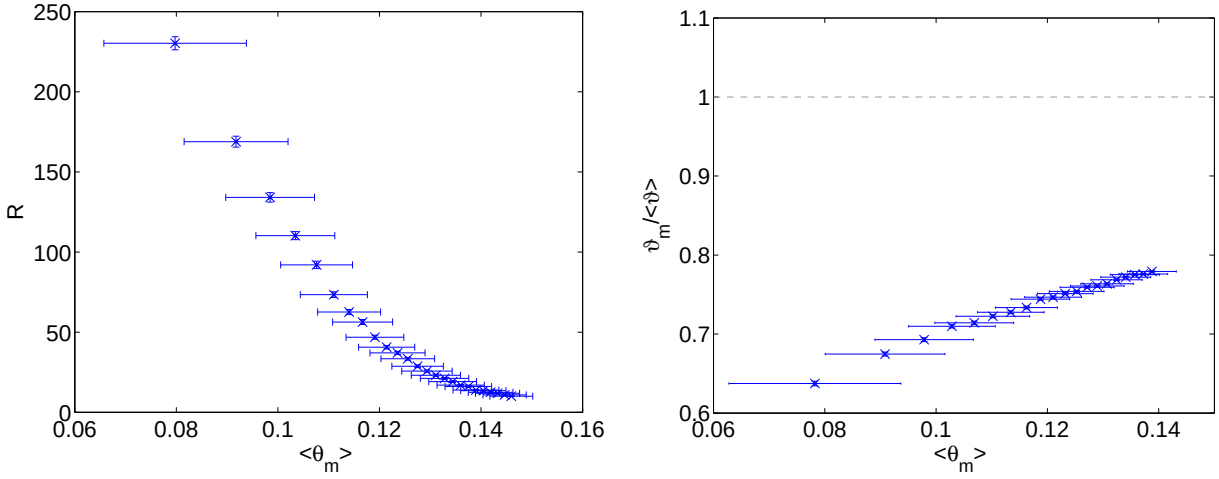

Figure 3.10.: Left: the IPR R of the eigenmodes, defined in Eq. (3.5), for the 25 smallest eigenvalues of the RMT model, plotted versus the average eigenvalue of that mode $\langle\theta_m\rangle$ (the maximum possible value for the IPR is $12^3 = 1\,728$). Right: intersection of the low eigenmodes of the RMT model with the underlying random potential as defined in Eq. (3.22), normalized by the average potential (to be compared to Fig. 3.6). The horizontal error bars show the variance of the eigenvalues rather than the numerical error in both plots. The data has been obtained by an ensemble average over 1 000 random matrices.

of the model. The approximate ratio of these variances has been obtained from lattice measurements by matching the ratio of the average determinants[7] of U (V) and u (v) which is $\langle\det U\rangle/\langle\det V\rangle \approx 1.6^2$ on our gauge configurations. The overall scale of the random numbers has been put in by hand to obtain desired properties of the RMT model, namely a gap at zero and a transition between a Poissonian and a GSE-like spacing distribution. To this end, we have chosen $\sigma_u^2 = 0.05^2$ and $\sigma_v^2 = 0.08^2$.

The eigenvalue density and spacing distribution of this model is shown in Fig. 3.9 for a lattice of spatial extent $n_s = 12$ and with $T = 1/4$. We observe a similar transition as in the spectrum of the staggered Dirac operator. Another feature that this model shares with the lattice Dirac operators is the decreasing localization of eigenmodes as the corresponding eigenvalues increase. This is shown in Fig. 3.10 along with the intersection of the modes with the underlying potential $\vartheta_{\vec{x}}$, defined equivalently to Eq. (3.6) by

$$\vartheta_m = \sum_{\vec{x}} |\Psi_{(m)}(\vec{x})|^2 \vartheta_{\vec{x}}\,. \tag{3.22}$$

Here, $\Psi_{(m)}(\vec{x})$ is the spatial profile of the eigenmode belonging to the m-th smallest

[7] For real quaternions of the form $q = c_0\mathbb{1} + i\sum_{j=1}^{3} c_j\sigma_j$, the determinant is just the sum over all squared parameters, i.e., $\det q = \sum_{\mu=0}^{3} c_\mu^2$ (σ_i are the Pauli matrices).

positive eigenmode of the random matrix M. As can be seen, the low modes have the tendency to be localized at islands of small random potential, like those of the lattice Dirac operators which are attracted by the small Polyakov loops. Hence, our model reproduces also this important effect.

To check the dependency of the random matrix model on the distribution of the Polyakov loop phase, we have studied the model with two further choices of that distribution. The first is the Haar measure $\sin^2\phi$ (valid at zero temperature), for which we have found that the model shows a similar behavior as discussed above. However, the gap in the spectral density is smaller and there are fewer Poissonian modes. The second distribution is obtained by the replacement $L \to -L$ in the Polyakov loop distribution in Fig. 3.7, which amounts to a change of the center sector. In this case, there are no Poissonian modes and the gap in the spectrum vanishes, i.e., a non-zero chiral condensate is present. This is consistent with the findings of a chiral condensate in non-physical center sectors discussed in the beginning of Sec. 3.1.

3.2. Spacing distributions of the overlap operator at non-zero density

The contents of this Section have been published in Ref. [80].

To obtain a better knowledge of the QCD phase diagram, it is crucial to study the theory not only at high temperature, but also at non-zero density. This amounts to a non-zero chemical potential. Non-perturbative techniques are again needed to get insight into non-analytical properties of the theory like phase transitions. Lattice simulations, which have been successfully used to understand the high-temperature phase of QCD, however suffer from the serious so-called sign problem at non-zero chemical potential, which is reviewed in Ref. [81]. The crux is that the chemical potential renders the fermion determinant complex. As a complex number cannot be interpreted as a probability, integration techniques based on importance sampling become very inefficient. This does not hold for quenched lattice simulations, where the fermion determinant does not enter the creation of gauge configurations. However, the quenched approximation works particularly bad at non-zero chemical potential both for lattice QCD [82] and for random matrix models of QCD [83].

In chiral random matrix ensembles, the chemical potential is mimicked by a real parameter, which controls the breaking of anti-hermiticity [83, 84]. The microscopic spectral densities and the lowest eigenvalue distributions of these models have been

calculated analytically [86, 87], and found to describe quenched QCD data very well [87, 88]. For the case of two-color QCD with chemical potential, which we consider in the following, the corresponding random matrix ensemble is the asymmetric real chiral ensemble introduced in Ref. [89]. This ensemble has been solved, i.e. the joint probability density function of the eigenvalues and the correlation functions have been computed analytically [90, 91].

The matrices of the ensembles discussed above generically have complex spectra. Thus, their eigenvalues have two degrees of freedom, and a straight-forward ordering of these eigenvalues does not exist. However, one can still define individual next-neighbors to obtain a spacing distribution. For the complex Ginibre ensemble, the spacing distribution of large matrices is not well approximated by a surmise from 2×2 matrices [92, 93], in contrast to the case of Hermitian Gaussian ensembles (see Sec. 2.4.4). However, in the case of real matrices with weakly broken hermiticity, the eigenvalues have to stay on the real axis unless they form a complex conjugate pair with another eigenvalue[8], as detailed in Sec. 3.2.1. If we consider the flow of the spectrum as the degree of the anti-hermiticity is increased, the real eigenvalues thus have only one degree of freedom, like the eigenvalues of the Hermitian Gaussian ensembles. This is our motivation to work out the spacing distributions of small real non-Hermitian random matrices. We assume that these distributions can yield an approximation for the spacing distribution of corresponding large random matrices in the spirit of Wigner's surmise. The random matrix model we consider is the real elliptic Ginibre ensemble, which has a tunable degree of non-hermiticity. Its jpdf of the eigenvalues has been derived in Ref. [38]. As discussed in the beginning of Sec. 3, chiral symmetry is irrelevant for the eigenvalue correlations in the bulk of the Dirac spectrum. Thus, the real elliptic Ginibre ensemble should reproduce the spacing distribution of the Dirac operator in two-color QCD with non-vanishing chemical potential away from the gap. This is implied by the anti-unitary symmetries of that operator (see Sec. 3.2.5.1 below).

Indeed, we find that the surmises derived for the small matrices can approximate the spectra of large random matrices very well. This holds in the case of weakly broken hermiticity, and different kinds of spacings have to be distinguished, as detailed below. These surmises also describe the spacing distributions of the overlap Dirac operator in two-color QCD at various small values of the chemical potential.

[8] This is not so for the complex (GUE, $\beta = 2$) or symplectic (GSE, $\beta = 4$) ensembles: in the former the eigenvalues are not restricted to form complex conjugate pairs, but can be distributed arbitrarily in the complex plane; in the latter the unperturbed matrices have two-fold degenerate eigenvalues due to Kramers' degeneracy and these split up and become complex conjugate pairs for arbitrary small anti-Hermitian perturbation.

This Section is organized as follows. We firstly introduce an ensemble of real random matrices with weakly broken anti-hermiticity and comment on the typical spectra of those matrices in Sec. 3.2.1. In Sec. 3.2.2, we consider by means of perturbation theory the dynamics of eigenvalues as the anti-Hermitian part is switched on. The surmises, i.e. the spacing distributions of small real random matrices with broken hermiticity, are derived in Sec. 3.2.3 for three kinds of spacings. They are applied to corresponding large random matrices in Sec. 3.2.4 and to the $SU(2)$ overlap operator with chemical potential in Sec. 3.2.5. We also briefly consider an imaginary chemical potential, in which case a different surmise applies, in Sec. 3.2.5.2.1.

3.2.1. Spectra of real random matrices

We consider a random matrix model that consists of real random matrices H and has one real parameter λ which controls the non-hermiticity of the matrices. If this parameter is zero, the matrices are taken from the GOE and thus Hermitian (and symmetric). In this case, the entries are Gaussian random numbers with mean zero and variance

$$\langle [H(\lambda=0)]_{ii}^2 \rangle = 1 \text{ , and } \quad \langle [H(\lambda=0)]_{ij}^2 \rangle = \frac{1}{2} \quad (i \neq j) \,. \tag{3.23}$$

For increasing λ, the non-hermiticity of H increases.

Real matrices have either real eigenvalues or pairs of complex conjugate eigenvalues, which is easily proven by the following consideration. Let ψ be an eigenvector of the real matrix H with the corresponding eigenvalue θ, i.e., $H\psi = \theta\psi$. By complex conjugation, we obtain $\theta^*\psi^* = H^*\psi^* = H\psi^*$, so θ^* is also an eigenvalue of H, with the eigenvector ψ^*. We denote real eigenvalues as 'on-axis' and eigenvalues with non-zero imaginary part as 'off-axis' in the following. We use this notation also for Dirac operator eigenvalues, with the only difference that the axis are swapped due to the anti-hermiticity of that operator at zero chemical potential (then on-axis refers to purely imaginary eigenvalues and off-axis to those with a non-zero real part).

We show a part of the typical spectrum of H with different magnitudes of the hermiticity-breaking part λ in Fig. 3.11. We treat off-axis spacings, i.e., the spacing between a complex conjugate pair, and on-axis spacings separately. Between the latter, we further distinguish between on-axis spacings with an interspaced complex pair (this means that the real part of the pair is inside the spacing) and those without. This is done because we found that the spacing distributions of these different kinds of spacings differ strongly, so it makes no sense to combine them all in one distribution. We

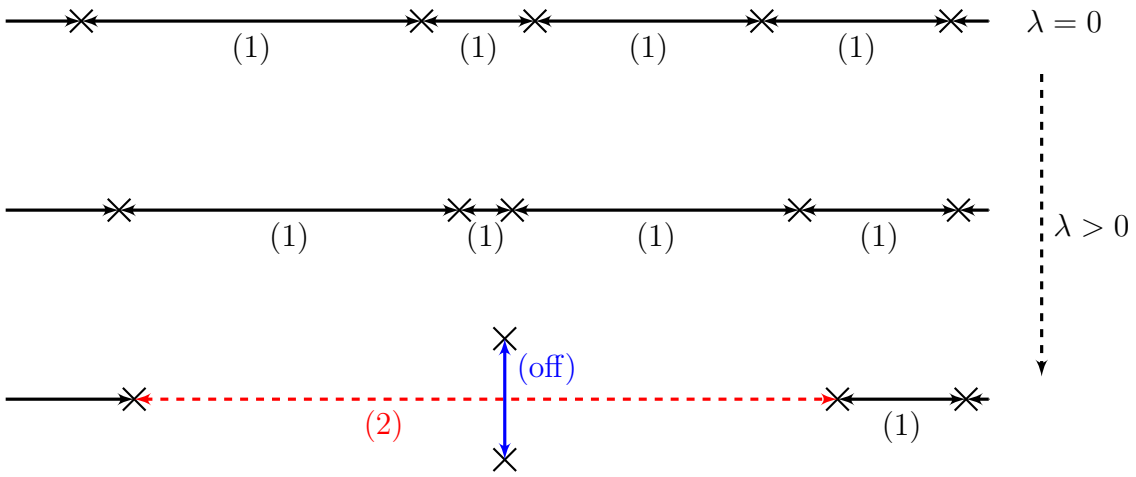

Figure 3.11.: A part of the spectrum of a typical random matrix H with increasing non-Hermitian perturbation, where the crosses mark the eigenvalues. The top panel is the unperturbed case, i.e. a real symmetric matrix from the GOE. Towards the bottom panel the antisymmetric part increases, which results in some eigenvalues forming complex conjugate pairs. Different types of level spacings are sketched: (1) spacings between eigenvalues that are on the real axis and have no interspaced complex conjugate pair, (2) spacings between on-axis eigenvalues with interspaced complex conjugate pair, (off) spacings between complex conjugate pairs called off-axis.

emphasize that this classification only makes sense if hermiticity is only mildly broken, since otherwise the eigenvalues are scattered over the complex plane. Thus, there are typically many complex pairs between each real spacing. Also, the distance between a complex conjugate pair cannot be considered a next-neighbor spacing any more, because they may be very far apart. This is why we consider only the weak non-Hermitian case, which we roughly define by the scale of the off-axis spacings being similar or smaller than the scale of the on-axis spacings. A review on random matrices that are weakly non-Hermitian according to this definition can be found in Ref. [94]. We do not treat the case of an on-axis spacing with two or more interspaced eigenvalue pairs, because this occurs only rarely in the weak non-Hermitian regime.

3.2.2. Eigenvalue dynamics in perturbation theory

We want to gain some insight into the dynamics of the eigenvalues of a real symmetric matrix H_0, that is perturbed by another real matrix λM with λ continuously increasing from 0. The eigenvalues of H_0 are denoted by θ_i and their corresponding eigenvectors by $|\psi_i\rangle$. We consider either symmetric or antisymmetric M in the beginning, to work out

the difference between them. The matrix elements of M in the eigenbasis of H_0,

$$M_{ij} = \langle \psi_i | M | \psi_j \rangle \,, \tag{3.24}$$

are real and symmetric or antisymmetric in $i \leftrightarrow j$, too, i.e.,

$$M_{ji} = \pm M_{ij} \,, \qquad \text{for } M^T = \pm M \,. \tag{3.25}$$

Ordinary perturbation theory up to second order yields for the eigenvalues

$$\theta_i \to \theta_i + \lambda M_{ii} \pm \lambda^2 \sum_{j \neq i} \frac{M_{ij}^2}{\theta_i - \theta_j} \,, \tag{3.26}$$

where the first oder contribution just induces a random walk of the eigenvalues without correlating them. For antisymmetric M, this term even vanishes exactly since $M_{ii} = -M_{ii} = 0$ in this case.

Omitting the random walk, the eigenvalue differences become

$$(\theta_i - \theta_j) \to (\theta_i - \theta_j) \left\{ 1 \pm 2\lambda^2 \frac{M_{ij}^2}{(\theta_i - \theta_j)^2} + \mathcal{O}\left[\frac{1}{(\theta_i - \theta_j)(\theta_{i,j} - \theta_{k \neq i,j})} \right] \right\} . \tag{3.27}$$

If θ_i and θ_j are much closer to each other than to any other eigenvalue, the third term in the curly brackets can be neglected in relation to the second one. Then, for real symmetric M (upper sign) the difference grows, which means that the eigenvalues repel as is well known. However, for real antisymmetric M (lower sign), which we will consider from now on, the eigenvalues feel an attraction, which is the stronger the closer they are. We recall that our investigations so far are based on the eigenvalues θ_i of the unperturbed matrix, which are real and remain so as long as ordinary perturbation theory is valid.[9]

However, when two eigenvalues θ_i and θ_j are very close, almost degenerate perturbation theory [95] has to be applied. Neglecting the second order contribution of all other eigenvalues, it yields for the perturbed eigenvalues

$$(\theta_i, \theta_j) \to \text{evs} \left[\begin{pmatrix} \theta_i & 0 \\ 0 & \theta_j \end{pmatrix} + \lambda \begin{pmatrix} 0 & M_{ij} \\ -M_{ij} & 0 \end{pmatrix} \right] , \tag{3.28}$$

where evs denotes the eigenvalues of the matrix and we have made use of the antisym-

[9] Ordinary perturbation theory only yields real shifts of the eigenvalues to all orders.

metry of M, see Eq. (3.25). The difference of the perturbed eigenvalues is

$$S = \sqrt{(\theta_j - \theta_i)^2 - 4\lambda^2 M_{ij}^2}\,. \tag{3.29}$$

Above some critical λ, the square root becomes negative and the eigenvalue difference purely imaginary, which is consistent with the fact that the complex eigenvalues of a real matrix come in complex conjugate pairs. More precisely, imaginary spacings occur for λ larger than

$$\lambda_{\text{crit}} = \frac{|\theta_j - \theta_i|}{2|M_{ij}|}\,, \tag{3.30}$$

which is specific to each individual eigenvalue pair. For the special case of $M_{ij} = 0$, this particular eigenvalue difference remains unperturbed for any λ (in this order of perturbation theory). For perturbations larger then λ_{crit}, we write the eigenvalue difference as

$$S = 2i|M_{ij}|\sqrt{\lambda^2 - \lambda_{\text{crit}}^2} = 2i|M_{ij}|\sqrt{\delta\lambda(2\lambda_{\text{crit}} + \delta\lambda)}\ , \text{ with } \quad \delta\lambda = \lambda - \lambda_{\text{crit}}\,, \tag{3.31}$$

which increases with the excess $\delta\lambda$ of the coupling over the critical coupling. As the spacing becomes imaginary, the eigenvalues are repelled in the complex plane by the perturbation.

The prediction of first order degenerate perturbation theory is that eigenvalue pairs leave the real axis perpendicular to it, as can be seen by an explicit calculation of $\theta_{i,j}$ in Eq. (3.28) for $\lambda > \lambda_{\text{crit}}$. We confirmed that this does indeed hold just after the creation of a complex conjugate pair by numerical simulations both with random matrices and the overlap operator. However, when the perturbation grows larger, the pairs start to move freely in the complex plane (but remain complex conjugate to each other).

3.2.3. Derivation of the surmises

The idea of Wigner surmises is to approximate spacing distributions of large random matrices by those of random matrices with the smallest possible size, typically 2×2 matrices. Note that in the perturbative treatment in Sec. 3.2.2 we have focused on a pair of nearest neighbor eigenvalues of an arbitrarily sized matrix, and ended up discussing a 2×2 matrix and its spacing. This can be seen as an indication that surmises computed for non-Hermitian 2×2 random matrices apply to corresponding large random matrices.

We recall that we distinguish between three different types of spacings in the systems

we finally want to describe (large random matrices and QCD): on-axis spacings without and with one interspaced complex conjugate eigenvalue pair, and off-axis spacings (see Fig. 3.11). For the first and third type we will deduce surmises from 2×2 matrices, computing the corresponding spacings. The spacings of the second type will be derived from the jpdf of the eigenvalues of 4×4 random matrices.

3.2.3.1. Considerations about real 2×2 matrices and their spacings

We consider a real traceless 2×2 matrix, that consists of a symmetric and an antisymmetric part, of the form

$$H = \begin{pmatrix} -a & b \\ b & a \end{pmatrix} + \lambda \begin{pmatrix} 0 & c \\ -c & 0 \end{pmatrix} , \tag{3.32}$$

with random numbers a, b and c that are Gaussian distributed with zero mean and unit variance. Note that the matrix H with $\lambda = 0$ is equivalent to a 2×2 GOE matrix, up to a common shift of the eigenvalues which does not alter the spacing. In the GOE the diagonal entries have twice the variance of the off-diagonal ones, but it can easily be shown that integrating out the part proportional to the identity makes these variances equal. We have done so in H to shorten and simplify the computations. The eigenvalues of H are $\pm\sqrt{a^2 + b^2 - c^2\lambda^2}$, which, for a particular draw of random numbers, turn imaginary beyond a critical coupling

$$\lambda_{\text{crit}} = \frac{\sqrt{a^2 + b^2}}{|c|} . \tag{3.33}$$

For $\lambda < \lambda_{\text{crit}}$ the spacing is $2\sqrt{a^2 + b^2 - c^2\lambda^2}$ and hence real, while for $\lambda > \lambda_{\text{crit}}$ the spacing is $2i\sqrt{c^2\lambda^2 - a^2 - b^2}$ and thus purely imaginary.

The probability that the matrix H has an imaginary spacing can be easily computed by integrating over a, b and c with the constraint that λ is above its critical value. This yields

$$p(\lambda) = (2\pi)^{-3/2} \int_{-\infty}^{\infty} da\, db\, dc\, e^{-(a^2+b^2+c^2)/2}\, \theta\left(c^2\lambda^2 - a^2 - b^2\right) = 1 - \frac{1}{\sqrt{1+\lambda^2}} . \tag{3.34}$$

As expected, the limiting cases are $p(\lambda \to 0) = 0$ and $p(\lambda \to \infty) = 1$. For $\lambda = 0$, there are no imaginary spacings, while for $\lambda \to \infty$, all spacings are imaginary. Of course, the plural here refers to the ensemble, as one realization of this random matrix has only one spacing.

3.2.3.2. On-axis without interspaced complex eigenvalues

For on-axis spacings without interspaced complex eigenvalues our surmise is the same as for the unperturbed ensemble, i.e. the GOE surmise,

$$P^1_{\text{on}}(s) = \frac{\pi}{2}\, s\, e^{-\frac{\pi}{4}s^2}\,, \tag{3.35}$$

because this is the distribution of *real* spacings of H independently of the coupling parameter λ. Note that this is not a completely trivial statement, because H is *not* taken from the GOE for $\lambda > 0$. Let us demonstrate the derivation of this distribution explicitly, as a typical example. We start with the non-normalized distribution of the spacing S,

$$\begin{aligned} Q^1_{\text{on}}(S) &= \int_{-\infty}^{\infty} da\, db\, dc\, e^{-(a^2+b^2+c^2)/2}\, \delta\left(S - 2\sqrt{a^2+b^2-c^2\lambda^2}\right) \theta\left(a^2+b^2-c^2\lambda^2\right) \\ &= 2\pi \int_{-\infty}^{\infty} dc \int_0^{\infty} dr\, r\, e^{-(r^2+c^2)/2}\, \delta\left(S - 2\sqrt{r^2-c^2\lambda^2}\right) \theta\left(r^2-c^2\lambda^2\right)\,. \end{aligned} \tag{3.36}$$

Performing the integration over r, the δ-function yields

$$r \to r_0 = \sqrt{S^2/4 + c^2\lambda^2}\,, \tag{3.37}$$

with the additional factor of

$$\left| \frac{d}{dr}\left(S - 2\sqrt{r^2-c^2\lambda^2}\right)\Big|_{r=r_0} \right|^{-1} = \frac{S}{4\sqrt{S^2/4+c^2\lambda^2}} = \frac{S}{4r_0}\,. \tag{3.38}$$

Thus, we obtain

$$Q^1_{\text{on}}(S) = \frac{\pi}{2}\int_{-\infty}^{\infty} dc\, S\, e^{-\frac{1}{2}\left[\frac{1}{4}S^2 + c^2(1+\lambda^2)\right]}\, \theta\left(\frac{S^2}{4}\right)\,. \tag{3.39}$$

The integration over c just gives a constant factor, and the θ-function forces the spacing S to be real as assumed. With the normalization defined in Eq. (2.77), indicated by $S \to s$, we obtain P^1_{on} as given in Eq. (3.35).

3.2.3.3. On-axis with interspaced complex eigenvalues

When two on-axis eigenvalues have an interspaced complex eigenvalue pair, we expect the latter to have a noticeable influence on the spacing between the on-axis eigenvalues.

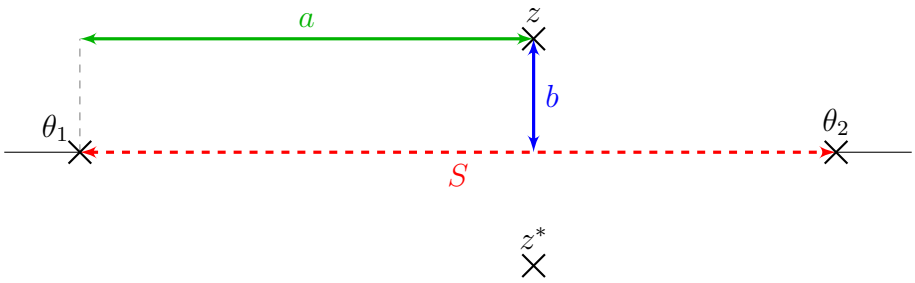

Figure 3.12.: Schematic spectrum of the matrix H used to derive the surmise P^2_{on}.

To obtain a surmise for the distribution of these spacings, we consider a 4×4 matrix

$$H = H_0 + \lambda A\,, \tag{3.40}$$

with H_0 taken from the GOE and an antisymmetric matrix A with probability density

$$w(A) \sim e^{-\frac{1}{2}\mathrm{tr}\left(AA^T\right)}\,, \tag{3.41}$$

i.e., Gaussian distributed entries having the same variance as the off-diagonal entries of H_0. This is the smallest possible matrix that can yield a surmise for this case as there are four eigenvalues which are relevant for the distribution of the spacing. The jpdf of the eigenvalues of H depends on the number of real and complex eigenvalues. For two real eigenvalues θ_1 and θ_2 and one complex conjugate pair z and z^*, it reads up to normalization [91]

$$P(\theta_1, \theta_2, z, z^*) \propto e^{-\theta_1^2-\theta_2^2-z^2-(z^*)^2}\,\mathrm{erfc}\left(\frac{\sqrt{1+\lambda^2}}{\sqrt{2}\lambda}|z-z^*|\right) 2i\Delta(\theta_1, \theta_2, z, z^*)\,, \tag{3.42}$$

with the Vandermonde determinant

$$\Delta(\theta_1, \theta_2, z, z^*) = (z^*-z)(z^*-\theta_2)(z^*-\theta_1)(z-\theta_2)(z-\theta_1)(\theta_2-\theta_1)\,, \tag{3.43}$$

where it is assumed that $\theta_2 > \theta_1$ and $\mathfrak{Im}\ z > 0$. To obtain the distribution of the spacing S between θ_1 and θ_2, we set $\theta_2 = \theta_1 + S$ and introduce new variables $a = \mathfrak{Re}\ z - \theta_1 \in (0, S)$ and $b = \mathfrak{Im}\ z \in (0, \infty)$, cf. Fig. 3.12. The range of a is chosen such that the real part of z (resp. z^*) is between θ_1 and θ_2. This results in

$$P(\theta_1, \theta_1 + S, \theta_1 + a + ib, \theta_1 + a - ib) \tag{3.44}$$
$$\propto S\, b \left[(a-S)^2 + b^2\right] \left(a^2 + b^2\right) e^{-\theta_1^2 - (\theta_1+S)^2 - 2(a+\theta_1)^2 + 2b^2}\ \mathrm{erfc}\left(\frac{\sqrt{2}\sqrt{1+\lambda^2}}{\lambda}\, b\right).$$

We integrate out θ_1, a and b, and perform an irrelevant rescaling $S \to 2S$ (this simplifies the computations and we have to normalize in the end anyway) to obtain the non-normalized spacing distribution

$$\int_0^\infty db \int_0^{2S} da \int_{-\infty}^\infty d\theta_1\, P(\theta_1, \theta_1 + 2S, \theta_1 + a + ib, \theta_1 + a - ib)$$
$$\propto S e^{-3S^2} \left\{\sqrt{\pi}\, e^{S^2}\, \mathrm{erf}(S) \left[\lambda^2\sqrt{1+\lambda^2}\left(3\lambda^2 + 8S^2\right) + 4\left(\sqrt{1+\lambda^2} - 1\right)\left(4S^4 - 8S^2 + 3\right)\right]\right.$$
$$\left. +8S\left[\left(\sqrt{1+\lambda^2} - 1\right)\left(2S^2 - 1\right) - \lambda^2\sqrt{1+\lambda^2}\right]\right\} = Q_{\mathrm{on}}^2(S;\lambda)\,. \tag{3.45}$$

With the normalization given in Eq. (2.77), indicated by the substitution $S \to s$, the spacing distribution reads

$$P_{\mathrm{on}}^2(s;\lambda) = CD\, Q_{\mathrm{on}}^2(Ds;\lambda)\,, \tag{3.46}$$

with

$$C = \left(\int_0^\infty dS\, Q_{\mathrm{on}}^2(S;\lambda)\right)^{-1} = \frac{12\sqrt{3}}{\sqrt{\pi}}\left[\lambda^2\sqrt{1+\lambda^2}\left(9\lambda^2 + 8\right) + 8\left(\sqrt{1+\lambda^2} - 1\right)\right]^{-1}, \tag{3.47}$$

and

$$D = C\int_0^\infty dS\, S\, Q_{\mathrm{on}}^2(S;\lambda) = \frac{C}{72}\left[26\left(\sqrt{1+\lambda^2} - 1\right) - 27\sqrt{2}\,\mathrm{arccot}(\sqrt{2})\right. \tag{3.48}$$
$$\left. +\sqrt{1+\lambda^2}\left(18\lambda^4 + 20\lambda^2 + 27\sqrt{2}\left(1+\lambda^2\right)^2\mathrm{arccot}(\sqrt{2})\right)\right].$$

The spacings distribution P_{on}^2 is plotted for various parameters λ in the left panel of Fig. 3.13.

We now consider the distribution for the limits $\lambda \to 0$ and $\lambda \to \infty$. In the first case, we obtain

$$\lim_{\lambda\to 0} P_{\mathrm{on}}^2(s;\lambda) = \frac{\xi^2}{8\pi}\, s\, e^{-3\xi^2 s^2}\left[4\xi^3 s^3 - 6\xi s + \sqrt{\pi}\, e^{\xi^2 s^2}(4\xi^4 s^4 - 4\xi^2 s^2 + 3)\ \mathrm{erf}(\xi s)\right], \tag{3.49}$$

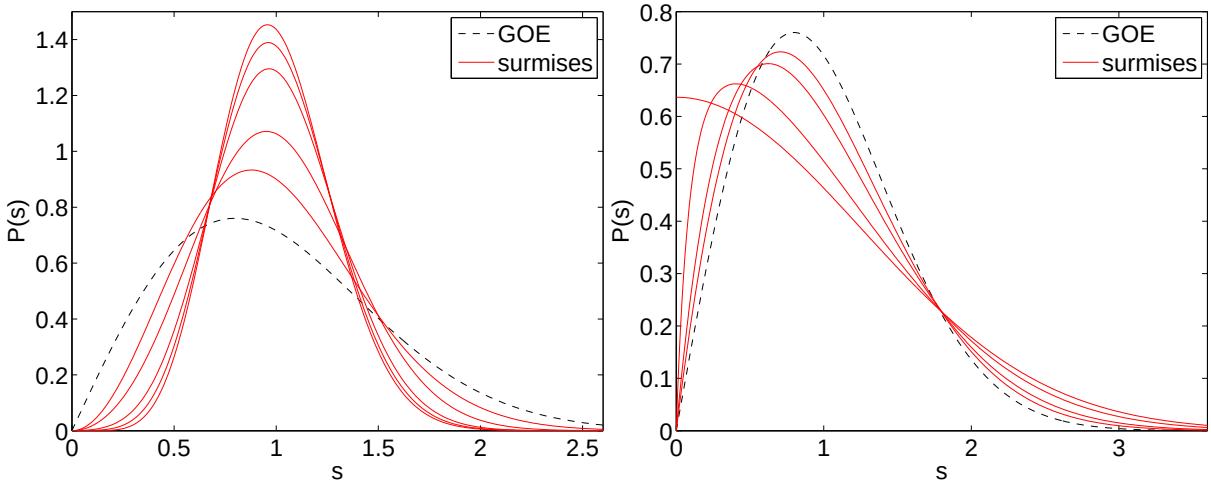

Figure 3.13.: Left: Wigner surmise $P^2_{\text{on}}(s;\lambda)$, Eq. (3.46), for on-axis eigenvalues with an interspaced complex conjugate eigenvalue pair for $\lambda = 0, 0.3, 0.5, 1, \infty$ (decreasing maxima). Right: Wigner surmise $P_{\text{off}}(s;\lambda)$, Eq. (3.55), for off-axis spacings and coupling parameters $\lambda = 0, 2, 10, \infty$ (decreasing maxima). Plotted for comparison is the Wigner surmise for the GOE (dashed), which is the surmise for the on-axis spacings with no interspaced complex pair, Eq. (3.35).

with

$$\xi = \lim_{\lambda\to 0} D = \frac{22 + 45\sqrt{2}\,\text{arccot}\sqrt{2}}{16\sqrt{3\pi}} \approx 1.2453\,. \tag{3.50}$$

The opposite limit $\lambda \to \infty$ yields

$$\lim_{\lambda\to\infty} P^2_{\text{on}}(s;\lambda) = 4\sqrt{3}\,\eta^2 s\, e^{-2(\eta s)^2}\,\text{erf}(\eta s)\,, \tag{3.51}$$

where

$$\eta = \lim_{\lambda\to\infty} D = \frac{2 + 3\sqrt{2}\,\text{arccot}\sqrt{2}}{2\sqrt{3\pi}} \approx 0.7510\,. \tag{3.52}$$

For infinitesimally small spacings s and arbitrary non-zero λ (including the limit $\lambda \to \infty$), the spacing distribution P^2_{on} is proportional to s^2. However, taking the limit $\lambda \to 0$, the first term in the Taylor expansion at $s = 0$ is proportional to s^6. One can understand the small-s behavior from the Vandermonde determinant in the joint probability density alone, i.e. by focusing on the eigenvalue repulsion and neglecting the exponential and erfc factors (which only contribute significantly at larger spacings). The

relevant integral is

$$\int_0^S da(z^*-\theta_2)(z^*-\theta_1)(z-\theta_2)(z-\theta_1)(\theta_2-\theta_1)\Big|_{z=\theta_1+a+ib,\,\theta_2-\theta_1=S}$$
$$= S\int_0^S da\,\left[(a-S)^2+b^2\right](a^2+b^2) = b^4S^2+\frac{2}{3}\,b^2S^4+\frac{1}{30}\,S^6\,. \tag{3.53}$$

This is indeed proportional to S^2 for small S, unless the b-dependent terms we have neglected become proportional to $\delta(b)$, which happens for $\lambda\to 0$. Then, the distribution is proportional to S^6 for small S. These considerations are unaltered by the rescaling $S\to s$.

3.2.3.4. Off-axis

For the behavior of the imaginary off-axis spacings, we assume that the complex conjugate eigenvalue pair forming the respective spacing is mainly relevant. Such a pair can already occur in a non-Hermitian real 2×2 matrix. We therefore consider the 2×2 matrix H given in Eq. (3.32) as a sufficient set-up to obtain a surmise for the off-axis spacings. This time, we are interested in the distribution of the imaginary spacings of this matrix. In analogy to Sec. 3.2.3.2 we define the non-normalized distribution $Q_{\text{off}}(S)$ similar to Eq. (3.36), but with different arguments of the delta and step function,

$$Q_{\text{off}}(S) = \int_{-\infty}^{\infty} da\,db\,dc\,e^{-(a^2+b^2+c^2)/2}\,\delta\left(S-2\sqrt{c^2\lambda^2-a^2-b^2}\right)\theta\left(c^2\lambda^2-a^2-b^2\right)\,. \tag{3.54}$$

For the normalized spacing distribution [see Eq. (2.77)] we obtain by a short calculation similar to the one in Sec. 3.2.3.2,

$$P_{\text{off}}(s;\lambda) = C\,D^2\,s\,e^{D^2s^2}\,\text{erfc}\left(Ds\sqrt{1+\lambda^2}/\lambda\right)\,, \tag{3.55}$$

with the constants

$$C=\frac{2}{\sqrt{1+\lambda^2}-1}\,,\text{ and}\qquad D=C\,\frac{\lambda\sqrt{1+\lambda^2}-\text{arsinh}(\lambda)}{2\sqrt{\pi}}\,. \tag{3.56}$$

For small s, this distribution is linear in s, just like the one of the GOE.

In the limiting case of $\lambda\to 0$, the distribution is

$$\lim_{\lambda\to 0} P_{\text{off}}(s;\lambda) = \frac{64}{9\pi}\,s\,\text{erfc}\left(\frac{4s}{3\sqrt{\pi}}\right)\,. \tag{3.57}$$

Note that in this limit the perturbation is formally switched off. However, for an infinite number of realizations of the random matrix H, off-axis eigenvalues will exist for arbitrary small perturbations. This is because the probability to encounter an imaginary spacing, given in Eq. (3.34), is greater than zero for arbitrary non-zero λ. Eq. (3.57) describes the (normalized) distribution of these spacings in the $\lambda \to 0$ limit (whereas Eq. (3.49) reflects the influence of these eigenvalues on the neighboring on-axis spacings in this limit). Even though the difference between Eq. (3.57) and the GOE spacing distribution is rather small, the two are clearly distinguishable in Fig. 3.13 (right).

For $\lambda \to \infty$ the distribution P_{off} is simply half a Gaussian,

$$\lim_{\lambda\to\infty} P_{\text{off}}(s;\lambda) = \frac{2}{\pi} \exp\left(-\frac{s^2}{\pi}\right) , \tag{3.58}$$

which is the spacing distribution of the antisymmetric part of H alone. Note that this limit is not uniform at $s = 0$, since $\lim_{s\to 0} \lim_{\lambda\to\infty} P_{\text{off}}(s;\lambda) = 2/\pi$, whereas $P_{\text{off}}(0;\lambda) = 0$ for finite λ. Spacings for various values of the coupling parameter λ are plotted in the right panel of Fig. 3.13 and this discontinuity is clearly visible. A similar effect has been observed for mixed symmetry classes of (small and large) random matrices in Ref. [53]. There, even a Gibbs-like overshoot of the curves near $s = 0$ has been observed, which is absent here.

For consistency, we have checked that the surmises P^1_{on} and P_{off} could equally well be obtained from the jpdf of the eigenvalues of the 2×2 matrix H, given in Ref. [91] (with either two real or a pair of complex conjugate eigenvalues).

In the following, we compare those surmises to the spacing distributions of appropriate large random matrices and the QCD Dirac operator with non-vanishing chemical potential.

3.2.4. Comparison of the surmises to large RMT spectra

To check the validity of the surmises calculated in Sec. 3.2.3, we apply them to the spectra of large dimensional $N \times N$ random matrices of the form

$$H = H_0 + \frac{\Lambda}{\sqrt{2N/\pi}}\, A\,, \tag{3.59}$$

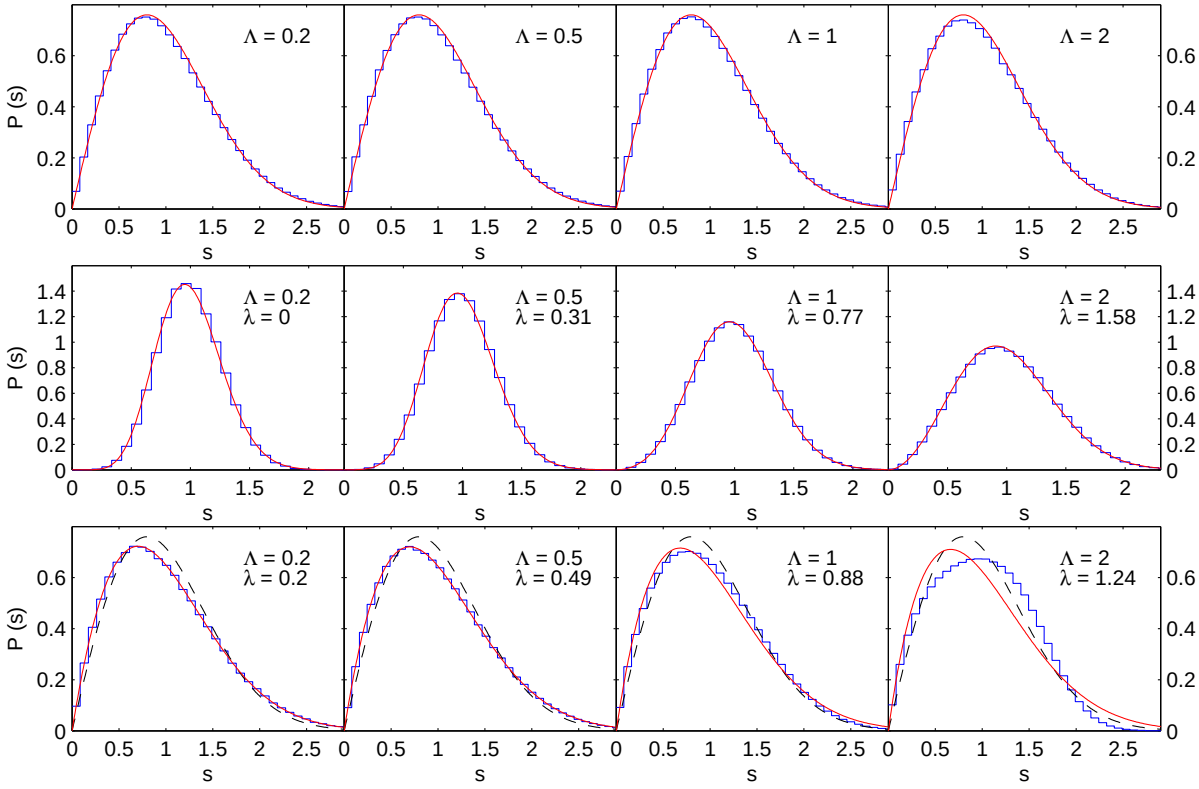

Figure 3.14.: Spacing distributions of 400×400 random matrices defined in Eq. (3.59), with various values of the coupling parameter Λ. Top: on-axis spacings of type 1, surmise given by the GOE, Eq. (3.35). Middle: on-axis spacings of type 2, surmise given by Eq. (3.46). Bottom: off-axis spacings, surmise given by Eq. (3.55); the dashed curve is the GOE spacing for comparison. For each value of Λ, $2 \cdot 10^5$ random matrices have been diagonalized.

where H_0 is real symmetric and taken from the GOE with, whereas A is real antisymmetric with probability density

$$w(A) \sim e^{-\frac{1}{2}\mathrm{tr}\left(AA^T\right)} . \tag{3.60}$$

This means that all elements of A are independently Gaussian distributed with the same variance like the off-diagonal entries of H_0 (as in the case of the small matrices used for the surmises). The coupling parameter Λ comes with a factor of $1/\sqrt{2N/\pi}$ in order to make it comparable to the one used in the surmises, λ. Furthermore, as far as the spacing distribution is concerned, this normalization makes Λ a universal, N-independent coupling parameter, see [53] for a detailed discussion. As also argued there, a constant spectral density of the large random matrices is necessary to apply the surmises for the spacing distributions obtained from small matrices of mixed universality classes. Oth-

erwise, different coupling strengths, i.e. surmises with different λ, are mixed. Therefore, we have only evaluated eigenvalues with real part in the interval $(-\sqrt{N}/4, \sqrt{N}/4)$, i.e., around the center of the real spectrum of H. The spectral density in this interval is almost, but not exactly, constant. We have thus measured the on-axis spacings in units of the local mean spacing (obtained by an ensemble average), which is equivalent to unfolding the spectrum. For the off-axis spacings, no unfolding has been done.

The numerically obtained spacing distributions of H are shown in Fig. 3.14 for various values of the coupling parameter Λ. As can be seen, the surmises for the on-axis spacings of both types (top and middle) describe the data very well for coupling parameters up to $\Lambda = 2$. The coupling parameters λ of the surmise for the on-axis spacings of type 2 have been obtained by a fit of P^2_{on} to the numerically obtained spacing distribution with minimized square deviation. As expected, the coupling λ increases with Λ.

For the off-axis spacings, we are able to predict the 2×2 coupling parameter λ through the frequency p of imaginary spacings by the following procedure. We numerically measure p for the large matrices in the spectral region we consider and obtain the coupling parameter by inverting Eq. (3.34), which yields $\lambda = \sqrt{1/(1-p)^2 - 1}$. This means that we match the frequency of imaginary spacings for the small and large random matrices. The surmises for the off-axis spacings with λ obtained this way describe the numerical data very well for $\Lambda = 0.2$ and 0.5, differ slightly for $\Lambda = 1$ and are far off for $\Lambda = 2$. Although the coupling parameter could also be determined by a fit of the surmise to the data as for the on-axis spacings of type 2 above, we observed that this does not yield an improved estimate. Note that the maxima of the surmises are always left of the maximum of the GOE, cf. Fig. 3.13 (right), in contrast to the maximum of the numerical data for $\Lambda = 2$. A reason for the break-down of the off-axis surmise at large couplings, while the on-axis surmises still work almost perfectly, could be the additional degree of freedom of the eigenvalues when they move in the complex plane.

3.2.5. Application to two-color QCD at non-zero density

3.2.5.1. Anti-unitary symmetries and hermiticity of the Dirac operator in two-color QCD

We show that the continuum and the overlap Dirac operator with $SU(2)$ gauge links both obey an anti-unitary symmetry squaring to unity. Therefore, the RMT counterpart of the Dirac operator at zero chemical potential μ is the GOE, while a non-zero μ requires the use of non-Hermitian random matrices like the ones considered above.

3.2.5.1.1. Continuum

We firstly consider the Euclidean continuum Dirac operator of two-color QCD, which at non-zero chemical potential μ is given by

$$D = \gamma_\nu D_\nu + m + \mu\gamma_4 \,, \tag{3.61}$$

with the covariant derivative $D_\nu = \partial_\nu + iA^a_\nu\tau_a$, where a sum over a from 1 to 3 and over ν from 1 to 4 is understood. τ_a are the Pauli matrices, and for the Euclidean γ matrices γ_ν, we use the Weyl representation

$$\gamma_a = \begin{pmatrix} 0 & i\tau_a \\ -i\tau_a & 0 \end{pmatrix} \text{, and} \quad \gamma_4 = \begin{pmatrix} 0 & \mathbb{1}_2 \\ \mathbb{1}_2 & 0 \end{pmatrix} . \tag{3.62}$$

At zero mass and chemical potential, this Dirac operator is anti-Hermitian and therefore has purely imaginary eigenvalues. The mass term has no effect on the eigenvalue correlations since it just shifts each eigenvalue by the same amount, which is why we consider the massless case in the following. The chemical potential, on the other hand, affects the spectrum in a more complicated way.

To obtain the anti-unitary symmetry of the $SU(2)$ Dirac operator, we use the fact that the $SU(2)$ group is pseudo-real, i.e.,

$$(i\tau_a)^* = \tau_2^\dagger (i\tau_a)\tau_2 \,. \tag{3.63}$$

Furthermore, we use the charge conjugation properties of gamma matrices,

$$(i\gamma_\nu)^* = C^\dagger (i\gamma_\nu) C \quad \text{, with} \quad C = \gamma_2\gamma_4 \,. \tag{3.64}$$

By multiplying the Dirac operator with the imaginary unit, which does not change the correlations of its eigenvalues, we obtain

$$iD = i\gamma_\nu \otimes \left(\partial_\nu \mathbb{1}_2 + A^a_\nu i\tau_a\right) + i\mu\gamma_4 \otimes \mathbb{1}_2 \,, \tag{3.65}$$

where the spin and gauge parts have been separated explicitly. From Eq. (3.63) and Eq. (3.64) it follows that iD obeys

$$[iD, OK] = 0 \,, \text{ with} \quad O = C \otimes \tau_2 \quad \text{satisfying} \quad (OK)^2 = OO^* = 1 \,, \tag{3.66}$$

where K is the complex conjugation operator. As a consequence, iD can be made real

by a unitary transformation that depends only on O. We therefore write

$$iD \cong D_s + D_a \,, \tag{3.67}$$

where $\cong$ implies that the two sides of the equation are connected by a unitary transformation, and we have split the operator into its real symmetric part D_s and real antisymmetric part D_a. The Hermitian part of iD is $iD(\mu = 0)$, while the anti-Hermitian part is $i\mu\gamma_4$. As the hermiticity is not changed by a basis transformation, we identify $D_s \cong iD(\mu = 0)$ and $D_a \cong i\mu\gamma_4$.

Thus up to a multiplication by i, the Dirac operator at $\mu = 0$ is real in a certain basis. For non-zero μ, it acquires an antisymmetric part, but remains real in that basis. Concerning the hermiticity, this is exactly the same setting as in the random matrix ensembles considered above, with the chemical potential μ taking the role of the coupling parameters λ and Λ.

Note that in the massless case, the Dirac operator also satisfies chiral symmetry, i.e., $\{D, \gamma_5\} = 0$, which means that its non-zero eigenvalues come in pairs $\pm\theta$. For the spacing distribution in the bulk, which we consider below, the chiral symmetry is however known to be irrelevant [47–51], as mentioned above.

3.2.5.1.2. Lattice

There are several ways to construct Dirac operators on a discrete space-time as discussed in Sec. 2.1.2.2. Some of those may have different anti-unitary symmetries than the continuum Dirac operator, as is the case for the staggered operator [74, 75]. Here, we consider the overlap operator defined in Eq. (2.26), which shares the anti-unitary symmetries of the continuum Dirac operator as we show in the following. At non-zero chemical potential, the overlap operator is defined by [88]

$$D^{\text{ov}}(\mu) = 1 + \gamma_5 \operatorname{sign}(\gamma_5 D^W(\mu)) \,, \tag{3.68}$$

where we have set the lattice spacing to unity (i.e., $a = 1$) and sign is the matrix sign function satisfying $(\operatorname{sign} A)^2 = \mathbb{1}$, which is explicitly defined below. The Wilson Dirac operator at non-zero chemical potential is given by [96]

$$D^W(\mu) = 1 - \kappa \sum_{i=1}^{3} \left(T_i^+ + T_i^-\right) - \kappa \left(e^{\,\mu}\, T_4^+ + e^{-\mu}\, T_4^-\right) \,, \tag{3.69}$$

with $\kappa = 1/(8 + 2m_w)$ and the hopping terms

$$(T_\nu^\pm)_{xx'} = (1 \pm \gamma_\nu)\, U_{\pm\nu}(x)\, \delta_{x\pm\hat{\nu},x'}\,. \tag{3.70}$$

$m_w \in (-2, 0)$ is the Wilson mass, and the gauge links $U_{\pm\nu}$ are elements of the $SU(2)$ group. The exponential factors $e^{\pm\mu}$ implement the quark chemical potential on the lattice. The argument of the sign function in Eq. (3.68) is Hermitian for $\mu = 0$ and non-Hermitian for $\mu \neq 0$.

The sign function is defined for a general $n \times n$ matrix A by

$$\mathrm{sign}(A) = G\,\mathrm{diag}[\mathrm{sign}(\theta_1), \ldots, \mathrm{sign}(\theta_n)]G^{-1}\,, \tag{3.71}$$

where we assume that A is diagonalizable, i.e., $A = G\,\mathrm{diag}[\theta_1, \ldots, \theta_n]G^{-1}$, with some invertible matrix G. Therefore, for every invertible matrix B holds

$$\begin{aligned}\mathrm{sign}\left(BAB^{-1}\right) &= \mathrm{sign}\left(BG\,\mathrm{diag}[\theta_1, \ldots, \theta_n](BG)^{-1}\right) \\ &= \left(BG\,\mathrm{diag}[\mathrm{sign}(\theta_1), \ldots, \mathrm{sign}(\theta_n)]G^{-1}B^{-1}\right) = B\,\mathrm{sign}(A)B^{-1}\,.\end{aligned} \tag{3.72}$$

If A is not diagonalizable, a spectral definition of $\mathrm{sign}(A)$ can still be derived using the Jordan decomposition [97]. As the eigenvalues of the argument of the sign function in Eq. (3.68) may become complex for non-zero chemical potential, we still need to extend the sign function to arbitrary complex numbers. To this end, we define [98]

$$\mathrm{sign}(z) = \mathrm{sign}\left(\mathfrak{Re}\, z\right)\,, \tag{3.73}$$

which is a choice that yields the correct physical result for the overlap Dirac operator in Eq. (3.68) (see Ref. [98]).

The operator we actually evaluate on the lattice is related to the overlap operator by a stereographic projection of its eigenvalues, defined by [99]

$$D^p = \frac{2D^{\mathrm{ov}}}{2 - D^{\mathrm{ov}}} = 2\,\frac{1 + \gamma_5\,\mathrm{sign}(\gamma_5 D^W)}{1 - \gamma_5\,\mathrm{sign}(\gamma_5 D^W)}\,. \tag{3.74}$$

For zero chemical potential, D^{ov} has eigenvalues on a circle, $\theta = 1 + \exp(i\varphi)$, in the complex plane, whereas D^p is anti-Hermitian and thus has purely imaginary eigenvalues. Furthermore, while the overlap operator fulfills the Ginsparg-Wilson relation [25] (note

that $a = 1$),

$$\{D^{\text{ov}}, \gamma_5\} = D^{\text{ov}} \gamma_5 D^{\text{ov}} \,, \tag{3.75}$$

the projected operator is exactly chiral, i.e., $\{D^p, \gamma_5\} = 0$ (but also non-local). Its non-zero eigenvalues therefore come in pairs $\pm i\theta$.

Considering the anti-unitary symmetries of the projected operator D^p, we first note that the gauge links obey

$$U^*_{\pm\nu}(x) = \tau_2^\dagger \, U_{\pm\nu}(x) \, \tau_2 \,, \tag{3.76}$$

as they are elements of $SU(2)$ and therefore can be written as linear combinations of $\mathbb{1}_2$ and $i\tau_a$. One can also show that

$$(\gamma_5 D^W)^* = O^\dagger (D^W \gamma_5) O \qquad \text{(note the ordering)}, \tag{3.77}$$

with O as defined in Eq. (3.66) for the continuum. Using the facts that O commutes with γ_5 and that γ_5 is real and its own inverse, we obtain

$$\gamma_5^* \, \text{sign}^*(\gamma_5 D^W) = O^\dagger \gamma_5 \, \text{sign}(D^W \gamma_5) O = O^\dagger \, \text{sign}(\gamma_5 D^W) \gamma_5 O \,, \tag{3.78}$$

where we have also made use of Eq. (3.72). Furthermore, sign is its own inverse, which yields

$$(D^p)^* = 2\, O^\dagger \, \frac{1 + \text{sign}(\gamma_5 D^W)\gamma_5}{1 - \text{sign}(\gamma_5 D^W)\gamma_5} \, O = 2\, O^\dagger \, \frac{\gamma_5 \, \text{sign}(\gamma_5 D^W) + 1}{\gamma_5 \, \text{sign}(\gamma_5 D^W) - 1} \, O = -O^\dagger D^p \, O \,. \tag{3.79}$$

Again multiplying with the imaginary unit, we obtain $[iD^p, OK] = 0$, so the Hermitian operator iD^p shares the anti-unitary symmetry from the continuum, compare to Eq. (3.66). We therefore expect its spacing distribution at vanishing μ to be similar to the one of the GOE. Again, a non-zero chemical potential destroys the hermiticity of iD^p, but keeps the anti-unitary symmetry, exactly as for the continuum Dirac operator. Note however, that μ enters the hermiticity breaking part of the operator iD^p non-linearly, unlike λ and Λ in the random matrix models.

Due to chiral and anti-unitary symmetry, for every eigenvalue θ of iD^p, $-\theta$, θ^* and $-\theta^*$ are also eigenvalues. Apart from the zero eigenvalues, there are thus three classes of eigenvalues: plus-minus pairs on the real or the imaginary axis and quartets of the form $(\theta, -\theta, \theta^*, -\theta^*)$. As μ is increased from zero, a quartet is typically formed when two pairs of real eigenvalues of iD_p come together and allow for its creation. Considering only the

μ	0.05	0.10	0.20	0.30
# configurations	60 000	30 000	20 000	20 000

Table 3.1.: Values of the chemical potential and corresponding number of quenched configurations used to determine the spectral properties of the overlap operator.

pair with positive real part and forgetting about chiral symmetry, the same happens in the spectra of the large random matrices as the degree of non-hermiticity is increased (see Sec. 3.2.1).

3.2.5.2. Numerical results

All the numerical computations have been done by N. Meyer on a lattice of extent 8^4 with Wilson gauge action, see Ref. [80] for more details. A number of 60 000 quenched gauge configurations has been created at $\beta = 2.2$. On subsets of these, a number of about 30 of the smallest eigenvalues of the overlap operator, given in Eq. (3.68), has been calculated for various values of the chemical potential and with a Wilson mass of $m_w = -1.4$. The number of configurations we used for the different values of the chemical potential μ are shown in Table 3.1.

We measure the spacing distributions of the projected overlap operator D^p, defined in Eq. (3.74), for various values of the chemical potential μ. As before, we distinguish between off-axis spacings and on-axis spacings with and without an interspaced complex pair. We only consider spacings between eigenvalues with an imaginary part in the spectral window $(0.5, 0.6)$. This ensures that these eigenvalues are in the bulk of the spectrum, and the eigenvalue density is roughly constant. This is necessary to apply the surmises, as argued in Sec. 3.2.4. As for the large random matrices considered in that Section, unfolding has only been done for the on-axis spacings.

The results are shown in Fig. 3.15. The numerical data are very well matched by the surmises derived from small matrices, as in the case of the large random matrices. Again, the coupling parameter λ is obtained by a fit for the on-axis spacings of type 2 and from the frequency p of real[10] spacings for the off-axis spacings. For the latter spacings, we observe that the discrepancy between the data and the surmise at large μ has the same tendency as in the case of the large random matrices, cf. Fig. 3.14 (bottom, right). This indicates that the spacing distributions of the large random matrices are able to describe the QCD results reasonably well, even at larger coupling. There is however no method

[10]Note that the off-axis spacings are imaginary in the case of the large random matrices, because the real and imaginary axis are swapped there.

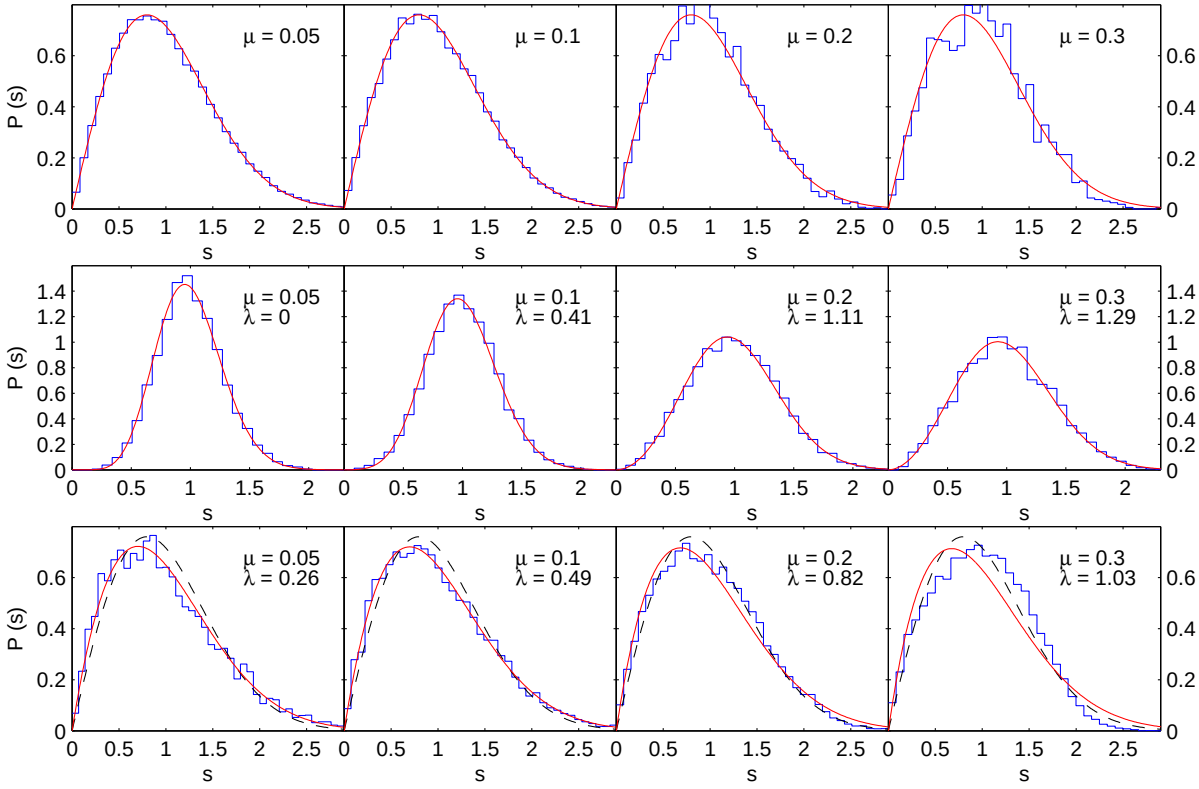

Figure 3.15.: Spacing distributions of the overlap operator with various real values of the chemical potential μ. Top: on-axis spacings of type 1, surmise given by GOE, Eq. (3.35). Middle: on-axis spacings of type 2, surmise given by Eq. (3.46). Bottom: off-axis spacings, surmise given by Eq. (3.55); the dashed curve is the GOE spacing distribution for comparison.

known to us to match the chemical potential μ and the coupling parameter Λ, which is why we show no direct comparison between QCD and large random matrices.

3.2.5.2.1. Imaginary chemical potential

Contrarily to a real chemical potential, an imaginary μ does not change the anti-hermiticity of either the continuum Dirac operator or of the projected overlap operator D^p. Instead, the anti-unitary symmetry of those operators is broken in this case. Therefore, these operators are in the same universality class like the GUE in the presence of a non-vanishing imaginary chemical potential. We thus expect a transition from GOE to GUE behavior of the spacing distribution as the imaginary chemical potential is increased from zero. A surmise for the spacing distribution of a mixed 2×2 random matrix of the form $H_{\mathrm{GOE}} + \lambda H_{\mathrm{GUE}}$, has been worked out in Refs. [52, 53] and is has been shown that it applies to large random matrices of that form very well. This distribution

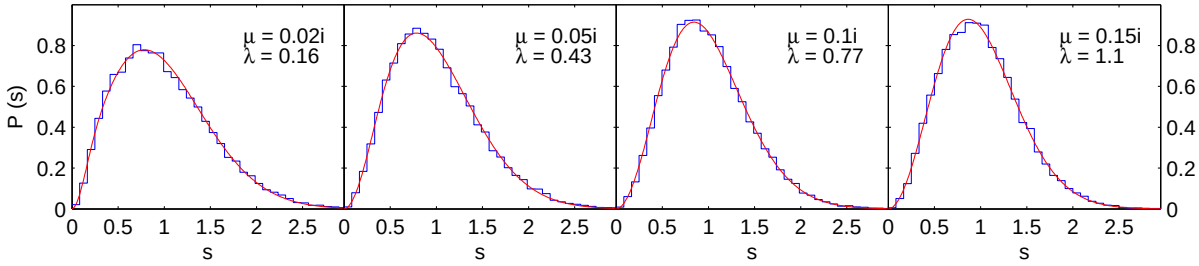

Figure 3.16.: Spacing distributions of the overlap operator with various imaginary values of the chemical potential μ, approximated by the surmise given in Eq. (3.80). For each μ, 5 000 configurations have been analyzed in the spectral window with imaginary parts of the eigenvalues between 0.65 and 0.8.

reads

$$P_{\mathrm{GOE}\to\mathrm{GUE}}(s) = Cs\, e^{-D^2 s^2}\, \mathrm{erf}\left(\frac{Ds}{\lambda}\right) , \tag{3.80}$$

where

$$C = 2\sqrt{1+\lambda^2}\, D^2 \text{ , and } \quad D = \frac{\sqrt{1+\lambda^2}}{\sqrt{\pi}}\left(\frac{\lambda}{1+\lambda^2} + \mathrm{arccot}\lambda\right) . \tag{3.81}$$

In Fig. 3.16, this surmise is compared to the spacing distribution of the projected overlap operator D^p for various imaginary values of the chemical potential. Again, unfolding has been done by measuring the spacings in units of the local mean spacing. The coupling parameter λ has been obtained by a fit of the surmise to the data with minimized square deviation. It can be seen that the surmise is in very good accordance with the numerical data also in this case.

4. Supersymmetry on the lattice

Supersymmetry is assumed to play an important role in the search for a unified theory which describes all known fundamental physical interactions. As a variety of important properties of supersymmetric theories (e.g. spontaneous breaking of SUSY) are not accessible via perturbation theory, other approaches are required. Promising candidates are numerical methods like the computation of path integrals on space time lattices which have been applied to QCD with great success. There is, however, a fundamental problem that supersymmetric theories on discrete space-time suffer from, which is the failure of the Leibniz rule on the lattice [100, 101]. The naive ansatz for a lattice action usually is not invariant under infinitesimal translations, which it has to be in order to fulfill SUSY. Nevertheless, it is possible to formulate lattice theories which are not fully supersymmetric but restore SUSY in the continuum limit. One way to ensure this is the orbifolding procedure [102] that allows to keep a subgroup of the original continuum symmetry on the lattice. For the theory of SUSYQM, which is one of the simplest supersymmetric models, even a lattice action that violates all continuum supersymmetries can yield sensible results. In this model, degenerate boson and fermion masses are obtained by merely including the Wilson mass of the fermions also in the bosonic derivative operator at non-zero lattice spacing and with interaction [103]. The quadratic terms in the action are then exactly supersymmetric and the only explicit breaking comes from the interaction term which connects bosons and fermions. This action also yields a continuum limit for the masses which is compatible with the correct values. Further improved actions for SUSYQM are discussed in Refs. [104, 110], where a lattice action preserving one exact supersymmetry, introduced in Ref. [103], is also studied numerically.

A different method to conserve full SUSY on the lattice by means of non-commuting fermionic and bosonic variables has been introduced in Refs. [105, 106]. However, it has been shown that this ansatz suffers from inconsistencies because the SUSY variation of field products is not uniquely defined in this case [107].

A rigorous no-go theorem for SUSY on the lattice has recently been established [18]. It has been shown there that a fully supersymmetric action, which incorporates boson-fermion interaction, necessarily has to be non-local. An approach to circumvent this

no-go theorem could be the use of a modified symmetry relation. We shortly review this ansatz in Sec. 4.1, and consider its consequences and a fundamental problem. In Sec. 4.2, we return to the naive supersymmetry, and show that it is possible to make a compromise between locality and SUSY. We demonstrate this numerically for the theory of SUSYQM.

4.1. The blocking approach to SUSY

A possible approach to overcome the problems of supersymmetric lattice theories that is based on a generalization of the Ginsparg-Wilson relation [25] has been introduced in Ref. [108]. The motivation for this ansatz, which we briefly review in Sec. 4.1.1, is the formal construction of a 'perfect' lattice action by a blocking procedure. The study of the properties of this action under symmetry transformations yields the so-called 'generalized Ginsparg-Wilson relation'. We derive a necessary condition for the solution of that relation and consider its consequences in Sec. 4.1.2. Our findings about actions that are explicitly obtained from the blocking of SUSYQM in the continuum are summarized in Sec. 4.1.3.

4.1.1. The generalized Ginsparg-Wilson relation

The starting point is a general N-dimensional continuum theory with the action $S^{\mathrm{co}}[\varphi]$, where φ is a multiplet containing all kinds of continuum fields. Furthermore, a perfect (see below) lattice action $S[\phi]$ with the lattice field multiplet ϕ is defined via

$$e^{-S[\phi]} = \mathrm{SDet}^{\frac{1}{2}}\alpha \int D\varphi \, e^{-\frac{1}{2}(\phi-\phi_f)_i^b \alpha_{ij}^{bc} (\phi-\phi_f)_j^c - S^{\mathrm{co}}[\varphi]} \,, \tag{4.1}$$

where SDet denotes the superdeterminant, b, c label the field species and $i, j \in n_1 \times n_2 \times \ldots \times n_N$ label the lattice sites. A sum over doubly occurring indices is understood here and in the following. We assume that the lattice has the same spacing of a in each direction. We denote α as blocking kernel and define the smeared continuum field by

$$(\phi_f)_i^b = \int d^D x \, f^{bc}(x - ai)\varphi^c(x) = f_{ix}^{bc}\varphi_x^c \,, \tag{4.2}$$

where f is a smearing function whose space-dependent part has a peak at 0, which may also mix different field species. In the last step of Eq. (4.2), we have introduced a compact notation for f and written the space-time variable as an index. Analogously to the lattice

indices, doubly occurring space-time indices are integrated over. By construction, the lattice theory based on the action S has the same partition function and yields the same correlation functions like the continuum theory[1] with the action S^{co}. This is why S is denoted as perfect action. In the language of renormalization group theory, S is an effective Wilsonian action.

Usually, S cannot be given explicitly, because this would require the calculation of the path integral over the continuum fields and is therefore equivalent to solving the continuum theory. If this is possible, there is no need to consider the theory on the lattice in the first place, as it is completely accessible analytically. However, one can show that the lattice action S inherits the symmetries of the continuum action in a certain sense. Precisely, S has to fulfill a generalized Ginsparg-Wilson relation given S^{co} is invariant under an infinitesimal linear symmetry transformation of the continuum fields $\varphi^b_x \to \varphi^b_x + \tilde{G}^{bc}_{xy}\varphi^c_y$. Here, $\tilde{G}$ is the infinitesimal generator of the transformation. This relation reads [108]

$$G^{bc}_{ij}\phi^c_j \frac{\partial S}{\partial \phi^b_i} = (G\alpha^{-1})^{bc}_{ij}\left(\frac{\partial S}{\partial \phi^c_j}\frac{\partial S}{\partial \phi^b_i} - \frac{\partial^2 S}{\partial \phi^c_j \partial \phi^b_i}\right) + \mathrm{STr}G - \mathrm{STr}\tilde{G}\,, \tag{4.3}$$

where STr denotes the supertrace and G is the lattice version of the generator $\tilde{G}$. For actions that contain polynomials in the fields of order three or larger, this relation becomes a very complicated non-linear differential equation which mixes different powers of fields. The derivation of Eq. (4.3) also requires that the transformation of the continuum fields can be represented as a linear transformation on the blocked lattice fields, i.e.,

$$f^{bc}_{iy}\,\tilde{G}^{cd}_{yx}\varphi^d_x = G^{bc}_{ij}(\phi_f)^c_j\,, \tag{4.4}$$

resulting in the additional constraint

$$f^{bc}_{iy}\,\tilde{G}^{cd}_{yx} = G^{bc}_{ij}f^{cd}_{jx}\,. \tag{4.5}$$

If a right-inverse of f exists (denoted by f^{-1}), this constraint defines the lattice symmetry generator via

$$G^{bc}_{ij} = f^{bd}_{iy}\,\tilde{G}^{de}_{yx}\,(f^{-1})^{ec}_{xj}\,. \tag{4.6}$$

[1]Note that the correlation functions of the continuum theory have to be taken with respect to the smeared fields ϕ_f in order for this statement to hold.

However, this definition does not ensure that Eq. (4.5) is fulfilled, because f^{-1} is no left inverse of f (there exists no left inverse of f since it maps from the continuum to the lattice).

The generalized Ginsparg-Wilson relation (4.3) is a deformation of the naive symmetry relation

$$G_{ij}^{bc}\phi_j^c \frac{\partial S}{\partial \phi_i^b} = 0\,, \tag{4.7}$$

which signals that the action S is invariant under the transformation generated by G. The generalized relation adds a non-trivial right hand side, which is why it is also called modified symmetry relation. It is known that there is no local lattice action with terms of higher order than quadratic that satisfies Eq. (4.7), if the generator G is a lattice derivative [18]. In this case, Eq. (4.7) means that the action has to be translationally invariant with respect to continuous shifts (generated by G). This is different from the discrete translational invariance under shifts of one lattice spacing that is usually demanded for lattice actions. We will refer to these types of translational invariance as continuous and discrete, respectively. In order to be fully supersymmetric in the naive sense, an action has to fulfill continuous translational invariance, since successive SUSY transformations can generate a translation. This is essentially how the above mentioned no-go theorem for local supersymmetric lattice actions is derived.

One may hope that the nonzero right-hand side of the generalized relation Eq. (4.3) in contrast to Eq. (4.7) allows for lattice actions that are both supersymmetric and local. The right-hand side can here be seen as a controlled breaking of SUSY on the lattice, which should vanish in the continuum limit. For the chiral symmetry, this is indeed the case, i.e., the right hand side of the Ginsparg-Wilson relation, given in Eq. (2.27), vanishes for $a \to 0$.

Solutions of Eq. (4.3) have been found for SUSYQM with a quadratic action [108]. However, it has not yet been possible to find solutions which incorporate an interaction term and thus higher orders polynomials in the fields (except for the zero mode sector with constant fields discussed in Sec. 4.1.3).

4.1.2. The relation for the anticommutator

In this Section, we consider a relation involving the anticommutator of two SUSY generators, given the lattice action under consideration fulfills Eq. (4.3) with respect to those generators. After an explicit derivation of this relation in Sec. 4.1.2.1, we consider its

consequences in Sec. 4.1.2.2.

4.1.2.1. Derivation of the relation

We assume that the action S fulfills relation (4.3) for $G = \epsilon M$ as well as $G = \bar{\epsilon}\bar{M}$. We use G as a placeholder for these two choices in the following. Here, M and $\bar{M}$ are traceless generators of SUSY transformations on the lattice, whereas ϵ and $\bar{\epsilon}$ are independent infinitesimal Grassmann numbers. Note that the latter anticommute with each other and with fermionic fields. We furthermore assume that the blocking matrix α only connects bosons with bosons and fermions with fermions, which carries over to its inverse α^{-1}.

Under an infinitesimal transformation of the fields $\phi \to \phi + G\phi$, the action becomes

$$S[(1+G)\phi] = S[\phi] + \delta S_G[\phi]\,, \tag{4.8}$$

with

$$\delta S_G[\phi] = (G\phi)^i_m \partial^b_i S = \left[(G\alpha^{-1})^S\right]^{bc}_{ij} \mathcal{D}^{cb}_{ji}\,, \tag{4.9}$$

where

$$\mathcal{D}^{cb}_{ji} = \left[(\partial^c_j S)(\partial^b_i S) - (\partial^c_j \partial^b_i S)\right]\,. \tag{4.10}$$

We introduced the notation $\partial^b_i = \partial/\partial\phi^b_i$ and the 'supersymmetrized' version of a matrix A, given by

$$A^S = \frac{1}{2}(A + A^D)\,. \tag{4.11}$$

where the 'supertranspose' is defined by

$$(A^D)^{bc}_{ij} = A^{cb}_{ij}(-1)^{|b||c|}\,. \tag{4.12}$$

The absolute value of an index is defined by $|b| = 0$ if the field ϕ^b is bosonic and $|b| = 1$ if ϕ^b is fermionic. Note that the original relation (4.3) contains $G\alpha^{-1}$ rather than $(G\alpha^{-1})^S$, but this is equivalent due to $\mathcal{D} = \mathcal{D}^S$.

We now introduce the composite transformation

$$\mathcal{T} = T_2 T_1 T_2^{-1} T_1^{-1} = (1+\epsilon M)\left(1+\bar{\epsilon}\bar{M}\right)(1-\epsilon M)\left(1-\bar{\epsilon}\bar{M}\right)\,, \tag{4.13}$$

which consists of four successive infinitesimal transformations. The action therefore transforms as

$$\begin{aligned} S[\mathcal{T}\phi] = S[\phi] + \delta S_{-\bar{\epsilon}\bar{M}}[\phi] + \delta S_{-\epsilon M}[\left(1-\bar{\epsilon}\bar{M}\right)\phi] + \delta S_{\bar{\epsilon}\bar{M}}[(1-\epsilon M)\left(1-\bar{\epsilon}\bar{M}\right)\phi] \\ + \delta S_{\epsilon M}[\left(1+\bar{\epsilon}\bar{M}\right)(1-\epsilon M)\left(1-\bar{\epsilon}\bar{M}\right)\phi]\,, \end{aligned} \tag{4.14}$$

where we successively used Eq. (4.8). After a short calculation using $\epsilon^2 = \bar{\epsilon}^2 = 0$ and the expansion

$$\begin{aligned} \delta S_{\bar{\epsilon}\bar{M}}[(1+\epsilon M)\phi] &= \delta S_{\bar{\epsilon}\bar{M}}[\phi] + (\epsilon M\phi)_i^b \partial_i^b \delta S_{\bar{\epsilon}\bar{M}}[\phi] \\ &= \bar{\epsilon}\,\delta S_{\bar{M}}[\phi] + (\bar{\epsilon}\epsilon M\phi)_i^b \partial_i^b \delta S_{\bar{M}}[\phi]\,, \end{aligned} \tag{4.15}$$

which holds equivalently for ϵM replaced by $\bar{\epsilon}\bar{M}$, we obtain

$$S[\mathcal{T}\phi] = S[\phi] - \bar{\epsilon}\epsilon\left(\Delta S_{M\bar{M}}[\phi] + \Delta S_{\bar{M}M}[\phi]\right)\,, \tag{4.16}$$

with

$$\Delta S_{M\bar{M}}[\phi] = (M\phi)_i^b \partial_i^b \delta S_{\bar{M}}[\phi]\ \text{, and} \qquad \Delta S_{\bar{M}M}[\phi] = (\bar{M}\phi)_i^b \partial_i^b \delta S_M[\phi]\,. \tag{4.17}$$

We suppress the dependencies on ϕ in the following. Using Eq. (4.9), we obtain

$$\Delta S_{M\bar{M}} = \left[(\bar{M}\alpha^{-1})^S\right]_{jk}^{cd} (M\phi)_i^b \left[(\partial_i^b\partial_k^d S)(\partial_j^c S) + (-1)^{|b||d|}(\partial_k^d S)(\partial_i^b\partial_j^c S) - (\partial_i^b\partial_k^d\partial_j^c S)\right]\,. \tag{4.18}$$

With $\delta S_M = (M\phi)_i^b \partial_i^b S$, this can be written as

$$\begin{aligned} \Delta S_{M\bar{M}} = \left[(\bar{M}\alpha^{-1})^S\right]_{jk}^{cd} \Big[&(-1)^{|d|}(\partial_k^d \delta S_M)(\partial_j^c S) + (-1)^{|d|+|c|}(\partial_k^d S)(\partial_j^c \delta S_M) \\ &- (-1)^{|d|+|c|}(\partial_k^d\partial_j^c \delta S_M) - (-1)^{|d|}(M_{ik}^{bd}\partial_i^b S)(\partial_j^c S) - (-1)^{|d|+|c|}(\partial_k^d S)(M_{ij}^{bc}\partial_i^b S) \\ &+ (-1)^{|d|+|c|}(M_{ij}^{bc}\partial_k^d\partial_i^b S) + (-1)^{|d|+|c|+|d||c|+|b||c|}(M_{ik}^{bd}\partial_i^b\partial_j^c S)\Big]\,. \end{aligned} \tag{4.19}$$

It is shown in App. A.2, that the three summands containing δS_M vanish when the sum $\Delta S_{\bar{M}M} + \Delta S_{M\bar{M}}$ is taken. Neglecting these, we obtain

$$\Delta S_{M\bar{M}} = -\left[(\bar{M}\alpha^{-1})^S \ominus M^T - M(\bar{M}\alpha^{-1})^S\right]_{ij}^{bc} \mathcal{D}_{ji}^{cb}\,, \tag{4.20}$$

where the fact that M and $\bar{M}$ only connect bosons with fermions and vice versa has

been used to simplify the sign factors. We have also introduced a new kind of matrix multiplication, defined by

$$(A \ominus B)_{ij}^{bc} = A_{ik}^{bd} \, (-1)^{|d|} B_{kj}^{dc} \, . \tag{4.21}$$

By the reformulation

$$(\bar{M}\alpha^{-1})^S \ominus M^T - M(\bar{M}\alpha^{-1})^S = \frac{1}{2} \left(\bar{M}\alpha^{-1} \ominus M^T - M\alpha^{-1} \ominus \bar{M}^T \right) - \left(M\bar{M}\alpha^{-1} \right)^S \, , \tag{4.22}$$

where we used the property $(\alpha^{-1})^D = \alpha^{-1}$ (which α^{-1} fulfills by construction), we obtain

$$\Delta S_{M\bar{M}} + \Delta S_{\bar{M}M} = \left[(\{M, \bar{M}\} \, \alpha^{-1})^S \right]_{ij}^{bc} \mathcal{D}_{ji}^{cb} \, . \tag{4.23}$$

On the other hand, the transformation $\mathcal{T}$ can be simplified due to the nilpotence of the Grassmann numbers,

$$\mathcal{T} = (1 + \epsilon M) \left(1 + \bar{\epsilon}\bar{M} \right) (1 - \epsilon M) \left(1 - \bar{\epsilon}\bar{M} \right) = 1 - \bar{\epsilon}\epsilon \{M, \bar{M}\} \, , \tag{4.24}$$

what yields

$$S[\mathcal{T}\phi] = S[(1 - \bar{\epsilon}\epsilon \left\{ M, \bar{M} \right\})\phi] = S[\phi] - \bar{\epsilon}\epsilon \left(\left\{ M, \bar{M} \right\})\phi \right)_i^b \partial_i^b S \, . \tag{4.25}$$

Combining Eqs. (4.16), (4.23) and (4.25), we obtain the final result

$$\left(\left\{ M, \bar{M} \right\} \phi \right)_i^b \partial_i^b S = \left[(\{M, \bar{M}\} \, \alpha^{-1})^S \right]_{ij}^{bc} \mathcal{D}_{ji}^{cb} \, , \tag{4.26}$$

which is exactly Eq. (4.9) with G replaced by $\{M, \bar{M}\}$. It is thus proven that the generalized Ginsparg-Wilson relation holds also for the anticommutator of two SUSY generators, if it holds for both the generators themselves. Eq. (4.26) is thus a necessary condition for a solution of the generalized Ginsparg-Wilson relation. This no great surprise, since the SUSY algebra is closed, so $\{\tilde{M}, \tilde{\bar{M}}\}$ is a generator of a symmetry of S^{co}. Furthermore, the action S inherits all symmetries of the continuum action S^{co} in the sense of relation (4.3), if S is obtained from S^{co} by a blocking procedure. However, our proof does not make direct use of the fact that S is derived from some continuum action via blocking. It only requires that the generalized Ginsparg-Wilson relation is fulfilled, which is a weaker condition. A consequence of this is that the additional constraint given

in Eq. (4.5) does not play a role[2].

4.1.2.2. Consequences of the relation for the anticommutator

In this Section, we address a fundamental problem that occurs in the solution of relation (4.3) which is associated with the relation for the anticommutator derived in Sec. 4.1.2.

As an example, we consider specific SUSY generators M and $\bar{M}$, which fulfill

$$\left\{M, \bar{M}\right\}_{ij}^{bc} \sim \delta_{bc} \nabla_{ij} \,, \tag{4.27}$$

with some lattice derivative operator ∇. This holds in a similar fashion for all supersymmetric theories, since the Poincaré algebra is a subset of the SUSY algebra (see Sec. 2.2). One of those theories is SUSYQM on the lattice (introduced in more detail in Sec. 4.2.1 below), to which Eq. (4.27) applies in this form.

Assuming the action S fulfills Eq. (4.9) with respect to those SUSY generators, Eq. (4.26) also holds and reads

$$(\nabla\phi)_i^b \, \partial_i^b S = \left[(\nabla\, \alpha^{-1})^S\right]_{ij}^{bc} \mathcal{D}_{ji}^{cb} \,. \tag{4.28}$$

This is a modified relation for continuous lattice translational symmetry, which reduces to the naive relation if the right hand side is zero. This actually happens with the usual assumptions that the derivative ∇ is antisymmetric, circulant[3] and assuming that the spatial part of α^{-1} is also circulant. In this case, we obtain

$$(\nabla\, \alpha^{-1})^S = \frac{1}{2}\nabla\, \alpha^{-1} + \frac{1}{2}\left(\nabla\, \alpha^{-1}\right)^D = \frac{1}{2}\nabla\, \alpha^{-1} + \frac{1}{2}(\alpha^{-1})^D \nabla^T = \frac{1}{2}\nabla\, \alpha^{-1} - \frac{1}{2}\nabla\alpha^{-1} = 0 \,, \tag{4.29}$$

where we used the fact that circulant matrices commute and $(\alpha^{-1})^D = \alpha^{-1}$. Thus, we are left with the naive symmetry relation, which has only non-local solutions. In order to make use of the modified relation, we therefore have to relax the assumptions we have made. This leaves us with the following choices (or combinations thereof) for the blocking matrix and the derivative operator[4] that is obtained by the anticommutator of the SUSY generators:

1. ∇ is not chosen circulant.

[2]Note however, that if M and $\bar{M}$ both fulfill the additional constraint, the latter holds also for $\{M, \bar{M}\}$ and its continuum counterpart.

[3]A circulant $N \times N$ matrix A fulfills $A_{ij} = A_{(i+1) \mod N,(j+1) \mod N}$ for all values of i and $j \in (0, N-1)$.

[4]Note that this derivative does not necessarily occur in the action of the theory.

2. α^{-1} is not chosen circulant.

3. ∇ is allowed to have a symmetric part.

At first glance, all of these are quite unnatural. The first and the second mean that the derivative in the symmetry generators respectively the blocking is not lattice translational invariant. The third option implies that even a quadratic action with discrete translational symmetry would not generally fulfill the naive symmetry relation $(\nabla\phi)_i^b\,\partial_i^b S = 0$ (in contrast to the case of an antisymmetric ∇). Nevertheless, such a quadratic action might fulfill the modified relation (4.28).

To gain insight into the consequences of the three choices, we firstly drop all of the assumptions. Furthermore, we restrict ourselves to a one-dimensional lattice theory which contains only a scalar field χ and is not supersymmetric. Therefore, the indices denoting the field species are dropped in the following. We denote the extent of the lattice by n and the spacing by a. We consider this the simplest setting in which translational invariance can be studied and assume that possible solutions of Eq. (4.28) for this theory can be generalized to supersymmetric theories. Moving to momentum space, that equation becomes

$$\nabla_{pq}\chi_{-q}\partial_p S = \gamma_{pq}\left[(\partial_q S)(\partial_p S) - (\partial_q\partial_p S)\right] , \tag{4.30}$$

where p and q denote lattice momenta, $\partial_p = \partial/\partial p$ and a sum over doubly occurring momenta is understood here and in the following. We have also introduced

$$\gamma_{pq} = (\nabla\,\alpha^{-1})^S_{pq} = \frac{1}{2}\left(\nabla_{p,-r}\alpha^{-1}_{rq} + \alpha^{-1}_{p,-r}\nabla_{qr}\right) . \tag{4.31}$$

Here, ∇ and α^{-1} are transformed to momentum space like tensors of rank two without discrete translational symmetry[5], while the field χ is transformed like a tensor of rank one. These transformations are described in App. A.1.

We assume that the action can be written as

$$S[\chi] = \sum_{D=1}^{\infty} T^{(D)}_{p_1,\ldots,p_D}\chi_{p_1}\,\cdot\,\ldots\,\cdot\,\chi_{p_D} , \tag{4.32}$$

where the tensor $T^{(D)}$ specifies the product of D-th order in the field. These tensors can be chosen symmetric in all indices without loss of generality.

[5]This is because we have dropped the constraint that these matrices are circulant.

Then, Eq. (4.30) is equivalent to the following set of constraints for the tensors $T^{(D)}$

$$T^{(D+2)}_{q,r,p_1,\ldots,p_D}\gamma_{qr} = \frac{1}{(D+2)(D+1)} \underset{p_1,\ldots,p_D}{\mathrm{SYMM}} \Bigg\{ D\, T^{(D)}_{q,p_2,\ldots,p_D} \nabla_{q,-p_1} - \gamma_{qr} \sum_{m=1}^{D+1} \left[m\, T^{(m)}_{q,p_1,\ldots,p_{m-1}} (D+2-m)\, T^{(D+2-m)}_{r,p_m,\ldots,p_D} \right] \Bigg\} , \tag{4.33}$$

which has to hold for every value of $p_1, \ldots, p_D$, while the other double indices are summed. SYMM denotes a symmetrization over all possible permutations of the momenta $p_1, \ldots, p_D$.

Starting from Eq. (4.33), we consider specific combinations of constraints for ∇ and α^{-1} in the following and analyze the consequences for the action S. We also consider polynomial solutions for the action.

4.1.2.2.1. ∇ not antisymmetric, both ∇ and α^{-1} circulant

It has been shown in Ref. [108], that the constraint (4.5) essentially means that the lattice derivative in the SUSY generators has to be of the SLAC type, i.e., $\nabla_{pq} = \delta(p+q)\, ip$. We ignore this constraint here and allow for derivatives of the form

$$\nabla_{pq} = \delta(p+q)[\nabla^S(p) + \nabla^A(p)] , \tag{4.34}$$

with a symmetric and antisymmetric part fulfilling $\nabla^S(p) = \nabla^S(-p)$ and $\nabla^A(p) = -\nabla^A(-p)$, respectively. Furthermore, α^{-1} is circulant and thus of the form $\alpha^{-1}_{pq} = \delta(p+q)\alpha^{-1}(p)$, which results in

$$\gamma_{pq} = \delta(p+q)\nabla^S(p)\alpha^{-1}(p) . \tag{4.35}$$

For a quadratic and discretely translationally invariant action, i.e., $T^{(2)}_{pq} = \delta(p+q)T^{(2)}(p)$, we obtain from Eq. (4.33)

$$T^{(2)}(p)\nabla^S(p) = 2\left[T^{(2)}(p)\right]^2 \nabla^S(p)\alpha^{-1}(p) , \tag{4.36}$$

which has to hold for all values of p (unless $\nabla^S(p) = 0$). This is solved by

$$T^{(2)}(p) = \frac{1}{2}\alpha(p) . \tag{4.37}$$

The action of the theory is therefore given by the blocking matrix. This is a problem, since in the continuum limit, the blocking matrix should be sent to infinity in order for the generalized relation to approach the naive relation. This is not possible here, because the action has to flow towards the (finite) continuum action for decreasing lattice spacing.

We assume that since not even the case of a quadratic action yields a sensible solution, this very likely also holds for actions which incorporate terms of higher order in the field.

Note that this does not rule out a Wilson mass, which is only included in the derivative operator in the action, but not in the generator of the translation. These need not be identical.

4.1.2.2.2. ∇ antisymmetric and circulant, α^{-1} not circulant

In this case, the derivative is of the form $\nabla_{pq} = \delta(p+q)\nabla(p)$ with $\nabla(p) = -\nabla(-p)$. Thus, Eq. (4.30) reads

$$\nabla(p)\chi_p\partial_p S = \gamma_{pq}\left[(\partial_q S)(\partial_p S) - (\partial_q\partial_p S)\right] \text{ , where } \quad \gamma_{pq} = \frac{1}{2}[\nabla(p) + \nabla(q)]\alpha^{-1}_{pq}\,. \quad (4.38)$$

Assuming a discretely translationally invariant action, the sum of momenta of fields in each term of S is zero (up to a projection to the first Brillouin zone, see App. A.1). Therefore, the sum of the momenta on the left hand side of Eq. (4.38) is also zero, since the derivative ∂_p removes a field of momentum p, which is restored by the multiplication of χ_p. On the right hand side, the sum of momenta can only be zero, if the momentum removed by ∂_p is the inverse of the one removed by ∂_q, i.e. $p = -q$. However, the right hand side is zero in that case, since $\gamma_{p,-p} = 0$. Thus, both sides have to be zero separately, which means that we again have to solve the naive symmetry relation.

The conclusion for this case is that the generalized Ginsparg-Wilson relation is as hard to solve as the naive symmetry relation, unless we do not demand a discretely translationally invariant action.

4.1.2.2.3. ∇ antisymmetric and not circulant, α^{-1} circulant

Here we have $\alpha^{-1}_{pq} = \delta(p+q)\alpha^{-1}(p)$ with $\alpha^{-1}(p) = \alpha^{-1}(-p)$ (since α^{-1} is symmetric) and thus

$$\gamma_{pq} = \frac{1}{2}[\alpha^{-1}(q) - \alpha^{-1}(p)]\nabla_{pq}\,. \quad (4.39)$$

Considering a discretely translationally invariant action, both sides of Eq. (4.30) contain field products whose momenta do not add up to zero. Therefore, we cannot rule out such an action as in the previous case.

4.1.2.2.4. Polynomial solutions

If a polynomial action is desired, there exists a maximum power of fields in the action denoted by Ω, so $T^{(D>\Omega)} = 0$. Given $\Omega > 2$, Eq. (4.33) is zero for $D > 2\Omega - 2$, whereas for $D = 2\Omega - 2$ it reads

$$0 = \underset{p_1,\ldots,p_{2\Omega-2}}{\text{SYMM}} \left\{ \gamma_{qr}\, T^{(\Omega)}_{q,p_1,\ldots,p_{\Omega-1}}\, T^{(\Omega)}_{r,p_\Omega,\ldots,p_{2\Omega-2}} \right\} , \tag{4.40}$$

where we have dropped the prefactors. A similar constraint has been discussed in Ref. [108] and it remains unclear if there exists a nontrivial solution.

4.1.3. Explicit blocking for SUSYQM in the continuum

In principle, a possible way of solving the generalized Ginsparg-Wilson relation is to construct an action by performing the blocking procedure defined in Eq. (4.1) explicitly. We show that this is possible for SUSYQM in the continuum (introduced in Sec. 2.2.1), where we use a slightly modified blocking that maps a continuum theory to an equivalent continuum theory rather than a lattice theory. In this blocking ansatz, the smeared fields are simply the fields of the original theory, i.e., the smearing function is $f^{ij}_{xy} = \delta_{ij}\,\delta(x-y)$, and both the original and the blocked fields live in the continuum.

For the theory of SUSYQM, the blocking can indeed be carried out analytically for the fermions and the auxiliary field. The original action is $\tilde{S}[\tilde{\Phi}]$, as given in Eq. (2.39), with the field multiplet $\tilde{\Phi}_b = \{\tilde{\chi}, \tilde{F}, \tilde{\psi}, \tilde{\bar{\psi}}\}_b$. We denote the blocked action by $S[\Phi]$, with the respective blocked field multiplet $\Phi_b = \{\chi, F, \psi, \bar{\psi}\}_b$. This action is defined via

$$e^{-S[\Phi]} = \text{SDet}^{1/2}\alpha \int D\tilde{\Phi}\, e^{-\tilde{S}[\tilde{\Phi}] - \frac{1}{2}[\Phi^b(t_1) - \tilde{\Phi}^b(t_1)]\alpha^{bc}(t_1,t_2)[\Phi^c(t_2) - \tilde{\Phi}^c(t_2)]} , \tag{4.41}$$

where sums over double indices and integrals over t_1 and t_2 are understood and we have chosen the blocking matrix of the form

$$\alpha^{bc}(t_1,t_2) = \delta(t_1 - t_2) \begin{pmatrix} b_2 & 0 & 0 & 0 \\ 0 & b_0 & 0 & 0 \\ 0 & 0 & 0 & -b_1 \\ 0 & 0 & b_1 & 0 \end{pmatrix}^{bc} . \tag{4.42}$$

We can only perform the blocking in the auxiliary and fermionic field sector analytically,

so the parameter b_2 is sent to infinity, which results in

$$\lim_{b_2\to\infty} e^{-\frac{1}{2}[\chi(t)-\tilde{\chi}(t)]b_2[\chi(t)-\tilde{\chi}(t)]} \sim \delta[\chi(t)-\tilde{\chi}(t)]\,. \tag{4.43}$$

Thus, the field $\tilde{\chi}$ is not modified by the blocking procedure and the path integral over $D\tilde{\chi}$ yields $\tilde{\chi}=\chi$. The remaining path integrals in Eq. (4.41) are Gaussian and can be performed analytically, which results in

$$\begin{aligned} S = \int dt \Bigg\{ &\frac{1}{2}(\partial_t\chi)^2 - \frac{b_0}{2(b_0-1)}F^2 - \frac{b_0}{b_0-1}FW - \frac{1}{2(b_0-1)}W^2 \\ &+\bar{\psi}\left[b_1 - b_1^2\left(\partial_t + \frac{\partial W}{\partial\chi} + b_1\right)^{-1}\right]\psi\Bigg\} - \log\det\left[\partial_t + \frac{\partial W}{\partial\chi} + b_1\right], \end{aligned} \tag{4.44}$$

where W is the same superpotential as in the definition of $\tilde{S}$, but with $\tilde{\chi}$ replaced by χ.

This blocked action has some interesting properties. In the limit $(b_0, b_1)\to\infty$, it becomes the original action $\tilde{S}$. The auxiliary field is integrated out for $b_0\to 0$, and the fermions are integrated out for $b_1\to 0$. For $b_0\to 0$ and $b_1\to\infty$, we obtain the the on-shell action given in Eq. (2.42). Furthermore, S fulfills the generalized Ginsparg-Wilson relation (4.3) modified for a continuum theory,

$$\left[G\Phi\right]^b(t_1)\frac{\partial S}{\partial\Phi^b(t_1)} = \left[G\alpha^{-1}\right]^{bc}(t_1,t_2)\left[\frac{\partial S}{\partial\Phi^c(t_2)}\frac{\partial S}{\partial\Phi^b(t_1)} - \frac{\partial^2 S}{\partial\Phi^c(t_2)\partial\Phi^b(t_1)}\right], \tag{4.45}$$

for either $G=\epsilon\tilde{M}$ or $G=\bar{\epsilon}\tilde{\bar{M}}$.

Upon integrating out the auxiliary field F and the fermions, the blocked action S becomes (up to a constant)

$$S^{\text{eff}} = \int dt\left[\frac{1}{2}(\partial_t\chi)^2 + \frac{1}{2}W^2\right] - \log\det\left[\partial_t + \frac{\partial W}{\partial\chi}\right], \tag{4.46}$$

which is exactly the same result that is obtained by integrating out the fermions and the auxiliary field from the original action $\tilde{S}$. This shows explicitly that the actions S and $\tilde{S}$ are equivalent, even if S contains different terms, depends on additional parameters b_0 and b_1, and is not naively supersymmetric. However, this result is not a surprise since the blocking procedure is defined such that it yields an equivalent theory. In lattice simulations, the fermionic fields and the auxiliary field have to be integrated out anyway. For a hypothetic lattice action that is directly obtained from a blocking procedure as considered above, one thus end with at the original action once actual computations

are performed. It therefore seems that the blocking in the fermionic and auxiliary field sector is of no great use concerning lattice simulations.

Nevertheless, we want to gain some intuition about the blocked action S. To this end, we consider constant fields, i.e. the zero mode sector of the theory. There is no distinction between continuum and lattice anymore in this case, since the dependence of the fields on time variable becomes trivial and the theory is effectively reduced to 0 dimensions. With constant fields, we have $\partial_t = 0$ and the action on a volume of V is (up to a constant)

$$\frac{S}{V} = -\frac{1}{b_0 - 1}\left[\frac{b_0}{2}F^2 + b_0 FW + \frac{1}{2}W^2\right] + \bar{\psi}\left(b_1 - \frac{b_1^2}{\frac{\partial W}{\partial \chi} + b_1}\right)\psi - \log\left(\frac{\partial W}{\partial \chi} + b_1\right). \quad (4.47)$$

In the zero mode sector, an action of SUSYQM that satisfies the generalized Ginsparg-Wilson relation has also been found in [108] by directly solving the related differential equations. The fermionic term of that action is $\lambda\bar{\psi}\chi\psi$, given in Eq. (118) of the latter reference. To match this term with the fermionic term in S, we demand

$$\frac{\partial W}{\partial \chi} + b_1 = \frac{b_1^2}{b_1 - \lambda\chi}, \quad (4.48)$$

which is solved by the superpotential

$$W = -\frac{b_1^2}{\lambda}\log\left(1 - \frac{\lambda\chi}{b_1}\right) - b_1\chi. \quad (4.49)$$

Plugged into the action (4.47) with $V = 1$, this yields

$$\begin{aligned} S = &-\frac{1}{b_0 - 1}\left\{\frac{b_0}{2}F^2 - b_0 F\left[\frac{b_1^2}{\lambda}\log\left(1 - \frac{\lambda\chi}{b_1}\right) + b_1\chi\right] + \frac{1}{2}\left[\frac{b_1^2}{\lambda}\log\left(1 - \frac{\lambda\chi}{b_1}\right) + b_1\chi\right]^2\right\} \\ &- \log\left(\frac{b_1^2}{b_1 - \lambda\chi}\right) + \lambda\bar{\psi}\chi\psi, \end{aligned} \quad (4.50)$$

which is very similar (but not identical) to the interacting solution of relation (4.3) in the zero mode sector given in Eqs. (115, 116) of [108],

$$\begin{aligned} S^{\text{ref}} = &-\frac{1}{2}F^2 + b_1\frac{1 + b_0}{b_0}\chi F - b_1^2\frac{1 + b_0}{2b_0^2}\chi^2 - b_1^4\frac{1 + b_0}{2b_0^2\lambda^2}\left[\log\left(1 - \frac{\lambda\chi}{b_1}\right)\right]^2 \\ &+ \left(1 + b_1^2\frac{1 + b_0}{b_0\lambda}F - b_1^3\frac{1 + b_0}{b_0^2\lambda}\chi\right)\log\left(1 - \frac{\lambda\chi}{b_1}\right) + \lambda\bar{\psi}\chi\psi, \end{aligned} \quad (4.51)$$

where we have set $N = a = 1$, and $a_{0,1} = 1/b_{0,1}$. Up to a constant, this action can be obtained from blocking by an $\tilde{F}$-dependent choice of the superpotential

$$W(\tilde{\chi}, \tilde{F}) = -\frac{b_1^2}{\lambda} \log\left(1 - \frac{\lambda\tilde{\chi}}{b_1}\right) - b_1\tilde{\chi} - \frac{1}{2(1+b_0)}\tilde{F}\,, \tag{4.52}$$

in the original action $\tilde{S}$. Previously, W has only been a function of the bosonic field, which has been used in the derivation of the blocked action in Eq. (4.44). However, the integral over $\tilde{F}$ is still Gaussian with this new choice of W, so the blocking can be performed analytically resulting in the desired action S^{ref}. Note that an $\tilde{F}$-dependent W only yields a supersymmetric action $\tilde{S}$ for constant fields, because the variation of $\tilde{F}$ with respect to SUSY vanishes in this case, cf. Eq. (2.41).

We have hence found that the solution of relation (4.3) in the constant field sector given in Ref. [108] can also be obtained by directly performing the blocking procedure. It therefore remains unclear whether there exist also solutions of that modified symmetry relation that cannot be obtained from blocking. This may well be possible, since that relation holds if the action under consideration is constructed by a blocking procedure, but the reverse is not necessarily true to our current knowledge.

4.2. Construction of a SUSY-improved action

The contents of this Section will be contained in an upcoming publication of the author and F. Bruckmann.

A fully supersymmetric lattice version of SUSYQM with a non-local action has been presented and numerically studied in Ref. [18]. It has been found there that the Ward identities related to all the supercharges of that theory are indeed zero, which signals a completely unbroken supersymmetry. However, the method used there to make the theory supersymmetric requires a non-local action, which causes serious problems when carried over to more realistic theories. Firstly, such an action renders the computations very costly, especially in theories that live in more than one dimension. Secondly, there may be fundamental problems with a non-local action in the continuum limit, as in the case of QED [109]. Furthermore, the mentioned method to construct the fully supersymmetric action is not generalizable to gauge theories in a straight-forward way.

We therefore follow another route, which is focused on finding a compromise between locality and SUSY, again in the framework of SUSYQM. To this end, we allow the interaction term to combine fields in a finite range and optimize the magnitude of these

combinations to minimize the breaking of continuous translational invariance. Due to the connection of SUSY and Poincaré symmetry, we assume that this also leads to an improvement of supersymmetry, which we confirm numerically. Contrary to most of the other approaches discussed above, our goal is to improve SUSY at non-zero lattice spacing rather then focusing on the continuum limit.

We organize this Section as follows. In Sec. 4.2.1, we introduce the lattice version of supersymmetric quantum mechanics. We show a way to construct a lattice model of SUSYQM which is not fully supersymmetric but improved in comparison to the naive discretization and still ultra-local, in Sec. 4.2.2. Concrete lattice models are introduced in Sec. 4.2.3, which are classified by the two different lattice derivatives we consider. Our numerical results are discussed in Sec. 4.2.4. We compute boson and fermion masses, which are degenerate for all the models. We also show that the improved models have smaller Ward identities, which indicates a smaller breaking of SUSY.

4.2.1. Supersymmetric quantum mechanics on the lattice

A lattice version of SUSYQM, which has been introduced in the continuum in Sec. 2.2.1, is obtained by discretizing the time variable t. We denote the number of lattice sites by n and the lattice spacing by a and introduce a periodic boundary condition both for fermions and bosons. All the fields acquire an index that denotes the lattice site and doubly occurring indices are implicitly summed from 0 to $n-1$. The lattice counterpart of the continuum action of SUSYQM, given in Eq. (2.39), reads

$$S = a\left[-\frac{1}{2}\chi_i(\nabla^2)_{ij}\chi_j + \bar{\psi}_i\nabla_{ij}\psi_j - \frac{1}{2}F_iF_i + \bar{\psi}_i\frac{\partial W_i}{\partial\chi_j}\psi_j - F_iW_i\right], \tag{4.53}$$

where the tilde has been removed from the fields to indicate that these are defined on the lattice. We choose a superpotential of

$$W_i = \tilde{m}_{ij}\chi_j + g\,T_{ijkl}\,\chi_j\chi_k\chi_l\,. \tag{4.54}$$

Here, ∇ is a lattice derivative, i.e., a difference operator, $\tilde{m}$ is a general mass term and the tensor T specifies the boson-fermion interaction term. g is the coupling parameter that defines the strength of that interaction. Each of these will be specified later as we construct concrete lattice models. This choice of W ensures that SUSY is not spontaneously broken in the corresponding continuum theory.

After integrating out the auxiliary field F, we obtain the on-shell lattice action

$$S^{\text{on}} = a\left[-\frac{1}{2}\chi_i(\nabla)^2_{ij}\chi_j + \bar{\psi}_i\left(\nabla_{ij} + \tilde{m}_{ij}\right)\psi_j + 3g\,T_{ijkl}\,\bar{\psi}_i\chi_j\chi_k\psi_l + \frac{1}{2}W_iW_i\right]. \tag{4.55}$$

The discretized SUSY generators M and $\bar{M}$ are obtained from their continuum counterparts defined in Eq. (2.37) via replacing the derivative ∂_t by the lattice derivative ∇. In the on-shell formulation, they yield the variation of the fields

$$M:\ \delta\bar{\psi}_i = 0\,, \qquad \delta\psi_i = -\epsilon\nabla_{ij}\chi_j + \epsilon W_i\,, \qquad \delta\chi_i = \epsilon\bar{\psi}_i\,, \tag{4.56}$$

$$\bar{M}:\ \bar{\delta}\bar{\psi}_i = \bar{\epsilon}\,\nabla_{ij}\chi_j + \bar{\epsilon}\,W_i\,, \qquad \bar{\delta}\psi_i = 0\,, \qquad \bar{\delta}\chi_i = -\bar{\epsilon}\psi_i\,. \tag{4.57}$$

The variation of the action in Eq. (4.55) with respect to these generators is

$$M:\ \epsilon\,\delta S[\chi,\bar{\psi}] = \epsilon\, g\bar{\psi}_i\left(3T_{ijkl}\chi_j\chi_k\nabla_{lm}\chi_m - \nabla_{ij}T_{jklm}\chi_k\chi_l\chi_m\right), \tag{4.58}$$

$$\bar{M}:\ \bar{\epsilon}\,\bar{\delta}S[\chi,\psi] = \bar{\epsilon}\, g\psi_i\left(3T_{ijkl}\chi_j\chi_k\nabla_{lm}\chi_m - \nabla_{ij}T_{jklm}\chi_k\chi_l\chi_m\right). \tag{4.59}$$

Contrary to the continuum theory, these variations do not vanish, as difference operators ∇ do not obey a Leibniz rule in general.

4.2.1.1. Ward identities

For SUSYQM, these exist two Ward identities associated with the SUSY generators M and $\bar{M}$. These are derived in App. A.3, and read

$$M:\ \left\langle\bar{\psi}_k\psi_l + \left(-\nabla_{lj}\chi_j + W_l\right)\chi_k\right\rangle = \left\langle\delta S[\chi,\bar{\psi}]\,\psi_l\chi_k\right\rangle, \tag{4.60}$$

$$\bar{M}:\ \left\langle\bar{\psi}_l\psi_k + \left(\nabla_{lj}\chi_j + W_l\right)\chi_k\right\rangle = \left\langle\bar{\delta}S[\chi,\psi]\,\bar{\psi}_l\chi_k\right\rangle, \tag{4.61}$$

where we have removed the Grassmann parameters ϵ and $\bar{\epsilon}$ compared to Eqs. (A.15) and (A.16). If the variations δS and $\bar{\delta}S$ of the action vanish, all the expectation values in Eqs. (4.60) and (4.61) are zero as well. Therefore, these expectation values are a measure for the breaking of supersymmetry.

There exists a connection between the two Ward identities, which can be shown as follows. We define

$$\mathcal{W}_{kl} = \left\langle\bar{\psi}_k\psi_l + \left(-\nabla_{lj}\chi_j + W_l\right)\chi_k\right\rangle, \tag{4.62}$$

$$\bar{\mathcal{W}}_{kl} = \left\langle\bar{\psi}_l\psi_k + \left(\nabla_{lj}\chi_j + W_l\right)\chi_k\right\rangle, \tag{4.63}$$

which are the expectation values on the left hand sides of Eqs. (4.60) and (4.61), respectively. The lattice action S is invariant under a time-reversal of the χ-field, i.e. a replacement $\chi_i \to \chi_{-i}$ (where $\chi_{-i} = \chi_{-i \mod n}$), after the fermions have been integrated out. Using this property and discrete lattice translational invariance, it is easily checked that $\mathcal{W}_{kl} = \bar{\mathcal{W}}_{lk}$. Because of the Ward identities, this symmetry under the exchange of the indices k and l holds also for the expectation values containing δS and $\bar{\delta} S$ in Eqs. (4.60) and (4.61).

4.2.2. Explicit method to construct the improved lattice action

Due to the connection of supersymmetry and Poincaré symmetry, a fully supersymmetric action has to be invariant under arbitrary shifts of the fields generated by the lattice derivative ∇. This is an additional requirement which is not equivalent to the invariance of the action under shifts of one lattice spacing, the latter of which all actions we consider in Sec. 4.2 fulfill. A consequence of this is that quadratic terms in the action are automatically invariant under arbitrary shifts if the lattice derivative ∇ is antisymmetric, which is usually the case. For the momentum space versions of the lattice derivative[6] ∇ and interaction tensor T, as defined in App. A.1, the invariance under arbitrary shifts is equivalent to

$$\big[\nabla(p) + \nabla(q) + \nabla(r) + \nabla(-p-q-r)\big] T(p,q,r) = 0 \tag{4.64}$$

for all possible values of the momenta p, q, and r. It is known that this equation cannot be fulfilled by a local interaction term [18]. However, one can minimize the magnitude of the left hand side with a T that is allowed to spread over a few lattice sites. This can be seen as a compromise between locality and supersymmetry. As an example we choose an ultra-local interaction tensor, which allows a hopping to the nearest neighbor, by the ansatz

$$T_{ijkl} = c_1\, \delta_{ijkl} + c_2\, \mathrm{SYMMT}\left\{\delta_{ijk,l+1}\right\} \text{ , with } c_1 + c_2 = 1\,, \tag{4.65}$$

where $\delta_{ijkl} = \delta_{ij}\delta_{ik}\delta_{il}$ and SYMMT$\{\}$ means a symmetrization in all indices and under time reversal. The approach we follow towards a small breaking of SUSY is the minimization of the quantity

$$B(T,\nabla) = \sum_{p,q,r=-\frac{\pi}{a}}^{\frac{\pi}{a}} \Big| \big[\nabla(p) + \nabla(q) + \nabla(r) + \nabla(-p-q-r)\big]\, T(p,q,r) \Big|^2 \tag{4.66}$$

[6] The lattice derivative is here considered as a tensor of rank 2.

with respect to c_1 and c_2 (for this example), where the sum is over all possible values of the momenta on the lattice (see App. A.1). For the lattice derivatives we consider, this minimization is independent of the lattice spacing, but depends weakly on the number of lattice points.

In the following, we consider a general interaction tensor T of the form

$$T_{ijkl} = \sum_{\alpha=1}^{N} c_\alpha \; T^\alpha_{ijkl} \;, \text{ with } \quad c_N = 1 - \sum_{\alpha=1}^{N-1} c_\alpha \,, \tag{4.67}$$

consisting of a number of N elementary parts T^α. In this context, we define an elementary tensor as a tensor that is the symmetrized version of just one δ function, i.e., $T^\alpha_{ijkl} = \text{SYMMT}\{\delta_{i,j+s_1^\alpha,k+s_2^\alpha,l+s_3^\alpha}\}$ with integers s_1^α, s_2^α, and s_3^α. The choice of c_N in Eq. (4.67) ensures that the sum over all c^α is 1, so that T approaches a δ function in the continuum limit. The measure for the breaking of SUSY defined in Eq. (4.66) is then

$$B(T,\nabla) = \sum_{p,q,r=-\frac{\pi}{a}}^{\frac{\pi}{a}} D(p,q,r) \left[\sum_{\alpha=1}^{N} c_\alpha \; T^\alpha(p,q,r) \right]^2 \,, \tag{4.68}$$

where we have introduced

$$D(p,q,r) = \left| \nabla(p) + \nabla(q) + \nabla(r) + \nabla(-p-q-r) \right|^2 . \tag{4.69}$$

To transform the constituents T^α of the interaction term to momentum space, we firstly have to do the symmetrizations explicitly. As an example, we consider

$$\begin{aligned} T^2_{ijkl} = \text{SYMMT}\left\{\delta_{ijk,l+1}\right\} = \frac{1}{8}\big(&\delta_{ijk,l+1} + \delta_{ij,k+1,l} + \delta_{i,j+1,kl} + \delta_{i+1,jkl} \\ &+ \delta_{ijk,l-1} + \delta_{ij,k-1,l} + \delta_{i,j-1,kl} + \delta_{i-1,jkl}\big) \,. \end{aligned} \tag{4.70}$$

In momentum space, this contribution reads according to Eq. (A.4)

$$T^2(p,q,r) = \frac{1}{4n}\big[\cos(ap) + \cos(aq) + \cos(ar) + \cos(ap+aq+ar)\big] \,. \tag{4.71}$$

The procedure is straight-forwardly generalized to other elementary contributions of the interaction term.

To find the minimum of B, we demand its first derivatives with respect to the c_β to

vanish, where $\beta = 1, \ldots, N-1$ and c_N is constrained according to Eq. (4.67). We obtain

$$\frac{dB(T,\nabla)}{dc_\beta} = \sum_{p,q,r=-\frac{\pi}{a}}^{\frac{\pi}{a}} D(p,q,r)\, T(p,q,r) \left[T^\beta(p,q,r) - T^N(p,q,r)\right] = 0\,. \tag{4.72}$$

From now on, the dependencies on the momenta p, q and r are implicitly understood and suppressed in the notation. Writing T as

$$T = \sum_{\alpha=1}^{N-1} c_\alpha \left(T^\alpha - T^N\right) + T^N\,, \tag{4.73}$$

we obtain

$$\frac{dB(T,\nabla)}{dc_\beta} = \sum_{\alpha=1}^{N-1} A_{\beta\alpha} c_\alpha + b_\beta = 0\,, \tag{4.74}$$

with the matrix

$$A_{\beta\alpha} = \sum_{p,q,r=-\frac{\pi}{a}}^{\frac{\pi}{a}} D \left(T^\alpha - T^N\right) \left(T^\beta - T^N\right) \tag{4.75}$$

and

$$b_\beta = \sum_{p,q,r=-\frac{\pi}{a}}^{\frac{\pi}{a}} D\, T^N \left(T^\beta - T^N\right)\,. \tag{4.76}$$

Solving Eq. (4.74) for c_β yields

$$c_\beta = -\sum_{\alpha=1}^{N-1} (A^{-1})_{\beta\alpha} b_\alpha\,. \tag{4.77}$$

For both improved models considered in Sec. 4.2.3 below, we have evaluated the $A_{\beta\alpha}$ and b_β in the limit $n \to \infty$. Therefore, the sum over the momenta becomes an integral that we have calculated numerically. This has to be considered the infinite volume limit, because the minimization is independent of the lattice spacing a for the lattice derivatives we have used. The final calculation of the c_β is then an elementary algebraic task.

As an estimate for the achieved improvement of the interaction tensor, we introduce

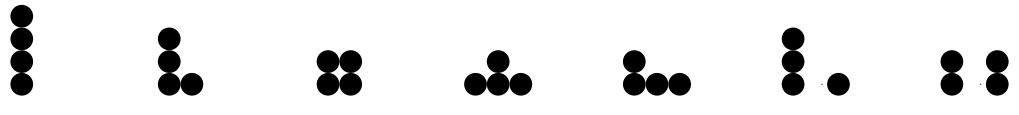

Figure 4.1.: Elementary contributions to the interaction tensor (not symmetrized with respect to time-reversal) up to a range of two lattice sites, defined in Eq. (4.82). Circles that are on top of each other are located at the same lattice site.

the quantity

$$Q(\nabla) = \frac{B(T, \nabla)}{B(T^{\text{naive}}, \nabla)}\,, \tag{4.78}$$

where $T^{\text{naive}}_{ijkl} = \delta_{ijkl}$ is the most local interaction tensor. Values of Q for the improved models are provided in the respective Sections.

4.2.3. Lattice discretizations

We consider four different discretizations based on the action given in Eq. (4.55). These contain different kinds of lattice derivatives and interaction terms which are described in detail in the following.

4.2.3.1. Naive and improved actions with the SLAC derivative

The derivative used in the first models is the SLAC derivative, which is defined in momentum space by

$$\nabla_{\text{SLAC}}(p) = ip\,. \tag{4.79}$$

This choice makes a Wilson mass obsolete as the SLAC operator has no doublers, which however comes at the cost of being non-local. Therefore, the mass matrix becomes trivial,

$$\tilde{m}_{ij} = m\,\delta_{ij}\,, \tag{4.80}$$

with the bare mass m. At first, we introduce the 'naive SLAC model', whose interaction tensor is given by

$$T^{\text{naive}}_{ijkl} = \delta_{ijkl}\,. \tag{4.81}$$

Secondly we construct an improved model with an interaction tensor that contains products of fields which are up to two lattice sites apart. Demanding symmetry and time-

reversal invariance, this tensor contains the contributions

$$\begin{aligned} T^1_{ijkl} &= \delta_{ijkl}\,, & T^2_{ijkl} &= \mathrm{SYMMT}\left\{\delta_{ijk,l+1}\right\}\,, \\ T^3_{ijkl} &= \mathrm{SYMMT}\left\{\delta_{ij,k+1,l+1}\right\}\,, & T^4_{ijkl} &= \mathrm{SYMMT}\left\{\delta_{i,j+1,k+1,l+2}\right\}\,, \\ T^5_{ijkl} &= \mathrm{SYMMT}\left\{\delta_{ij,k+1,l+2}\right\}\,, & T^6_{ijkl} &= \mathrm{SYMMT}\left\{\delta_{ijk,l+2}\right\}\,, \\ T^7_{ijkl} &= \mathrm{SYMMT}\left\{\delta_{ij,k+2,l+2}\right\}\,, \end{aligned} \tag{4.82}$$

where again SYMMT{} induces a symmetrization of all indices and under time reversal. The shape of these contributions is schematically depicted in Fig. 4.1. The interaction tensor thus reads

$$T_{ijkl} = \sum_{\alpha=1}^{7} c_\alpha\, T^\alpha_{ijkl}\,, \text{ with } \quad \sum_{\alpha=1}^{7} c_\alpha = 1\,. \tag{4.83}$$

The coefficients c_α have been determined as described in Sec. 4.2.2, resulting in

$$\begin{aligned} &c_1 = 0.0754\,; && c_2 = 0.3389\,; && c_3 = 0.2057\,; && c_4 = 0.1687\,; \\ &c_5 = 0.1597\,; && c_6 = 0.0421\,; && c_7 = 0.0095\,. \end{aligned} \tag{4.84}$$

We refer to this choice of the interaction tensor as the 'improved SLAC model'. This model yields an improvement of $Q(\nabla_{\mathrm{SLAC}}) \approx 2.3 \cdot 10^{-6}$ as defined in Eq. (4.78).

4.2.3.2. Naive and improved actions with a Wilson mass

In these models, we insert a symmetric difference operator into the action, which is defined by

$$(\nabla_{\mathrm{symm}})_{ij} = \frac{1}{2a}\left(\delta_{i+1,j} - \delta_{i-1,j}\right)\,. \tag{4.85}$$

A Wilson mass has to be included to remove the doublers, so the mass matrix is

$$\tilde{m}_{ij} = m\,\delta_{ij} - \frac{ra}{2}\left(\delta_{i+1,j} - 2\delta_{ij} + \delta_{i-1,j}\right)\,, \tag{4.86}$$

where we have chosen $r = 1$ for the Wilson mass parameter. For the 'naive Wilson model', we have inserted the naive interaction term as defined in Eq. (4.81). The contributions to the improved interaction term are again the ones from Eq. (4.82). This time, the constants that are obtained by a minimization of $B(T, \nabla_{\mathrm{symm}})$ are

$$\begin{aligned} &c_1 = 0.0414\,; && c_2 = 0.2349\,; && c_3 = 0.1668\,; && c_4 = 0.2265\,; \\ &c_5 = 0.2014\,; && c_6 = 0.1133\,; && c_7 = 0.0157\,; \end{aligned} \tag{4.87}$$

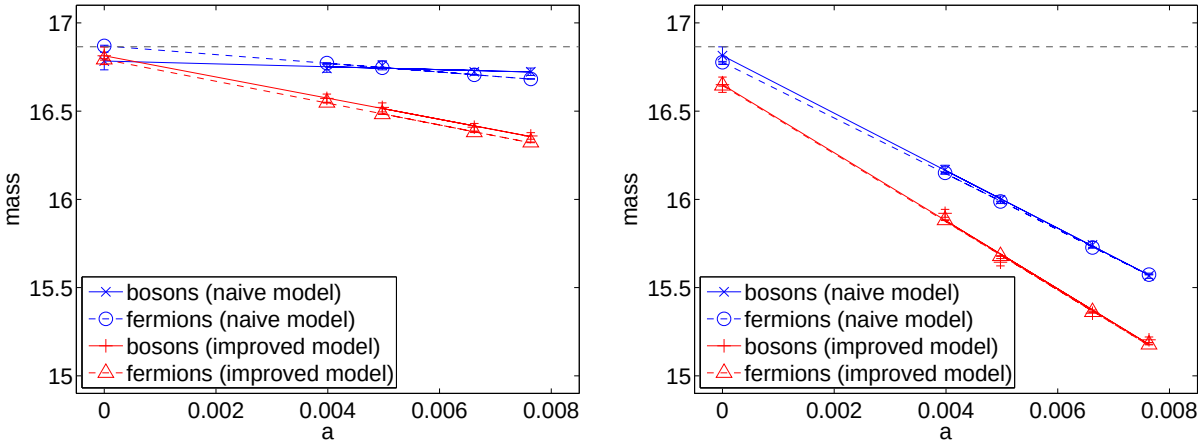

Figure 4.2.: Masses for the SLAC models (left) and Wilson models (right) for $m = 10$ and $g = 100$. The linear fits have been obtained by minimized square deviation. The horizontal dashed line is the exact continuum mass (= 16.865).

We call the model that results from this choice the 'improved Wilson model'. Here, we obtained a improvement of $Q(\nabla_{\text{symm}}) \approx 5.2 \cdot 10^{-4}$ as defined in Eq. (4.78).

4.2.4. Numerical results

In this Section, we give the numerical results for the masses and Ward identities we have measured with the actions defined in Sec. 4.2.3. For each model, we have chosen a bare mass of $m = 10$ and a volume of $na = 1$, which ensures that the Compton wavelength of the lowest mode fits easily into the volume. All the configurations for the χ-field have been obtained by a Hybrid Monte Carlo algorithm (see Sec. 2.3.2). The effective action we have used for this algorithm is obtained by integrating out the fermions from the on-shell action defined in Eq. (4.55), with the result

$$S^{\text{eff}} = a \left[-\frac{1}{2}\chi_i (\nabla)^2_{ij} \chi_j + \frac{1}{2} W_i W_i \right] - \log \det M \,, \tag{4.88}$$

where the fermion matrix is given by

$$M_{ij} = \nabla_{ij} + \tilde{m}_{ij} + 3g\, T_{ijkl} \chi_k \chi_l \,. \tag{4.89}$$

For further details on the creation of the configurations, the reader is referred to Ref. [110], where the same Hybrid Monte Carlo algorithm has been used.

model	$m_{\text{boson}}^{\text{continuum}}$	$m_{\text{fermion}}^{\text{continuum}}$
naive SLAC	16.784 (94)	16.870 (5)
improved SLAC	16.813 (50)	16.793 (4)
naive Wilson	16.815 (50)	16.778 (5)
improved Wilson	16.650 (43)	16.645 (4)
exact	16.865	16.865

Table 4.1.: Continuum mass extrapolations for the various actions.

4.2.4.1. Masses

According to previous works, the naive SLAC model [110] as well as the naive Wilson model [103] defined in Sec. 4.2.3 should have degenerate boson and fermion masses. In order to check this and to see if it holds also for the improved models, we have calculated these masses for all the models we have defined. To this end, the propagators $\langle\bar{\psi}_0\psi_k\rangle$ for the fermion and $\langle\chi_0\chi_k\rangle$ for the boson have been computed. The fermionic bilinears in the expectation values are replaced by a matrix element of the inverse fermionic matrix M when $\bar{\psi}$ and ψ are integrated out. For the lattice sizes we consider, this matrix can be obtained by standard numerical methods. The masses have been obtained by linear fits to the respective propagator in a logarithmic representation as described in [110]. Unlike there, we use a simple Gaussian filter[7] to smoothen the fermionic propagator for the SLAC models, because more complicated filters have given only negligibly different results.

We have chosen a coupling constant of $g = 100$, which is in the regime of strong coupling, to be able to compare our results with previous works which have used the same value of g. For each lattice size and model an ensemble of 10^6 configurations has been created, which is sufficient to obtain small errors for the propagators. As shown in Fig. 4.2, fermion and boson masses are fairly equal inside the error bars for all models and lattice spacings. For the naive SLAC model, the masses are compatible to the ones obtained in [110], where the same model has been considered. This holds also for the masses of the naive Wilson model, which were computed in [103]. The values of the respective continuum extrapolations, which have been determined by a linear fit with minimized square deviation, are given in Tab. 4.1.

The (degenerate) exact continuum mass can easily be obtained by a numerical treatment of the Hamiltonian of SUSYQM given in Eq. (2.44) [110]. We observe that both naive models are closer to this continuum mass for all values of the lattice spacing. The reason for this is presumably the larger extension of the interaction term in the improved

[7]Defined by the replacement of the propagator $\langle\bar{\psi}_0\psi_k\rangle \to c\sum_l e^{-(k-l)^2/2}\langle\bar{\psi}_0\psi_l\rangle$, with $c = 1/\sum_k e^{-k^2/2}$.

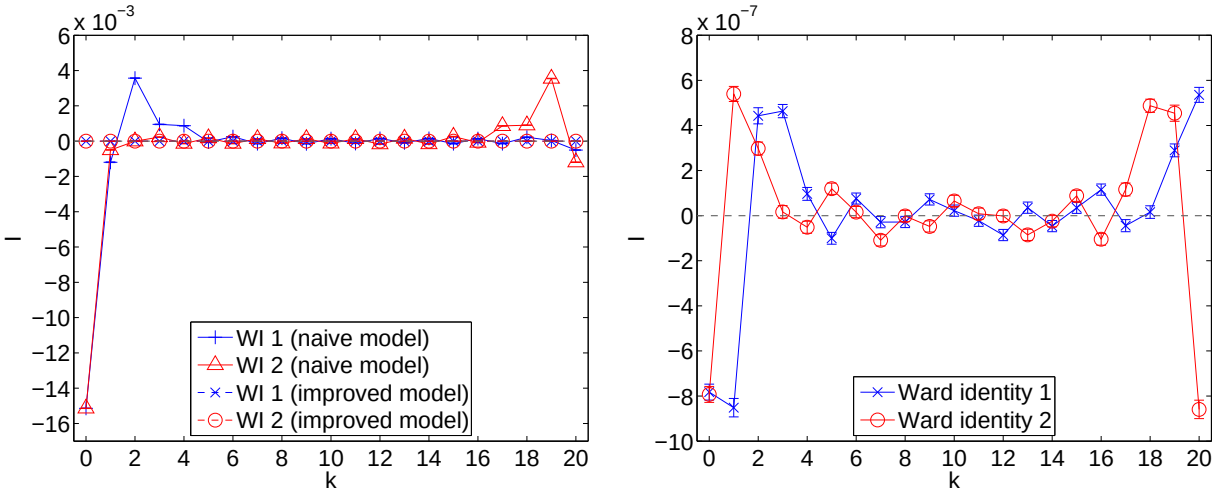

Figure 4.3.: Functions I associated with the Ward identities, defined in Eq. (4.90) and Eq. (4.91) for both SLAC models (left) and the improved SLAC model alone (right) for $n = 21$, $m = 10$ and $g = 800$. Note the different scales of the axes.

models, as the extension is zero in the continuum. This seems to be the prize one has to pay for the improved supersymmetry. However, the masses of the improved models also clearly flow towards the correct continuum mass, even if the linear extrapolations may not exactly hit that value.

4.2.4.2. Ward identities

For all models, we have computed two quantities associated with the two Ward identities (WIs) discussed in Sec. 4.2.1.1,

$$\text{WI 1:} \quad I_1(k) = \left\langle \bar{\psi}_k \psi_0 + (-\nabla_{0j}\chi_j + W_0)\,\chi_k \right\rangle = \left\langle \delta S[\chi, \bar{\psi}]\,\psi_0 \chi_k \right\rangle , \tag{4.90}$$

$$\text{WI 2:} \quad I_2(k) = \left\langle \bar{\psi}_0 \psi_k + (\nabla_{0j}\chi_j + W_0)\,\chi_k \right\rangle = \left\langle \bar{\delta} S[\chi, \psi]\,\bar{\psi}_0 \chi_k \right\rangle . \tag{4.91}$$

Here, we have set the index l in Eqs. (4.60) and (4.61) to zero without loss of generality, because these expectation values are only functions of the difference $l - k$ because of lattice translational invariance. Due to the Ward identities, each of the the functions I_1 and I_2 is equally well defined by the expectation values of two different observables, see Eqs. (4.90) and (4.91). Both of these observables can be measured on the lattice. In the plots addressed below, we show only the expectation values related to δS and $\bar{\delta} S$, because these suffer from far smaller numerical errors. However, we have checked that the respective other expectation value belonging to the same Ward identity is equal within the error bars. Due to the connection between the Ward identities explained in

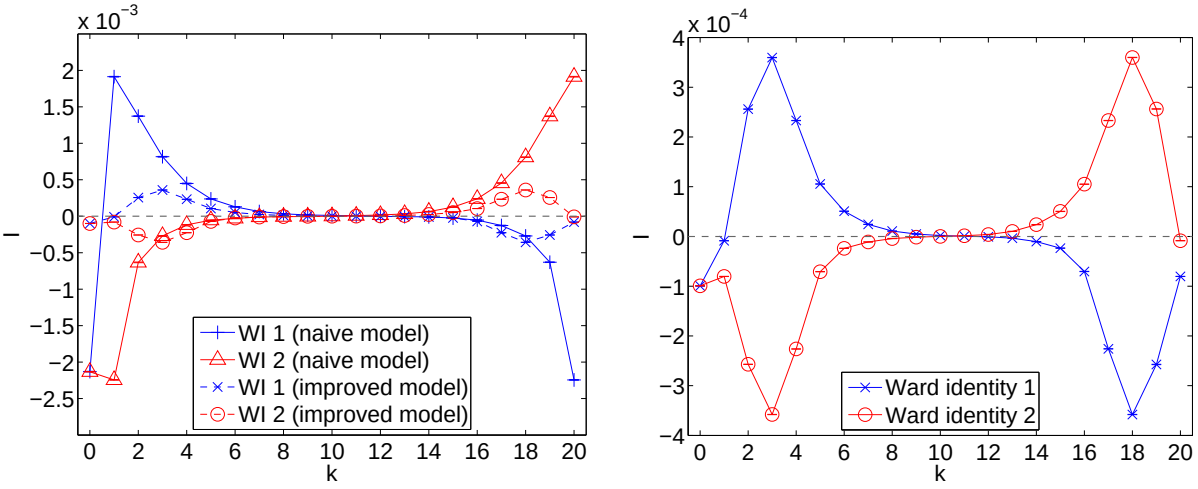

Figure 4.4.: Functions I associated with the Ward identities, defined in Eq. (4.90) and Eq. (4.91) for both Wilson models (left) and the improved Wilson model alone (right) for $n = 21$, $m = 10$ and $g = 800$. Note the different scales of the axes.

Sec. 4.2.1.1, the functions I_1 and I_2 are related via $I_1(k) = I_2(-k \mod n)$. We have chosen a very strong coupling of $g = 800$ and a small lattice size of $n = 21$ for all the models to have a strongly broken SUSY in the naive models.

As shown in Fig. 4.3, the scale of the Ward identities in the improved SLAC model is smaller by four orders of magnitude compared to the naive model. The number of configurations is 10^7 for the naive SLAC model and 10^8 for the improved SLAC model. In the latter case, better statistics are required to get reliable results due to the small value of the Ward identities.

The same Ward identities have been computed for the Wilson models. They are shown in Fig. 4.4, where again 10^7 field configurations have been evaluated for the naive model and 10^8 for the improved model. There clearly is an improvement, which however is much less than in the SLAC model. One reason for this could be the different values of Q that have been achieved, because these differ by two orders of magnitude. Presumably, the SLAC derivative is also more suited to allow for a supersymmetric interaction term in the first place. This assumption is backed by the fact that the only possible construction of an exactly supersymmetric lattice action with interaction requires the use of the SLAC derivative [18].

5. Summary and conclusions

5.1. Analysis of quark spectra on the lattice with two-color QCD

We have studied quenched $SU(2)$ lattice QCD in the deconfined phase at high temperature. For the same setting, previous works have shown that the low eigenmodes of the overlap and the staggered Dirac operator are localized and the corresponding eigenvalues are uncorrelated. These effects vanish for larger eigenvalues, i.e., those are correlated according to RMT predictions and their eigenmodes delocalize.

We have shown that there is a correlation between the localized low eigenmodes of the two mentioned Dirac operators in the sense that these eigenmodes are placed in the same volumes in space-time (for the same gauge configurations). Furthermore, we have found that the low eigenmodes of the Dirac operators are attracted by small local Polyakov loops. This means that both the staggered and the overlap operator are sensitive to the same physical structure in the gauge background. A possible explanation for this finding is that the small Polyakov loops create small local Matsubara frequencies. Those can compensate for the anti-periodic fermionic boundary conditions and thus trap low eigenmodes.

These observations have motivated a new kind of random matrix model for the staggered Dirac operator. This model is based on a decomposition of that operator into a part containing temporal and a part containing spatial derivatives. In the eigenbasis of the temporal component, the staggered operator takes a form similar to a condensed matter Hamiltonian in three dimensions, with an on-site potential and next-neighbor interactions. Here, the potential emerges from the local traced Polyakov loops. As we have found, these are only weakly correlated, and can therefore provide the Poissonian ingredient at the low end of the spectrum.

Hence, we have constructed a random matrix model with a (chiral) on-site potential consisting of uncorrelated entries. The distribution of the latter has been chosen so as to match the distribution of local Polyakov loops obtained from lattice data. Addition-

ally, uncorrelated Gaussian random numbers have been introduced to mimic the three dimensional next-neighbor interactions. As we have numerically verified, this model reproduces the important properties of the Dirac spectra mentioned above, i.e., there is a gap, localized low modes and a transition from Poissonian to RMT spectral statistics. For future investigations, it would be interesting to solve the random matrix model analytically and to compare further predictions of the model to lattice data. Furthermore, the random matrix model could be adapted to the more realistic case of three-color QCD with dynamical quarks. In this setting, some of the phenomena discussed above (localization of low modes and a transition from Poisson to RMT statistics) have recently been found in the spectrum of the Dirac operator [60].

We have also studied lattice QCD at non-zero quark density, where we have firstly made some general considerations about spectra of real weakly non-Hermitian matrices. We have shown that the eigenvalues of real symmetric matrices attract each other under weak antisymmetric perturbations. The eigenvalues stay real until two of them meet and form a complex conjugate pair that moves out into the complex plane. We have identified three different kinds of level spacings, those between the conjugate pairs which we call off axis, and spacings on the real axis with or without an interspaced complex pair. For each of those kinds, we have derived a surmise for the spacing distribution from small real Gaussian random matrices with a tunable degree of non-hermiticity. The surmise for the on-axis spacings without interspaced pair is identical to the GOE surmise. For the other kinds of spacings, we obtain formulas that depend on the magnitude of the antisymmetric part via a real parameter.

These surmises approximate the spacing distributions of large Gaussian random matrices in the regime of weak anti-hermiticity very well. For the spacings in the bulk of the overlap Dirac operator of quenched two-color QCD with small chemical potential, they provide equally good approximations. This is expected due to the anti-unitary symmetry and hermiticity properties of the overlap operator. For on-axis spacings with an interspaced pair the surmise parameter has been obtained by a fit to the numerically obtained spacing distributions. For the off-axis spacings, this parameter has been predicted by matching the frequency of those spacings between surmise and data.

We have also measured spacing distributions for two-color QCD with imaginary chemical potential and verified that they follow a mixed-symmetry surmise.

In contrast to the joint probability density of the eigenvalues, the spacing distributions of the large random matrices we have considered have not been worked out analytically. However, the analytic surmises provide sufficient approximations for those matrices as

well as two-color QCD in the regime of weak non-hermiticity, as we have shown.

A conclusion for the QCD part of this work is that random matrix theory has once again proven its power to describe eigenvalue correlations in quark spectra. For QCD at high temperature, the ensembles from chiral RMT do not work in the low end of the spectrum. However, we have shown that a random matrix model of a similar structure like a condensed matter Hamiltonian reproduces many features of the low-lying quark spectrum for quenched two-color QCD. As mentioned above, it would be promising to modify this random matrix model in order to describe three-color QCD.

In the case of a non-zero chemical potential, our findings certainly cannot be carried over to three-color QCD (unless the staggered operator with adjoint gauge links is considered). This is because the anti-unitary symmetries of the Dirac operator are different for $SU(3)$ gauge links. However, we assume that the surmises we have derived for the spacing distributions apply also to the case of dynamical two-color QCD. Further applications are likely to be found in completely different physical systems with the same anti-unitary symmetries and in the regime of weak non-hermiticity, as encountered e.g. in quantum scattering [94].

5.2. Supersymmetry on the lattice

We have studied the blocking approach to lattice SUSY. At first, we have considered the generalized Ginsparg-Wilson relation, which can be seen as a modified symmetry relation for a lattice theory. We have derived a necessary condition for a supersymmetric action on the lattice to fulfill this relation. Furthermore, we have shown that this condition is as hard to solve as the naive symmetry relation, when the lattice derivative and the blocking matrix fulfill certain common constraints. We have explicitly dropped those constraints and discussed the consequences.

For SUSYQM in the continuum, we have considered a blocking in the fermionic and auxiliary field sector, which can be carried out analytically. The resulting blocked action depends on two additional parameters and interpolates between the on-shell and the off-shell action, but it is completely equivalent to the original action. This can be seen explicitly by integrating out the fermions and the auxiliary field, in which case both actions coincide. For numerical simulations, where these integrations have to be carried out analytically anyway, we thus obtain no new equivalent actions with this kind of blocking. In the zero mode sector, i.e. with constant fields, we have furthermore discussed the connection between the blocked action and a known solution of the generalized

Ginsparg-Wilson relation.

We conclude our considerations about the blocking approach to lattice supersymmetry with the following remarks. While we have not been able to solve the generalized Ginsparg-Wilson relation for the case of SUSY, we have at least enlightened some of the related problems. We have shown that some common assumptions have to be dropped in order to allow for a sensible solution of the mentioned relation. It remains an open question whether an action that is suited for numerical computations can be found as a solution of that relation.

We have also constructed lattice actions of supersymmetric quantum mechanics which are improved with respect to SUSY and compared them to naive discretizations. One type of model contains the SLAC derivative in the kinetic terms of the action, while the other incorporates the naive symmetric difference operator and consequently a Wilson mass term. We have made a compromise between supersymmetry and locality by allowing the interaction term of the improved actions to connect fields in a finite range of two lattice spacings or less. Via numerical lattice simulations we have determined boson and fermion masses which have turned out to be degenerate for each model. The masses of the naive models are closer to the exact continuum mass than the masses of the improved models for all values of the lattice spacing. However, all models show a clear tendency towards the correct value in the continuum limit. To quantify the breaking of supersymmetry, we have also measured Ward identities, which are much smaller for the improved models than for the naive ones. We therefore conclude that the improved actions indeed have better properties with respect to SUSY, which comes at the cost of a slower convergence of the masses in the continuum limit.

The method we have developed to construct improved lattice actions could also be applied to higher dimensional Wess-Zumino type models. This would not render numerical simulations overly expensive, because the interaction terms we have used are ultra-local. Our method can also be generalized to interaction terms which are polynomials of higher rank or have a higher range in a straight-forward way. Therefore, this method could be an ingredient for the construction of supersymmetric lattice actions of more realistic models than SUSYQM, possibly in combination with other improvement techniques.

A. Appendix

A.1. Fourier transforms

We define the Fourier transform of a lattice tensor $T_{j_1,\ldots,j_M}$ of rank M by

$$T_{p_1,\ldots,p_M} = n^{-\frac{M}{2}} \sum_{j_1,\ldots,j_M=0}^{n-1} T_{j_1,\ldots,j_M}\; e^{ia\sum_{k=1}^{M} p_k j_k}\,, \tag{A.1}$$

where is the n number of sites and a the spacing of the resp. lattice. The momenta can take values of

$$p = \frac{2\pi}{na}\, z \text{ , with } \quad \begin{cases} z \in \mathrm{Z} = -\frac{n-1}{2}, \ldots, \frac{n-1}{2} & \text{for } n \text{ odd,} \\ z \in \mathrm{Z} = -\frac{n}{2}, \ldots, \frac{n}{2} - 1 & \text{for } n \text{ even.} \end{cases} \tag{A.2}$$

In this work, we often consider tensors which are discretely translational invariant, i.e. invariant under an increase of all their indices by one, in which case we obtain

$$T_{p_1,\ldots,p_M} = \delta_P\left(\sum_{i=1}^{M} p_i\right) T(p_1,\ldots,p_{M-1})\,, \tag{A.3}$$

with the reduced form of T, given by

$$T(p_1,\ldots,p_{M-1}) = n^{-\frac{M}{2}+1} \sum_{j_1,\ldots,j_{M-1}=0}^{n-1} T_{j_1,\ldots,j_{M-1},0}\; e^{ia\sum_{k=1}^{M-1} p_k j_k}\,. \tag{A.4}$$

We have also introduced a periodic δ function, defined by

$$\delta_P(q) = \delta\left[\mathrm{BZ}(q)\right] \text{ , with } \qquad \mathrm{BZ}(q) = -\frac{\pi}{a} + \left(q + \frac{\pi}{a}\right) \bmod \frac{2\pi}{a}\,. \tag{A.5}$$

BZ denotes the projection to the first Brillouin zone.

We use the bracket notation for the arguments of reduced tensors as in Eq. (A.4), and the index notation for non-reduced tensors as in Eq. (A.1).

A.2. Remaining calculations for Sec. 4.1.2.1

We claimed that the terms contributing to $\Delta S_{M\bar{M}}$ given in Eq. (4.19) containing δS_M vanish, if $\Delta S_{\bar{M}M}$, i.e., the same terms with M and $\bar{M}$ exchanged, are added. The former terms read

$$\begin{aligned}&\left[(\bar{M}\alpha^{-1})^S\right]_{ij}^{bc}\left[(-1)^{|c|}(\partial_j^c\delta S_M)(\partial_i^b S)+(-1)^{|b|+|c|}(\partial_j^c S)(\partial_i^b\delta S_M)-(-1)^{|b|+|c|}(\partial_j^c\partial_i^b\delta S_M)\right]\\&=-\left[(\bar{M}\alpha^{-1})^S\right]_{ij}^{bc}\left[(\partial_i^b S)(\partial_j^c\delta S_M)+(\partial_j^c S)(\partial_i^b\delta S_M)-(\partial_j^c\partial_i^b\delta S_M)\right]\,,\end{aligned}\tag{A.6}$$

where we have used that $|b|+|c|=1$ (otherwise, $\left[(\bar{M}\alpha^{-1})^S\right]_{ij}^{bc}$ is zero). We insert

$$(\partial_i^b\delta S_M)=\left[(\bar{M}\alpha^{-1})^S\right]_{kl}^{de}\left[(\partial_i^b\partial_l^e S)(\partial_k^d S)+(\partial_i^b\partial_k^d S)(\partial_l^e S)-(\partial_i^b\partial_l^e\partial_k^d S)\right]\,,\tag{A.7}$$

and obtain

$$\begin{aligned}\left[(\bar{M}\alpha^{-1})^S\right]_{ij}^{bc}\left[(M\alpha^{-1})^S\right]_{kl}^{de}\;&\big\{(\partial_i^b S)(\partial_j^c\partial_l^e S)(\partial_k^d S)+(\partial_j^c S)(\partial_i^b\partial_k^d S)(\partial_l^e S)\\&+(\partial_i^b S)(\partial_j^c\partial_k^d S)(\partial_l^e S)+(\partial_j^c S)(\partial_i^b\partial_l^e S)(\partial_k^d S)\\&-(\partial_i^b S)(\partial_j^c\partial_l^e\partial_k^d S)-(\partial_j^c\partial_i^b\partial_l^e S)(\partial_k^d S)\\&-(\partial_j^c S)(\partial_i^b\partial_l^e\partial_k^d S)-(\partial_j^c\partial_i^b\partial_k^d S)(\partial_l^e S)\\&-(-1)^{|c|}(\partial_i^b\partial_l^e S)(\partial_k^d\partial_j^c S)-(-1)^{|c|}(\partial_i^b\partial_k^d S)(\partial_l^e\partial_j^c S)\\&+(\partial_j^c\partial_i^b\partial_l^e\partial_k^d S)\big\}\,.\end{aligned}\tag{A.8}$$

All terms in the curly brackets in each separate line are antisymmetric under the simultaneous exchange of the index pairs $(b,i)\leftrightarrow(d,k)$ and $(c,j)\leftrightarrow(e,l)$, what is equivalent to the exchange of $M\leftrightarrow\bar{M}$. Therefore, they vanish in the sum $\Delta S_{M\bar{M}}+\Delta S_{\bar{M}M}$.

A.3. Derivation of the Ward identities

To obtain Ward identities, we consider the generating functional of SUSYQM on the lattice, defined by

$$Z[J]=\frac{1}{\mathcal{N}}\int D\Phi\; e^{-S[\Phi]+J_i^b\Phi_i^b}\,,\tag{A.9}$$

with the action S defined in Eq. (4.53), the field multiplet $\Phi_i^b=\{\chi_i,F_i,\psi_i,\bar{\psi}_i\}^b$ and the currents J. The index i labels the lattice sites, while the index b labels the field species. Doubly occurring indices are implicitly summed over. $\mathcal{N}$ is the partition function defined

by

$$\mathcal{N} = \int D\Phi \; e^{-S[\Phi]} \,. \tag{A.10}$$

An infinitesimal transformation of the fields

$$\Phi_i^b \to \Phi_i^b + (\delta\Phi)_i^b = \Phi_i^b + G_{ij}^{bc}\Phi_j^c \,, \tag{A.11}$$

with the infinitesimal generator G, yields to leading order

$$\begin{aligned} Z[J] &\to \frac{1}{\mathcal{N}} \int D\Phi \, \mathrm{SDet}\,[1+G] \, e^{-S[\Phi]-\delta_G S[\Phi]+J_i^b(\Phi_i^b+G_{ij}^{bc}\Phi_j^c)} \\ &\approx Z[J](1+\mathrm{STr}[G]) + \frac{1}{\mathcal{N}} \int D\Phi \left(J_i^b G_{ij}^{bc}\Phi_j^c - \delta_G S[\Phi]\right) e^{-S[\Phi]+J_m^f\Phi_m^f} \,, \end{aligned} \tag{A.12}$$

where $\delta_G S$ is the variation of the action with respect to the transformation. This has to be equal to $Z[J]$, because the transformation is equivalent to a mere change of variables in the path integral. For a traceless G, we can therefore conclude

$$\frac{1}{\mathcal{N}} \int D\Phi \left(J_i^b G_{ij}^{bc}\Phi_j^c - \delta_G S[\Phi]\right) e^{-S[\Phi]+J_m^f\Phi_m^f} = 0 \,. \tag{A.13}$$

Ward identities are obtained by deriving this expression with respect to currents and setting these to zero, e.g.

$$\begin{aligned} &\frac{\partial}{\partial J_k^d}\frac{\partial}{\partial J_l^e}\left[\frac{1}{\mathcal{N}} \int D\Phi \left(J_i^b G_{ij}^{bc}\Phi_j^c - \delta_G S[\Phi]\right) e^{-S[\Phi]+J_m^f\Phi_m^f}\right]_{J=0} \\ &= \frac{1}{\mathcal{N}} \int D\Phi \left(- \delta_G S[\Phi]\Phi_k^d\Phi_l^e + G_{ki}^{db}\Phi_i^b\Phi_l^e + \Phi_k^d G_{li}^{eb}\Phi_i^b\right) e^{-S[\Phi]} \\ &= \frac{1}{\mathcal{N}} \int D\Phi \left(- \delta_G S[\Phi]\Phi_k^d\Phi_l^e + (\delta\Phi)_k^d\Phi_l^e + \Phi_k^d(\delta\Phi)_l^e\right) e^{-S[\Phi]} = 0 \,. \end{aligned} \tag{A.14}$$

The infinitesimal generator is either $G = \epsilon M$ or $G = \bar{\epsilon}\bar{M}$, whose action is defined in Eqs. (4.56) and (4.57). We specify $\Phi_k^d = \chi_k$ and $\Phi_l^e = \psi_l$ or $\bar{\psi}_l$, to obtain the Ward identities (in the on-shell formulation)

$$M: \;\; \epsilon \left\langle \bar{\psi}_k\psi_l + (-\nabla_{lj}\chi_j + W_l)\,\chi_k \right\rangle = \epsilon \left\langle \delta S[\chi,\bar{\psi}]\,\psi_l\chi_k \right\rangle , \tag{A.15}$$

$$\bar{M}: \;\; \bar{\epsilon} \left\langle \bar{\psi}_l\psi_k + (\nabla_{lj}\chi_j + W_l)\,\chi_k \right\rangle = \bar{\epsilon} \left\langle \bar{\delta} S[\chi,\psi]\,\bar{\psi}_l\chi_k \right\rangle , \tag{A.16}$$

where δS and $\bar{\delta} S$ are given in Eq. (4.58) and Eq. (4.59), respectively, and the average is defined by the path integral, i.e.,

$$\left\langle O[\chi, \bar{\psi}, \psi] \right\rangle = \frac{1}{\mathcal{N}} \int D\chi D\psi D\bar{\psi}\; O[\chi, \psi, \bar{\psi}]\; e^{-S^{\mathrm{on}}[\chi, \psi, \bar{\psi}]} \,. \tag{A.17}$$

Bibliography

[1] ATLAS Collaboration, submitted to Phys. Lett. B (2012), 1207.7214v1 .

[2] CMS Collaboration, submitted to Phys. Lett. B (2012), 1207.7235v1 .

[3] P. W. Higgs, Phys. Rev. Lett. **13**, 508 (1964).

[4] D. J. Gross and F. Wilczek, Phys. Rev. Lett. **30**, 1343 (1973).

[5] K. Fukushima and T. Hatsuda, Rept. Prog. Phys. **74**, 014001 (2011), 1005.4814v2 .

[6] L. Susskind, Phys. Rep. **104**, 181 (1984).

[7] G. Bertone, D. Hooper, and J. Silk, Phys. Rept. **405**, 279 (2005), hep-ph/0404175v2 .

[8] top500.org (June 2012).

[9] top500.org (November 1999).

[10] C. Alexandrou, PoS **LAT2010**, 001 (2010), 1011.3660 .

[11] O. Philipsen, arXiv.org (2012), 1207.5999v1 .

[12] H. Nielsen and M. Ninomiya, Nucl. Phys. **B185**, 20 (1981).

[13] R. Narayanan and H. Neuberger, Nucl. Phys. **B412**, 574 (1994), hep-lat/9307006 .

[14] R. Narayanan and H. Neuberger, Nucl. Phys. **B443**, 305 (1995), hep-th/9411108 .

[15] H. Neuberger, Phys. Lett. **B417**, 141 (1998), hep-lat/9707022 .

[16] J. Giedt, PoS **LAT2006**, 008 (2006), hep-lat/0701006 .

[17] S. Catterall, PoS **LAT2010**, 002 (2010), 1010.6224 .

[18] G. Bergner, JHEP **1001**, 24 (2010), 0909.4791v2 .

[19] M. E. Peskin and D. V. Schroeder, *An Introduction to Quantum Field Theory*, 1st ed. (Perseus Books, 1995).

[20] HotQCD Collaboration, Phys. Rev. **D85**, 054503 (2012), 1111.1710v2 .

[21] C. Gattringer and C. B. Lang, *Quantum Chromodynamics on the Lattice: An Introductory Presentation, Lect. Notes Phys. 788* (Springer, Berlin Heidelberg, 2010).

[22] K. G. Wilson, Phys. Rev. **D10**, 2445 (1974).

[23] J. Kogut and L. Susskind, Phys. Rev. **D11**, 395 (1975).

[24] F. Gliozzi, Nucl. Phys. **B204**, 419 (1982).

[25] P. H. Ginsparg and K. G. Wilson, Phys. Rev. **D25**, 2649 (1982).

[26] P. Hasenfratz, V. Laliena, and F. Niedermayer, Phys. Lett. **B427**, 125 (1998), hep-lat/9801021v2 .

[27] E. Noether, Nachr. v. d. Ges. d. Wiss. zu Göttingen , 235 (1918).

[28] H. Kalka and G. Soff, *Supersymmetrie*, 1st ed. (Teubner, Stuttgart, 1997).

[29] S. R. Coleman and J. Mandula, Phys. Rev. **159**, 1251 (1967).

[30] R. Haag, J. T. Łopuszański, and M. Sohnius, Nucl. Phys. **B88**, 257 (1975).

[31] S. P. Martin, arXiv.org (2011), hep-ph/9709356v6 .

[32] N. Metropolis, A. W. Rosenbluth, M. N. Rosenbluth, A. H. Teller, and E. Teller, J. Chem. Phys. **21**, 1087 (1953).

[33] S. Duane, A. Kennedy, B. J. Pendleton, and D. Roweth, Phys. Lett. **B195**, 216 (1987).

[34] M. L. Mehta, *Random Matrices*, 3rd ed. (Elsevier/Academic Press, Amsterdam, 2004).

[35] T. Guhr, A. Müller-Groeling, and H. A. Weidenmüller, Phys. Rep. **299**, 189 (1998).

[36] G. Akemann, J. Baik, and P. Di Francesco, eds., *The Oxford Handbook of Random Matrix Theory* (Oxford University Press, Oxford, 2011).

[37] J. Ginibre, J. Math. Phys. **6**, 440 (1965).

[38] N. Lehmann and H.-J. Sommers, Phys. Rev. Lett. **67**, 941 (1991).

[39] T. A. Brody, J. Flores, J. B. French, P. A. Mello, A. Pandey, and S. S. M. Wong, Rev. Mod. Phys. **53**, 385 (1981).

[40] R. G. Edwards, U. M. Heller, J. Kiskis, and R. Narayanan, Phys. Rev. Lett. **82**, 4188 (1999).

[41] H. Markum, R. Pullirsch, and T. Wettig, Phys. Rev. Lett. **83**, 484 (1999), hep-lat/9906020 .

[42] E. P. Wigner, in *Conference on Neutron Physics by Time-of-Flight* (Oak Ridge National Laboratory Report No. 2309, 1957) p. 59.

[43] J. Verbaarschot and T. Wettig, Ann. Rev. Nucl. Part. Sci. **50**, 343 (2000), hep-ph/0003017 .

[44] M. E. Berbenni-Bitsch, S. Meyer, A. Schäfer, J. J. M. Verbaarschot, and T. Wettig, Phys. Rev. Lett. **80**, 1146 (1998).

[45] F. Basile and G. Akemann, JHEP **0712**, 043 (2007), 0710.0376 .

[46] T. Banks and A. Casher, Nucl. Phys. **B169**, 103 (1980).

[47] A. M. Halasz and J. Verbaarschot, Phys. Rev. Lett. **74**, 3920 (1995), hep-lat/9501025 .

[48] R. Pullirsch, K. Rabitsch, T. Wettig, and H. Markum, Phys. Lett. **B427**, 119 (1998), hep-ph/9803285 .

[49] D. Fox and P. B. Kahn, Phys. Rev. **134**, B1151 (1964).

[50] T. Nagao and M. Wadati, J. Phys. Soc. Jpn. **60**, 3298 (1991).

[51] T. Nagao and M. Wadati, J. Phys. Soc. Jpn. **61**, 78 (1992).

[52] G. Lenz and F. Haake, Phys. Rev. Lett. **67**, 1 (1991).

[53] S. Schierenberg, F. Bruckmann, and T. Wettig, Phys. Rev. **E85**, 061130 (2012), 1202.3925v1 .

[54] F. Bruckmann, T. Kovács, and S. Schierenberg, Phys. Rev. **D84**, 034505 (2011), 1105.5336 .

[55] F. Farchioni, P. de Forcrand, I. Hip, C. B. Lang, and K. Splittorff, Phys. Rev. **D62**, 014503 (2000), hep-lat/9912004 .

[56] P. Damgaard, U. Heller, R. Niclasen, and K. Rummukainen, Nucl. Phys. **B583**, 347 (2000), hep-lat/0003021 .

[57] A. M. Garcia-Garcia and J. C. Osborn, Phys. Rev. **D75**, 034503 (2007), hep-lat/0611019v3 .

[58] T. G. Kovács, Phys. Rev. Lett. **104**, 031601 (2010), 0906.5373v2 .

[59] T. G. Kovács and F. Pittler, Phys. Rev. Lett. **105**, 192001 (2010), 1006.1205v1 .

[60] T. G. Kovács and F. Pittler, Talk presented at the XXIX International Symposium on Lattice Field Theory - Lattice 2011, Lake Tahoe, California, USA (2011), 1111.3524v1 .

[61] P. W. Anderson, Phys. Rev. **109**, 1492 (1958).

[62] S. Dürr and C. Hoelbling, Phys. Rev. **D69**, 034503 (2004), hep-lat/0311002v2 .

[63] S. Dürr, C. Hoelbling, and U. Wenger, Phys. Rev. **D70**, 094502 (2004), hep-lat/0406027v2 .

[64] F. Bruckmann and E.-M. Ilgenfritz, Phys. Rev. **D72**, 114502 (2005), hep-lat/0509020 .

[65] S. Chandrasekharan and N. Christ, Nucl. Phys. B - Proc. Suppl. **47**, 527 (1996), hep-lat/9509095v2 .

[66] M. Stephanov, Phys. Lett. **B375**, 249 (1996), hep-lat/9601001 .

[67] P. N. Meisinger and M. C. Ogilvie, Phys. Lett. **B379**, 163 (1996), hep-lat/9512011 .

[68] S. Chandrasekharan and S. Huang, Phys. Rev. **D53**, 5100 (1996), hep-ph/9512323 .

[69] C. Gattringer, P. E. L. Rakow, A. Schäfer, and W. Söldner, Phys. Rev. **D66**, 054502 (2002), hep-lat/0202009 .

[70] C. Gattringer and S. Schaefer, Nucl. Phys. **B654**, 30 (2003), hep-lat/0212029v2 .

[71] V. G. Bornyakov, E. V. Luschevskaya, S. M. Morozov, M. I. Polikarpov, E.-M. Ilgenfritz, and M. Müller-Preussker, Phys. Rev. **D79**, 054505 (2009), 0807.1980v3 .

[72] T. G. Kovács, PoS **LAT2008**, 198 (2008), 0810.4763 .

[73] E. Bilgici, F. Bruckmann, C. Gattringer, and C. Hagen, Phys. Rev. **D77**, 094007 (2008), 0801.4051v2 .

[74] E. Follana, C. T. Davies, and A. Hart (UKQCD and HPQCD Collaborations), PoS **LAT2006**, 051 (2006).

[75] F. Bruckmann, S. Keppeler, M. Panero, and T. Wettig, Phys. Rev. **D78**, 034503 (2008), 0804.3929 .

[76] M. Falcioni, M. Paciello, G. Parisi, and B. Taglienti, Nucl. Phys. **B251**, 624 (1985).

[77] M. Albanese *et al.* (APE Collaboration), Phys.Lett. **B192**, 163 (1987).

[78] R. V. Gavai, S. Gupta, and R. Lacaze, Phys. Rev. **D77**, 114506 (2008), 0803.0182 .

[79] P. Hernández, K. Jansen, and M. Lüscher, Nucl. Phys. **B552**, 363 (1999), hep-lat/9808010v2 .

[80] J. C. R. Bloch, F. Bruckmann, N. Meyer, and S. Schierenberg, JHEP **1208**, 066 (2012), 1204.6259v1 .

[81] P. de Forcrand, PoS **LAT2009**, 010 (2009), 1005.0539v2 .

[82] J. B. Kogut, M.-P. Lombardo, and D. K. Sinclair, Phys. Rev. **D51**, 1282 (1995), hep-lat/9401039v1 .

[83] M. A. Stephanov, Phys. Rev. Lett. **76**, 4472 (1996), hep-lat/9604003v2 .

[84] J. C. Osborn, Phys. Rev. Lett. **93**, 222001 (2004), hep-th/0403131 .

[85] K. Splittorff and J. J. M. Verbaarschot, Nucl. Phys. **B683**, 467 (2004), hep-th/0310271 .

[86] G. Akemann, J. C. Osborn, K. Splittorff, and J. J. M. Verbaarschot, Nucl. Phys. **B712**, 287 (2005), hep-th/0411030 .

[87] G. Akemann, J. C. R. Bloch, L. Shifrin, and T. Wettig, Phys. Rev. Lett. **100**, 032002 (2008), 0710.2865 .

[88] J. C. R. Bloch and T. Wettig, Phys. Rev. Lett. **97**, 012003 (2006), hep-lat/0604020 .

[89] G. Akemann, M. J. Phillips, and H.-J. Sommers, J. Phys. A: Math. Theor. **42**, 012001 (2009), 0810.1458v2 .

[90] G. Akemann, M. J. Phillips, and H. J. Sommers, J. Phys. A: Math. Theor. **43**, 085211 (2010), 0911.1276 .

[91] G. Akemann, M. Kieburg, and M. J. Phillips, J. Phys. A: Math. Theor. **43**, 375207 (2010), 1005.2983 .

[92] R. Grobe, F. Haake, and H.-J. Sommers, Phys. Rev. Lett. **61**, 1899 (1988).

[93] G. Akemann, E. Bittner, M. J. Phillips, and L. Shifrin, Phys. Rev. **E80**, 065201 (2009), 0907.4195 .

[94] Y. V. Fyodorov and H.-J. Sommers, J. Phys. A: Math. Gen. **36**, 3303 (2003).

[95] K. Gottfried and T.-M. Yan, *Quantum Mechanics: Fundamentals*, 2nd ed. (Springer, New York, 2004).

[96] P. Hasenfratz and F. Karsch, Phys. Lett. **B125**, 308 (1983).

[97] G. Golub and C. V. Loan, *Matrix Computations* (The John Hopkins University Press, 1989).

[98] J. C. R. Bloch and T. Wettig, Phys. Rev. **D76**, 114511 (2007), 0709.4630 .

[99] H. Neuberger, Phys. Rev. **D57**, 5417 (1998), hep-lat/9710089 .

[100] P. Dondi and H. Nicolai, Nuovo Cimento A **41**, 1 (1977).

[101] M. Kato, M. Sakamoto, and H. So, JHEP **0805**, 057 (2008), 0803.3121v3 .

[102] D. B. Kaplan, E. Katz, and M. Ünsal, JHEP **0305**, 037 (2003), hep-lat/0206019v3 .

[103] S. Catterall and E. Gregory, Phys. Lett. **B487**, 349 (2000), hep-lat/0006013v2 .

[104] J. Giedt, E. Poppitz, R. Koniuk, and T. Yavin, JHEP **0412**, 033 (2004), hep-lat/0410041v2 .

[105] A. D'Adda, I. Kanamori, N. Kawamoto, and K. Nagata, Nucl. Phys. **B707**, 100 (2005), hep-lat/0406029v2 .

[106] A. D'Adda, I. Kanamori, N. Kawamoto, and K. Nagata, Nucl. Phys. Proc. Suppl. **140**, 754 (2005), hep-lat/0409092v1 .

[107] F. Bruckmann and M. de Kok, Phys. Rev. **D73**, 074511 (2006), hep-lat/0603003v2 .

[108] G. Bergner, F. Bruckmann, and J. M. Pawlowski, Phys. Rev. **D79**, 115007 (2009), 0807.1110v2 .

[109] L. H. Karsten and J. Smit, Phys. Lett. **B85**, 100 (1979).

[110] G. Bergner, T. Kaestner, S. Uhlmann, and A. Wipf, Ann. Phys. **323**, 946 (2008), 0705.2212v2 .

Acknowledgements

First and foremost, I would like to thank Falk Bruckmann who has been my supervisor during my work on this thesis. He has always taken the time to answer my questions and to discuss ideas I had come up with. Practically all the work I have done for my thesis was in close cooperation with Falk. He also gave me the opportunity to visit various conferences with interesting topics at very nice places.

I also want to thank Tamás Kovács, who has been working with Falk and me on high temperature QCD. His interesting findings in preceding publications have been the groundwork for our research. Has has also provided us with all the necessary lattice data.

I would also like to thank Tilo Wettig, who strongly supported me in the publication of the results of my diploma thesis.

Thanks also go to Nils Meyer and Jacques Bloch, with whom I worked on QCD at non-zero chemical potential. Nils also did all the numerical lattice calculations.

Furthermore, I thank Jan Pawlowski and Georg Bergner for all the fruitful discussions during our work on lattice supersymmetry.